Interaction of Pluronic polymers with sugar surfactant in microemulsions designed for decontamination

Sebastian Höhn

December 2015

Interaction of Pluronic polymers with sugar surfactant in microemulsions designed for decontamination

Dissertation

zur Erlangung des akademischen Grades eines

Doktors der Naturwissenschaften (Dr. rer. nat.)
der Fakultät für Chemie der Universität Bielefeld

vorgelegt von

Sebastian Höhn

(geb. Schmid)

aus Kempten (Allgaeu)

Altenplos, Dezember 2015

Erstgutachter: Prof. Dr. Thomas Hellweg
Zweitgutachter: Prof. Dr. Andreas Brockhinke

Die vorliegende Arbeit wurde in der Zeit von Juni 2009 bis März 2012 und von März 2013 bis Oktober 2013 an der Universität Bayreuth am Lehrstuhl für Physikalische Chemie I, sowie an der Universität Bielefeld im Bereich Physikalische und Biophysikalische Chemie unter Betreuung von Herrn Prof. Dr. Thomas Hellweg angefertigt.

Greed has poisoned men's souls,
has barricaded the world with hate [...]
We think too much and feel too little.
More than machinery, we need humanity.
More than cleverness, we need kindness
and gentleness.

Sir Charles Spencer Chaplin jr.
The Great Dictator

Contents

Chapter 1

Prelude

1.1 Abstract

Chemical warfare agents are one of the great threads of our time, irrelevant whether they are from regular military arsenals or synthesized in the laboratories of terrorist groups.
Most hazardous chemicals and the most chemical warfare agents are hydrophobic, while the decontamination agents usually are hydrophilic. Microemulsions are stable mixtures of two immiscible components, oil and water, which are separated by a surfactant film. Due to the coexistence of hydrophilic and hydrophobic domains in microemulsions they are interesting decontamination media. The huge internal interface, separating the two solvents, allows interaction of the decontamination agents and enzymes with the hazardous agents. One limiting factor for applications is the high demand of sugar surfactant to form stable microemulsions. By adding small amounts of amphiphilic diblock copolymers the surfactant efficiency is dramatically enhanced, an effect discovered over a decade ago and known as the efficiency boosting effect. Usually amphiphilic AB diblock copolymers were used in C_iE_j-surfactant systems. To our knowledge no systematic investigation of the effect of commercially available ABA triblock copolymers on microemulsion systems based on sugar surfactants exists up to now. In this thesis the influence of different commercially available triblock copolymers (Pluronics or Poloxamers) on two systems is shown in dependency of the polymer composition and size. In this work technical grade sugar surfactants (Simulsol SL55), with varying compositions due to production process and raw material as systems for application and n-decyl-β-D-maltoside ($C_{10}G_2$) as pure model system were investigated.
Especially the Pluronic polymers with a high PEO content were able to increase the surfactant effi-

ciency, while the large polymers lead to the formation of extended lamellar phases. In this case, the bicontinuous region relevant for decontamination is reduced. The influence of the Pluronic polymers on the internal structure sizes was investigated by SAXS- and SANS-experiments. We were able to show that at high surfactant concentrations the efficiency boosting polymers increase the resulting domain size. All other polymers show only a small influence on the domain size and correlation length. At low surfactant concentrations, as reached in the model system based on $C_{10}G_2$, the resulting internal structures are larger. Therefore, no significant difference in the structure sizes of the polymer free and the polymer containing microemulsion systems were observed. But upon the application of Pluronic polymers the stabilization of larger microemulsion sizes was achieved. Compared to the pure systems, containing only APG as surfactant, the structure sizes were almost twice as big due to use of small amounts of polymer.

Related to the fact, that the added block copolymers are part of the amphiphilic interface, where the decontamination takes place, the influence of different polymers on the interfacial film is of high interest. Therefore, we investigate the model system based on n-decyl-β-D-maltoside ($C_{10}G_2$) and cyclohexane by PCS and NSE. Here, the large polymers reduce the motion of the membrane dramatically. This effect is closely connected to the size of the applied polymer.

A major goal was the development of a skin friendly microemulsion system, the last chapter is dedicated to the newly developed microemulsion systems suitable for skin decontamination purposes. These microemulsions are based on ingredients which are used in the food production or pharmaceutical application. The used oils should be suitable solvents for the removal of the chemical warfare agents. In the case of the co-surfactants we concentrated on substances that were used pharmaceutically and additionally exhibit an anaesthetic effect.

Again, the replacement of small amounts of the surfactant by Pluronic polymers leads to an increase of the surfactant efficiency and increased the stability of the microemulsion.

The new systems, in combination with DFPase as an active decontaminant, offer an efficient, skin and environmentally friendly alternative to the used emulsions based on tetrachloroethylene (C8).

1.2 Zusammenfassung

Chemiewaffen, gleich ob sie aus den Arsenalen von Staaten oder aus den Kellerlaboren terroristischer Vereinigungen stammen, sind eine der großen Bedrohungen unserer Zeit. Während verschiedene giftige Chemikalien und die meisten chemischen Kampfstoffe hydrophob sind, ist der Großteil der Dekontaminationsmittel hydrophil. Mikroemulsionen stellen daher interessante Dekontaminationsmedien dar, da sie eine Öl- und eine Wasserphase bieten. An der ausgedehnten internen Grenzfläche, die die beiden Lösungsmittel separiert, können die Dekontaminationsmittel und Enzyme mit den chemischen Kampfstoffen interagieren. Ein großer Nachteil von Mikroemulsionen auf Zuckertensidbasis ist hierbei die geringe Tensideffizienz.

Die zum Teil dramatische Effizienzsteigerung, die bei Tensiden in Mikroemulsionssystemen durch Polymerzusatz beobachtet wurde, ist seit über einer Dekade als Efficiency boosting Effekt bekannt. Bisher lag der Schwerpunkt auf amphiphilen A-B Block-Copolymeren in C_iE_j Systemen. Bis zum heutigen Tag existiert unseres Wissens nach keine systematische Untersuchung der Interaktion kommerziell erhältlicher ABA - Block-Copolymere mit Mikroemulsionssystemen auf der Basis von Zuckertensiden. Die vorliegende Arbeit schließt diese Lücke. Dabei liegt der Schwerpunkt auf dem Einsatz von kommerziell erhältlichen ABA Blockcopolymeren (Pluronics) und deren Einfluss auf die Effizienz der Zuckertenside in Abhängigkeit der Polymerstruktur und Polymergröße. In dieser Arbeit wurden sowohl technische Zuckertenside (Simulsol SL55) mit produktionsbedingt wechselnden Zusammensetzungen als anwendungsrelevante Systeme und n-Decyl-β-D-maltosid ($C_{10}G_2$) als reines Modellsystem untersucht.

Dabei konnte gezeigt werden, dass vor allem die Pluronic Polymere mit hohem PEO Gehalt effizienzsteigernd auf die Tensidsysteme wirken. Die größeren Polymere zeigen im Phasenverhalten verstärkt die Tendenz zur Ausbildung ausgedehnter lamellarer Bereiche. Hierbei wird der für Dekontaminationszwecke notwendige bikontinuierliche Bereich geschmälert. Für die anschließende Charakterisierung wurde der Einfluss der Polymere auf die Größenverhältnisse innerhalb der Mikroemulsionssysteme durch SAXS- und SANS- Experimente untersucht. So konnte gezeigt werden, dass bei großen Tensidkonzentrationen die effizienzsteigernden Pluronics in Abhängigkeit der Polymergröße die resultierende Domänengröße erhöhen. Alle anderen Polymere zeigen nur einen geringen Einfluss auf die resultierenden Domänengrößen und Korrelationslängen. Bei niedrigen Tensidkonzentrationen, wie sie im reinen $C_{10}G_2$-System erreicht werden, sind die resultierenden internen

Strukturen größer. Hier ist kein signifikanter Unterschied in den Strukturgrößen zwischen den polymerfreien und den polymerhaltigen Systemen mehr festzustellen. Durch den Einsatz der Pluronic Polymere lassen sich jedoch deutlich größere Mikroemulsionsstrukturen stabilisieren. Im Vergleich zu den Basissystemen, deren einzige Tenside APG sind, können die Strukturgrößen durch Einsatz geringer Mengen Polymer nahezu verdoppelt werden.
Zusätzlich wurde der Einfluss auf die Dynamik der Membranen im reinen $C_{10}G_2$ System durch DLS und NSE Experimente im Vergleich zu polymerfreien Systemen betrachtet. Durch die großen Polymere im amphipilen Film wird die Dynamik der untersuchten Systeme deutlich reduziert. Dieser Effekt korreliert mit der Größe der eingesetzten Polymere.
Da die Weiterentwicklung der Mikroemulsionen hin zu hautfreundlichen Systemen im Hinblick auf die Human-Dekontamination ein wichtiger Aspekt unserer Forschungsarbeiten ist, wird den Modifikationen der technischen Systeme hin zu hautfreundlichen Systemen ein eigenes Kapitel gewidmet. Diese neu entwickelten Mikroemulsionen basieren auf Komponenten, die Zulassungen als pharmazeutische oder Lebensmittelzusatzstoffe haben. Die Ölphasen wurden so gewählt, dass sie als geeignete Lösemittel in der Lage sind chemische Kampfstoffe von Oberflächen zu entfernen. Im Falle der Cotenside wurden mit Benzylalkohol und Eugenol Alkohole gewählt, die neben einer pharmazeutischen Anwendung auch zusätzlich anaesthetische Eigenschaften zeigen.
Durch geeignete Pluronic Polymere kann auch hier die Effizienz der verwendeten Zuckertenside deutlich gesteigert werden und die Stabilität der Mikroemulsionen erhöht werden. Somit bieten diese Systeme in Kombination mit dem Enzym Diisopropylfluorophosphatase (DFPase), das Nervenkampfstoffe spaltet, eine effiziente, haut- und umweltverträgliche Alternative zu den bislang genutzten Emulsionen auf der Basis von Tetrachlorethylen.

Chapter 2

Introduction

2.1 Motivation and structure

The use of sarin in Syria in autumn 2013 proves that we have not overcome the era of chemical warfare agents. As long as these weapons of mass destruction exist and are used against mankind, the development of appropriate new and improvement of the existing decontaminants is of utmost importance.

This thesis is an important contribution in this context. The results of this work were obtained at the universities of Bayreuth and Bielefeld and this work contains new findings about microemulsions used as carrier media for decontamination processes. Beginning with an overview of the chemical warfare agents and decontamination the theoretical background is explained. A brief introduction of the topics of surfactants, microemulsions, and decontamination will be given.

Chapter 3 introduces the theoretical concepts of microemulsions, based on thoughts and observations about surfactant geometry. A closer look at the polymer-surfactant system is given, concentrating on the important *efficiency boosting effect* discovered by STREY *et al.* over a decade ago. The foundations of the used methods and analytical aspects are introduced, containing scattering methods such as photon correlation spectroscopy (PCS) and small angle X-ray (SAXS) and neutron (SANS) scattering. PCS offers information about the polymer influence on the surfactant film dynamics, while SAXS and SANS are used for the investigation of the internal structure sizes in the microemulsion systems.

The experimental part provides information about the methods used, describes the standard procedures resulting in the phase diagrams and contains details about the sample preparation. The

results of this work are separated in three chapters. The first deals with the important aspect for technical usage, the efficiency boosting in application. Based on the water / Lanol 99 / Simulsol 55 / n-pentanol system the changes upon replacement of surfactant by Pluronic polymers are shown.
The next chapter concentrates on the influence of the polymer on the internal film separating the oil and water domains. Here, the focus is on the model system water / cyclohexane / n-decyl-β-D-maltoside ($C_{10}G_2$) / n-pentanol and variations thereof prepared with deuterated solvents.
In the last chapter, the modifications of the microemulsion systems targeting the formation of an efficient skin friendly decontaminant are summed up. Variations of the oil phase, the cosurfatant and the surfactant are highlighted. In all cases the formation of a stable bicontinuous microemulsion was possible.

2.2 Chemical warfare agents

Chemical warfare agents (CWA) are all toxic substances, which are developed, produced or stored with the aim to decimate the enemy forces. Their application target can include plants, animals or humans, ranging from harassing agents, forcing short time disabling (such as lachrymatory agents) to the fast reacting nerve agents with a high lethality rate [2, 8, 11].
The use of hazardous chemical substances in warfare is documented throughout the whole history of mankind [8, 21]. But never before the use of chemical warfare agents reached the level, that started by a release of chlorine by the German imperial army on April 22nd in 1915 in West Flanders, driving Europe to a new kind of chemical warfare [29]. This gas attack, comparable to the one depicted in figure 2.1, was the prelude of an intense 'chemists war'. Depending on the source, up to 1.24 million injured and 80-91000 fatal gas casualties made World War I the sad peak in the history of the use of CWA [8].
The low costs and the simple synthesis in proportion to the resulting effect lead to a massive stockpile and further investigation of CWA. In Germany alone up to 70000 t of CWA, among them 12000 t Tabun and 25000 t Sulfur Mustard, were synthesized and stockpiled until 1945[28].
With the appearence of the religious group of Aum Shinrikyo in Japan and the release of Sarin in Matsumoto (June 1994) and the Sarin gas attack to the Tokyo subway on 20 March 1995, the first terrorist attacks were performed with CWA. Seven people died and over 200 were injured in Matsumoto, in Tokyo more than 5500 victims were affected containing 12 fatalities [24, 10]. In

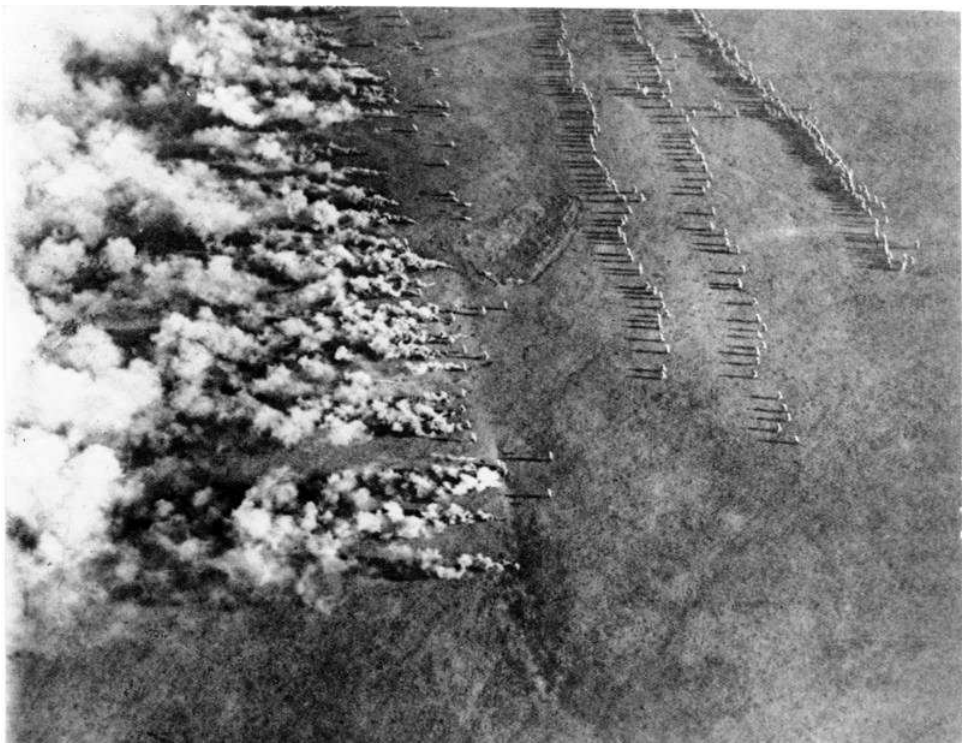

Figure 2.1: World War I, German Gas Attack. Picture: Creative Commons - Bundesarchiv, Bild 183-F0313-0208-007 / CC-BY-SA.

both cases the low number of casualties is owed to the low purity and the inefficiency of the Sarin used by the terrorists [8, 23].

Hence, there is a change in the threat scenarios from conflicts between nations to local assaults on civilian population. To what extent states suspected as supporters of the international terrorism, offered CWA to terror groups is unclear [8]. The synthesis of CWA is relatively simple and the necessary starting materials are easily purchased on the global market. In a test performed in 2002, HÖFER was able to buy all reactants for the synthesis of sulfur mustard and a nerve agent on a kilogram-scale without any troubles or request [8]. Instructions for CWA synthesis can be found in many established textbooks for organic chemistry [33, 27] or are available in free online encyclopaedia (for example HD synthesis pathways are given on wikipedia) [1]. Additionally the actual political situation in many states that did not sign the CWC, among them the Irak, Lybia, Egypt and Syria, can currently be described as very tense or even out of control.

Despite of their relatively low toxicity compared to nerve agents, blister and blood agents are a high potential threat. Widely used industrial chemicals, such as hydrogen cyanide or phosgene, are

comparatively easy to obtain and hard to control [29, 8, 11].

2.2.1 Classification and toxicity of CWA

The warfare agents can be classified into several categories according to the way they affect the human body (examples of the chemical structure are given in figure 2.2).

The most dangerous class are the nerve agents (see table 2.1). The high toxicity of these organophosphates is based on their ability to inhibit the function of the enzyme acetylcholinesterase by covalently binding to the active center. This results in a continuous stimulus of the nerves by the transmitter acetylcholine, which is no longer deactivated[11, 21].

The first member of this group was Tabun, developed in 1937 as insecticide by the IG Farben / Bayer AG. Following the nomenclature of the allied armed forces, Tabun is the first member of the G-Series (G for German, because it was developed by german scientists) and therefore named GA. Furthermore, the G-series consists of Sarin (GB, 1939), Soman (GD, 1944) and Cyclo-Sarin (GF, 1949). On allied side, the so called V-Series was developed containing VX, which has the highest toxicity of all nerve agents.[17, 8]

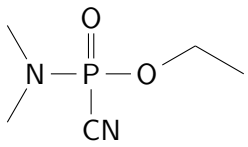

Tabun (**GA**)

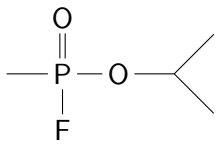

Sarin (**GB**)

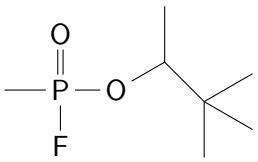

Soman (**GD**)

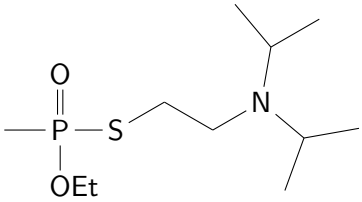

VX

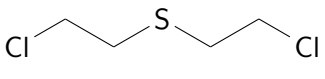

S-LOST, mustard gas (**HD**)

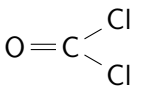

phosgene

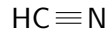

hydrogen cyanide

*Figure 2.2: Chemical structures of the most important nerve agents and one member of blister (**HD**), chocking (Phosgene) and blood agents (HCN).*

The second group consists of the skin or blister agents, including the S-LOST (sulfur mustards, Yperite, HD) and N-LOST (nitrogen mustards, HN1 to HN3) series, are known to cause severe damage on skin and eye. With a reduced toxicity compared to the nerve agents, they are simple to synthesize and show a higher persistence. Figure 2.3 shows the reaction route for S-LOST synthesis, which has been extensively used during World War I [26]. S-LOST is highly persistent and able to remain on the ground for days up to weeks depending on the weather conditions, leading to the application as an area-denial weapon. This high persistence makes them a thread still nowadays, as the toxicity of the S-Lost disposed in the Baltic sea after World War II is still high.

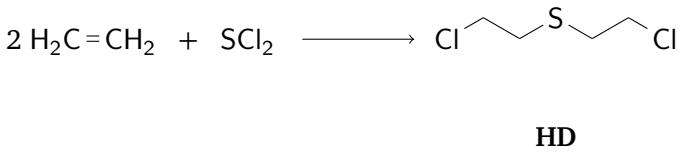

HD

Figure 2.3: Historical synthesis route of S-Lost by reaction of sulfur dichloride and ethene.

The remaining groups of chocking and blood agents have lower importance. Among these phosgene and hydrogen cyanide which are both widely used for industrial processes[29, 11].
The toxicity of the most relevant lethal CWAs is given in table 2.1. Here, LD50 is the lethal dose, at which 50 % of the exposed individuals will die as a result of their injuries. LD50 is given for contact with skin. For incorporation by inhalation the product of concentration c and exposure time t is taken into account (LCt50). The values are estimates of lethal doses on man. For comparison, the values for S-Lost are added.

2.2.2 Chemical Weapons Convention - CWC

In spite of the early proscription in the Hague Treaty of 1899 and 1907 as well as the Geneva Protocol (1925), CWA were (and are used up to date) as weapons of mass destruction[11]. Ratification of the Geneva Protocol of 1925 was performed slowly (ratified in USA and Japan after 1970) and the first use of biological and chemical warfare agents was banned [18].
With the commencement of the Chemical Weapons Convention (CWC) in 1997, which has been ratified by 147 states until December 2001, a serious reduction of the CWA stockpiles was achieved. The key issues of the CWC are the prohibition of the development, the production and the use of CWA. Furthermore, each ratifying state undertakes destruction of all CWA and production facilities[14]

Table 2.1: LD50 and LCt50 values of the most relevant nerve agents and sulfur mustard (HD) for comparison. a) data from [17], b) data from [8].

		LCt50 Inhalation mg·min/m^3	LD50 Skin mg/individual	Ref.
Tabun	GA	200	4000	a)
Sarin	GB	100	1700	a)
Soman	GF	100	300	a)
VX	VX	50	10	a)
S-LOST	HD	1500	10000	b)

The independent Organisation for the Prohibition of Chemical Weapons (OPCW) located in Den Haag, Netherlands administrates and controls the compliance of the CWC, supporting the states in the destruction process. According to the reports of the OPCW 55 939 t of the declared 71 196 t CWA have been destroyed to date (information dated 2013-02-28), that is a destruction rate of 78.5 %[15]. The CWC was signed and ratified by 189 states as of September 2013. In addition to Israel and Burma, which have signed but not yet ratified the CWC, five states have not signed nor ratified the treaty. These states are North Korea, Angola, Egypt, South Sudan and Syria.[13]
Actual reports of the use of weapons of mass destruction in the Ghouta chemical attacks in Syria on 21 August 2013, show that there is - unfortunately - still a need of effective decontamination methods [22].

2.3 Decontamination of CWA

Decontamination is generally defined as the inactivation or removal of chemical or biological threats to a non-hazardous level. This can be performed by physical removing such as washing or wiping of the hazard or by chemical neutralisation of the dangerous substances [23, 19, 16].
The decontamination methods are separated in two major fields: the human decontamination and the decontamination of equipment and infrastructure. The primary target of human decontamination is the quick removal of the contaminant using mild reagents. The second field forces the complete removal of hazardous material from different surfaces[23].

2.3.1 Decontaminants I - Solvent

A detailed compendium on the actually used decontamination reagents and methods can be found for example in the textbooks from LUKEY [10], HURST [9], and RICHARDT [19]. Here just a short overview is given.

Solid decontaminants, such as absorber powder, sponges or resins are only important in the field of human decontamination. They usually remove the CWA physically from the contaminated surface and are far from the wetting properties of liquid systems.

Aqueous decontamination has been performed during the World War I by 'bleach' solutions (usually containing calcium hypochlorite) [10]. The high availability and the high efficiency of soap and hypochlorite solutions or even pure water, makes them important decontaminants[6, 3]. The major disadvantage is the poor solubility of the CWA in water and the resulting lack of ability to eluate CWA from plastics or paint coatings[19]. Moreover most aqueous decontamination media are highly corrosive.

Non-aqueous solvents are able to remove even thickened CWA from surfaces. Stored as pre-mixed solution in containers, these decontaminants are ready-to-use. Usually the required amount of decontaminant per surface area is lower than in aqueous solutions. Deployment of organic solvents inevitably leads to their disadvantages, namely they are harmful to health and environment and often flammable.

A possibility to combine the advantages of both systems is the use of macro- and microemulsions.

In case of the macroemulsions, water in oil emulsions are preferred, where the continuous oil-phase is able to react as solvent for the hazardous substances. There are several approaches for the use of these systems, as example the German Armed Forces used the so-called "German (Makro-) Emulsion" or "C8", a mixture of Tetrachlorethylene, HTH (Ca-hypochlorite) and an anionic, technical grade surfactant mixture (Marlowet)[2].

But also the thermodynamically stable microemulsions have successfully been tested as carrier materials for decontamination processes [20, 12, 30, 25]. Their advantages over the macroemulsions, such as the larger interfacial area (approximately 100 times larger) and the ultra-low interfacial tension and viscosity are combined with high solubilisation capacities for both, water and oil soluble agents. This makes them ideal systems for decontamination processes [2, 30, 31].

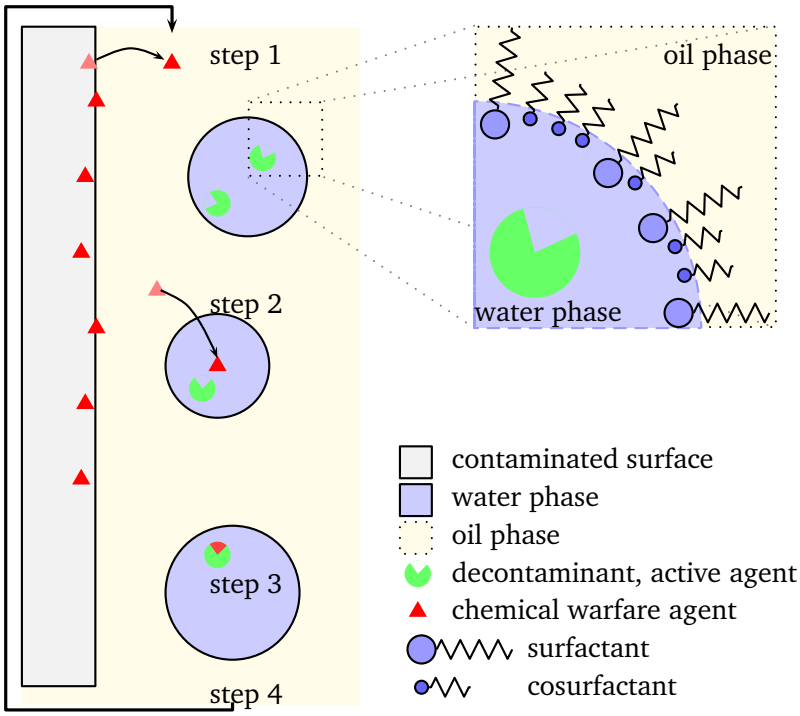

Figure 2.4: Decontamination scheme: Removal of CWA from a surface and decontamination with a water in oil droplet microemulsion. Step 1: Extraction of the CWA by the oil phase. Followed by phase transfer into water phase (Step 2). In step 3 the decontamination of CWA by the active agent takes place. The last step (step 4) is the regeneration of the microemulsion.

2.3.2 Decontaminants II - Active reagent

The inactivation of CWA by chemical decontamination can be achieved by three different mechanisms:

Oxidation [5, 19], (alkaline) hydrolysis [23, 19] , or enzymatic decontamination [31, 20, 10, 25].

The most promising method is the enzymatic decontamination. In contrast to the other methods it is usually non-corrosive, fast and the active agent is not needed in equal molarity as the CWA.

The advantage of an enzyme in combination with a skin friendly and environmentally compatible microemulsion system lead to an universally applicable decontamination system [2, 32].

The enzyme of the squid *Loligo vulgaris* (see figure 2.5) is known to detoxify nerve agents as reported by RICHARDT and co-workers [20, 19, 4, 31]. The proposed mechanism for a decontaminated surface is shown in figure 2.4 for a water in oil microemulsion. In the first step, the hazardous agent is dissolved from the surface by the continuous oil phase of the microemulsion. After phase transfer

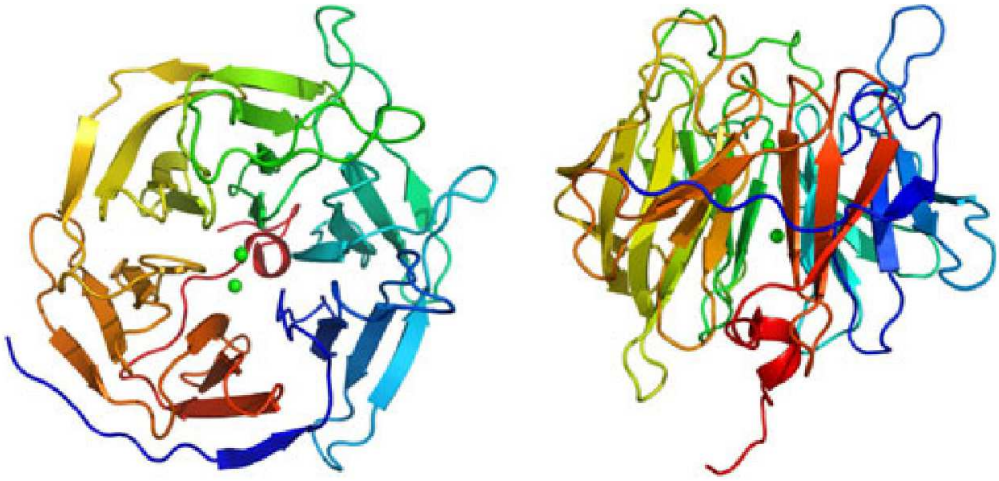

Figure 2.5: Tertiary structure of diisopropyl fluorophosphatase (DFPase) in top and side views. Picture and description from Wellert, S., Eur. Biophys. J. (2011) 40,761–774. Copyright Springer Verlag. Reproduced with permission

of the CWA into the water phase (step 2), it is destroyed by the active agent (step 3). The last step is the regeneration of the microemulsion, restarting the decontamination cycle [2].

2.3.3 The ideal decontaminant

The requirements to an ideal skin-decontaminant are collected from different military sources and summarised in table 2.2. As can be seen, these requirements are manifold. But the major part of them are covered by the newly developed microemulsion systems, as shown in the chapter 7.
The most critical factor in the skin decontamination process is time. The CWA has to be removed quickly from the skin, to minimize transdermal penetration. At this juncture it is not relevant whether the removal is performed with a sponge, wet tissues or by washing with water or decontamination solution. The most important is the removal of the CWA within the first two minutes [10, 8].
The necessary short time window for the CWA removal demands a fast recognition of the CWA by the victims. Here, the limits of decontamination are shown because most CWA are, when free from impurities, colorless oily liquids with almost no or at least a slightly fruity odour [11, 29].

Table 2.2: Requirements of an ideal skin decontamination medium according to references [10, 8, 23, 6, 7].

Aspect	Properties of the ideal decontamination media
Safety	non irritating and non allergic
	non hazardous
	environmentally compatible
	non corrosive
Usability	easy to employ
	quick to hand
	single and mass use devices available
Stability	Temperature range from -40 °C to +50 °C
	long storage life
	no separation effects
Economy	low costs
	available in large amounts
	easy to scale-up
	constant quality
Efficiency	quick and complete decontamination
	no formation of toxic products
	no increase of percutaneous uptake

2.4 References

[1] 2014. URL: http://de.wikipedia.org/wiki/Senfgas#Herstellung_von_S-Lost.

[2] H.J. Altmann and A. Richardt. "Decontamination of Warfare Agents". In: ed. by A. Richardt and M-M. Blum. Wiley VCH, 2008. Chap. Decontamination of Chemical Warfare Agents.

[3] S. Bjarnason et al. "Comparison of selected skin decontaminant products and regimens against VX in domestic swine." In: *Hum Exp Toxicol.* 27.3 (2008), pp. 253–261.

[4] J. Gäb et al. "Monitoring the hydrolysis of toxic organophosphonate nerve agents by diisopropyl fluorophosphatase (DFPase) in aqueous buffer and bicontinuous microemulsions with 1H-31P-HSQC NMR spectroscopy." In: *Anal. Bioanal. Chem.* 396.3 (2010), pp. 1213–1221.

[5] F. Gonzaga et al. "New microemulsions for oxidative decontamination of mustard gas analogues and polymer-thickened half-mustard". In: *New J. Chem.* 25 (2001), pp. 151–155.

[6] K.A. Hanssen et al. "Evaluation of Decontamination Systems Challenged With Nerve Agents". In: *Conference paper.* 2006.

[7] T. Hellweg. "Microemulsions: A Versatile Carrier for Decontamination Agents". In: *Decontamination of Warfare Agents*. Ed. by A. Richardt and M.-M. Bum. Wiley-VCH, Weinheim, 2008.

[8] M. Höfer. "Ein Überblick: Chemische Kampfstoffe". In: *Chemie in unsrer Zeit* 36.36 (2002), p. 148.

[9] C.G. Hurst. "Medical Aspects of Chemical and Biological Warfare - Textbook of Military Medicine". In: ed. by R. Zajtchuk and R.F. Bellamy. Office of The Surgeon General Department of the Army, United States of America, 1997. Chap. Chapter 15: Decontamination, p. 351.

[10] B.J. Lukey et al. "Chemical Warfare Agents - Chemistry, Pharmacology, Toxicology and Therapeutics". In: ed. by J.A. Roman, B.J. Lukey, and H. Salem. CRC Press, 2008. Chap. Chemical Warfare Agent Decontamination from Skin, p. 611.

[11] H. Marquardt and S.G. Schaefer. *Lehrbuch der Toxikologie*. Ed. by H. Marquardt and S.G. Schaefer. BI-Wissenschafts-Verlag, 1994.

[12] F.M. Menger and M.J. Rourk. “Deactivation of mustard and nerve agent models via low-temperature microemulsions”. In: *Langmuir* 15.2 (1999), pp. 309–313.

[13] *Non-Member States*. OPCW. URL: http://www.opcw.org/.

[14] OPCW. *Convention on the prohibition of the development, production and use of chemical weapons and on their destruction*. 2005.

[15] OPCW. *Demilitarisation*. 2014. URL: http://www.opcw.org/.

[16] OPCW. *Facts About Personal Cleaning and Disposal of Contaminated Clothing*. 2014. URL: http://www.opcw.org/.

[17] OPCW. *Types of chemical agents*. 2014. URL: http://www.opcw.org/.

[18] *Protokoll ueber das Verbot der Verwendung von erstickenden, giftigen oder aehnlichen Gasen sowie von bakteriologischen Mitteln im Kriege*. 1925.

[19] A. Richardt and M.M. Blum. *Decontamination of Chemical Warfare Agents*. Wiley VCH, 2008.

[20] A. Richardt, M.M. Blum, and S. Mitchell. “Was wissen Calamari über Sarin? Enzymatische Dekontamination von Nervenkampfstoffen.” In: *Chemie in unserer Zeit* 40.4 (2006), pp. 252–259.

[21] H. Salem, A.L. Ternay, and J.K Stuart. “Chemical Warfare Agents - Chemistry, Pharmacology, Toxicology and Therapeutics”. In: ed. by J.A. Roman, B.J. Lukey, and H. Salem. CRC Press, 2008. Chap. Brief History and use of Chemical Warfare Agents in Warfare and Terrorism, p. 12.

[22] A. Sellstroem, s. Cairns, and M. Barbeschi. “United Nations Mission to Investigate Allegations of the Use of Chemical Weapons in the Syrian Arab Republic - Report on Allegations of the Use od Chemical Weapons in the Ghouta Area of Damascus on 21 August 2013”. In: *United Nations Mission Report* (2013), pp. 1–41.

[23] F. Sidell and D. Franz. *Medical Aspects of Chemical and Biological Warfare - Textbook of Military Medicine*. Ed. by R. Zajtchuk and R.F. Bellamy. Office of The Surgeon General Department of the Army, United States of America, 1997.

[24] F. Sidell, E.T. Takafuji, and D. Franz. “Medical Aspects of Chemical and Biological Warfare - Textbook of Military Medicine”. In: ed. by R. Zajtchuk and R.F. Bellamy. Office of The Surgeon General Department of the Army, United States of America, 1997. Chap. Overwiew: Defense against the effects of chemical an biological warfare agent, p. 1.

[25] R. Stehle et al. “An enzyme containing microemulsion based on skin friendly oil and surfactant as decontamination medium for organo phosphates: Phase behavior, structure, and enzyme activity”. In: *Journal of colloid and interface science* 413 (2014), pp. 127–132.

[26] F. R. Tang and W. K. Loke. “Sulfur mustard and respiratory diseases”. In: *Critical Reviews in Toxicology* 42.8 (2012), pp. 688–702.

[27] F. Ullmann. *Ullmanns Encyklopaedie der Technischen Chemie, Band 21; Schwefel bis Sprengstoffe,* ed. by E. Bartholome et al. 4th Ed. Vol. 84. 8. WILEY-VCH Verlag, 1982, pp. 322–322.

[28] unknown. *Deutscher Bundestag: Drucksache 13/2733 vom 24.10.1995*. 1995.

[29] H.-W. Vohr. *Toxikologie Band 2: Toxikologie der Stoffe*. Ed. by H.-W. Vohr. Vol. 2. Wiley VCH Verlag GmbH & Co KGaA, 2010.

[30] S. Wellert et al. “Structure of biodiesel based bicontinuous microemulsions for environmentally compatible decontamination: A small angle neutron scattering and freeze fracture electron microscopy study”. In: *J.Colloid Interf.Sci.* 325.1 (2008), pp. 250–258.

[31] S. Wellert et al. “Temperature dependence of the surfactant film bending elasticity in a bicontinuous sugar surfactant based microemulsion: a quasielastic scattering study”. In: *Physical Chemistry Chemical Physics* 13.8 (2011), pp. 3092–3099.

[32] S. Wellert et al. “The DFPase from loligo vulgaris in sugar surfactant based bicontinuous microemulsions: Structure, dynamics and enzyme activity”. In: *European Biophys. J.* 40 (2011), pp. 761–774.

[33] T. Weyl and Houben J. *Methoden der organischen Chemie*. Ed. by Houben J. Weyl T. and Buechel K.H. G. Thieme-Verlag, 1955.

Chapter 3

Theoretical background

3.1 Sugar surfactants

The words detergents (from latin *detergere*), surfactants (surface active agents) or amphiphiles are usually describing the same group of chemical substances. History of mankind is closely related to the usage of such surfactants, the first reports are found written in Sumerian cuneiform script, dated about 2500 BC [24].

Usually surfactants consist of a hydrophilic head group and a hydrophobic or lipophilic hydrocarbon chain. Due to this amphiphilic (from greek: loving both) structure the molecules adsorb at interfaces (for example the oil-water interface) and reduce the surface tension. At concentrations above the critical micelle concentration (CMC) spontaneously self-organization of the molecules occurs and a wide variety of structures such as the well known micelles are formed. Surfactants are classified by the character of the hydrophilic head group (see figure 3.1). Among the ionic surfactants the anionic surfactants with negatively, cationic surfactants with a positively charged head group and amphoteric surfactants with compensated positive and negative charges in the head group are distinguished [24, 25, 21, 19].

The hydrophilic head group of the non-ionic surfactants consists of polar groups, such as alcohols, polyalkylethers or glucoside ethers. With the increasing interest in renewable raw materials and the demand for environmental harmless substances the sugar surfactants gain growing attention. These surfactants can be synthesized from fatty alcohols and sugars (glucosides, saccharides or sorbitols) and are dermatologically mild surfactants with very good biodegradability [80, 64].

We focus on the alkyl polyglucosides (APG), where the glucosidic head group and the alkyl chain

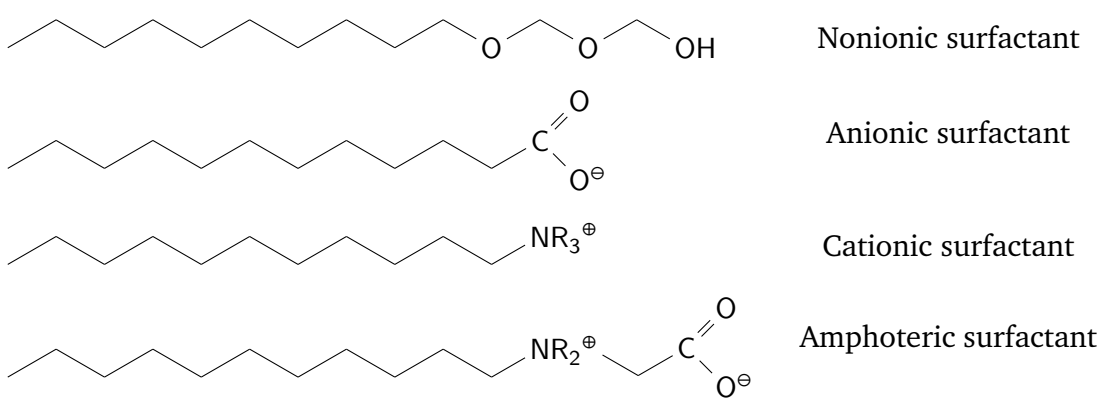

Figure 3.1: Surfactant classification by the composition of the different head groups. In all examples the lipophilic tail on the left side is represented by a decyl-chain.

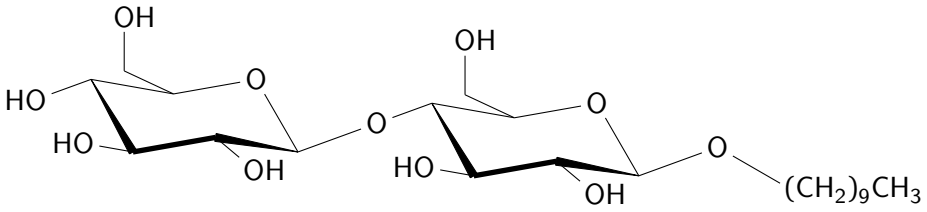

Figure 3.2: Alkyl polyglucoside: n-decyl-β D- *maltoside* $C_{10}G_2$

are linked via an ether bond as shown in figure 3.2. They are usually abbreviated as C_nG_m. Here, n is the number of carbon atoms of the alkyl chain, usually n is in the range of $6 \geq n \geq 14$. The polymerization degree of the glucosidic head group m is between $1 \geq m \geq 2$.

Sugar surfactants show no significant dehydration of the surfactant head group upon increasing the temperature. The reason is the strong hydrogen bond between the hydroxyl groups of the sugar unit and the water.

3.2 Microemulsions

Microemulsions are mixtures of at least two immiscible components stabilized in the easiest case just by a surfactant. The hydrophilic solvent is usually water, the hydrophobic solvent is denoted as oil in the following. The resulting microemulsions are clear, thermodynamically stable, nanostructured liquids [20, 95, 42]. If based on sugar surfactants, microemulsions consist of at least four components: Water, oil, sugar surfactant and a co-surfactant. As co-surfactant usually medium chain

alcohols are used. [94]

The phase behaviour depends on the composition of the microemulsion, the notation is given either in mass fractions (α, γ, δ and ϵ) or in the respective volume fractions (Φ).

3.2.1 Notation of the microemulsion composition

The following notation will be used in the ensuing work. It is based on the nomenclature introduced by KAHLWEIT [54] and modified to our needs where necessary. The composition is described by the three mass fractions: α for the oil in the oil-water mixture, γ for the surfactant and δ for the co-surfactant[104].

$$\alpha = \frac{m_{oil}}{m_{oil} + m_{water}} \tag{3.1}$$

$$\gamma = \frac{m_{surfactant}}{m_{oil} + m_{water} + m_{surfactant}} \tag{3.2}$$

$$\delta = \frac{m_{alcohol}}{m_{oil} + m_{water} + m_{surfactant} + m_{alcohol}} \tag{3.3}$$

It is important to notice, that we took γ_s, which is the pure surfactant concentration in our concerns. Hence, in contrast to the original work, we are neglecting the concentration of co-surfactant in the interfacial film.

For the small angle scattering experiments often the volume fractions of the components are taken into account. They are given corresponding to the mass fractions as Φ_a (for α), Φ_c (for γ) and Φ_d (for δ).

In addition, to study only surfactant and co-surfactant, the influence of amphiphlic polymers on microemulsions is investigated in this work. Assuming the added polymer being completely part of the amphiphilic film without formation of micelles or dissolving in the water or oil domain leads to a new definition of γ. Due to that consideration the mass amount of the polymer is part of the surfactant amount γ. Equation 3.1 changes to:

$$\gamma = \frac{m_{amphiphile}}{m_{oil} + m_{water} + m_{amphiphile}} \tag{3.4}$$

$$\text{with} \qquad m_{amphiphile} = m_{surfactant} + m_{polymer}$$

Furthermore, the polymer content in the sugar surfactant-polymer mixture is given as ϵ according to equation 3.2.1

$$\epsilon = \frac{m_{polymer}}{m_{surfactant} + m_{polymer}} \tag{3.5}$$

With these parameters each point in the phase triangle of the microemulsion systems can be described.

3.2.2 Phase behaviour of microemulsions

Ternary Microemulsion systems

Based on the work of FRIEBERG and KILPATRICK *et al.* [74, 29, 73, 61], KAHLWEIT and coworkers were able to show that the phase behaviour of ternary microemulsion systems is closely connected to the corresponding three binary base systems built from the seperate components [55, 59, 56]. As shown in Figure 3.3, the phase behaviour of the microemulsion can be drawn as a phase prism with the tuning parameter on the ordinate. In case of the C_iE_j surfactants, usually the temperature is used to change the phase behaviour. Metaphorically speaking, the phase prism is formed by simply stacking the isothermal Gibbs triangles of the ternary system on top of each other[57, 92]. The pure components water (A), oil (B) and surfactant (C) are located in the edges, the phase inversion can easily be achieved by changing the temperature [95].

As shown in figure 3.3 on the left, the phase behaviour of the system water (A) - oil (B) is nearly completely dominated by an extended miscibility gap. The binary mixtures water (A) - surfactant (C) and oil (B) - surfactant (C) show lower miscibility gaps at low temperatures, which are usually below the melting point of the mixture [65, 96, 32]. The system (A)-(C) has an additional upper miscibility gap, the lower critical point cp_β at temperature T_β is given in the literature as the cloud point and can be used to test the quality of the used surfactant[87].

With respect to the complexity of the phase behaviour of microemulsion systems it is useful to investigate several cuts through the phase prism. Usually a constant oil to water composition (α) is chosen, leading to the typical T(γ)-sections.

Such a cut is schematically shown in figure 3.4. Here, the phase diagram is measured at a constant α by varying the amount of surfactant (γ) as a function of the temperature T [96, 92].

These phases were first described by WINDSOR (and denoted as Windsor type I-IV)[106]. In this work the arabic notation introduced by KNICKERBOCKER *et al.* [63] will be used. The number of

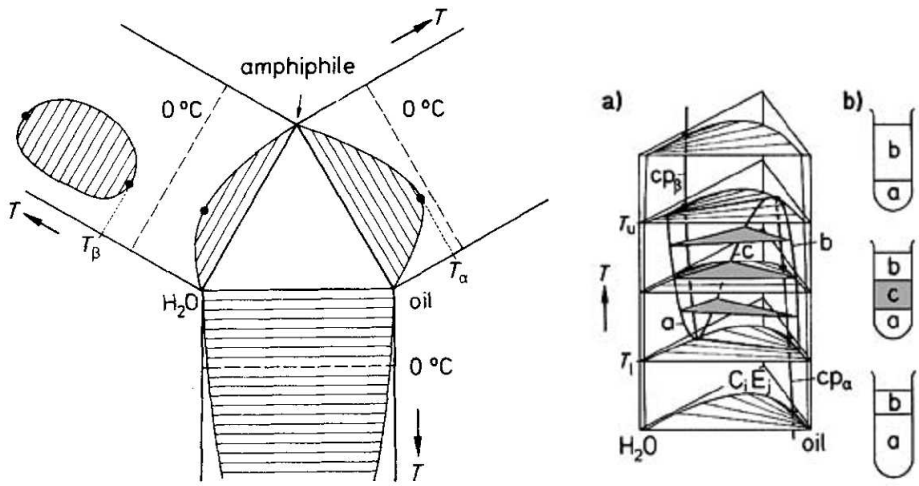

Figure 3.3: left: Phase behaviour of a ternary system shown as an unfolded phase prism consisting of three binary systems; right: a) resulting phase prism of the ternary system with broken critical line and resulting three phase body. The sketches in b) show the corresponding phase volume of a sample as a function of T. Pictures and description from Kahlweit, M. and Strey, R.: Phase Behavior of Ternary Systems of the Type H_2O-Oil-Nonionic Amphiphile (Microemulsions), Angew. Chem. Int. Ed. Engl. 1985, 24, 654-668. Copyright Wiley-VCH Verlag GmbH & Co. KGaA. Reproduced with permission.

coexisting liquid phases is given by $\underline{2}$, $\overline{2}$ and 3, the line denotes the phase where the predominant amount of amphiphile is dissolved. The pure microemulsion phase is denoted by 1.

The observed phase boundaries form the so-called *Kahlweit fish*. Using the schematic drawing in figure 3.4, the phase behaviour is explained. The test tubes show the existing phases, according to the following colour code: light blue denotes the water phase, yellow the oil phase and cyan is the microemulsion phase.

Following the red line in figure 3.4 we start at low temperatures. Here, we observe two phases denoted as $\underline{2}$ (or Windsor I), a surfactant-rich water phase with o/w micelles coexisting with an excess oil phase. An increase of the temperature leads to the formation of a third type (3 or Windsor Type III), where a water phase, a microemulsion phase and an oil phase coexist. Due to the shape of the phase boundaries this region is called the fish body. At high temperatures the single phase microemulsion disappears and a surfactant rich w/o microemulsion with an excess water phase appears. This situation is labelled as $\overline{2}$ or Windsor type II.

Starting at point $\tilde{T}$ in figure 3.4 with the binary water and oil system, small amounts of surfactant

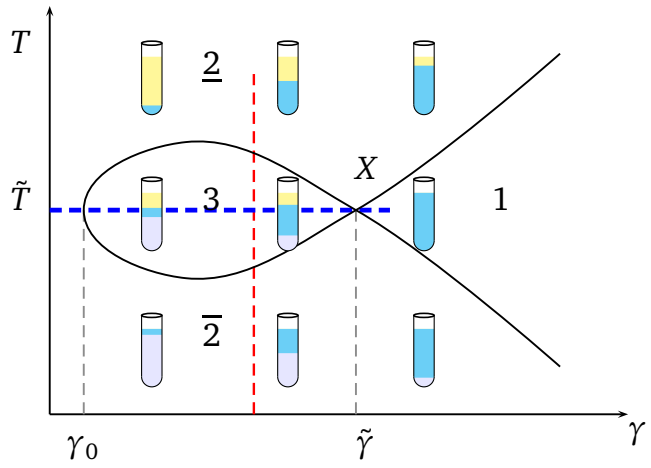

Figure 3.4: Schematic cut through the phase prism at a constant water to oil ratio α, showing the typical Kahlweit-fish. At γ_0 starts the formation of a microemulsion middle phase. A crucial point is the fish-tail-point or X-point, located at $\tilde{T}$ and $\tilde{\gamma}$. Here, the minimum amount of surfactant for complete microemulsion formation is reached. The tubes are schemes of the coexisting phases, light blue denotes a water rich, yellow an oil rich and cyan the microemulsion phase. Further information in the text.

are added. Following the dashed blue line, γ is slowly increased. First only two phases, namely pure water and pure oil, coexist. Upon surfactant addition, the surfactant dissolves monomerically in the two phases and enriches at the oil-water interface. When the amount of amphiphile at the interface reaches γ_0, both phases and the interfacial layer are saturated with surfactant molecules. With the formation of a third phase, the microemulsion phase, the so-called three phase fish body is reached. Staying at intermediate temperatures and further increasing the mass fraction γ of surfactant, the microemulsion phase grows until at $\tilde{\gamma}$ the one phase region (1 or Windsor Type IV) is reached. This point, where the three phase body meets the one phase region, is the crucial $\tilde{X}$-point or fish-tail-point, where all water and oil molecules are solubilized. The corresponding $\tilde{\gamma}$-value is the minimum amount of surfactant needed to solubilize water and oil and is a measure for the surfactant efficiency. The temperature $\tilde{T}$ is the phase inversion temperature (PIT).

Quaternary microemulsion systems

At the very beginning of microemulsion research in 1954, WINDSOR expected the co-surfactants to be essential in microemulsion formulation [106]. In 1967, SHINODA and SAITO were able to present co-surfactant free ternary microemulsions based on C_iE_j surfactants [91, 82]. When sugar surfactants

are applied in the microemulsion formulation, a temperature dependent phase inversion is replaced by the addition of co-surfactants [99]. Hence, the usage of a co-surfactant becomes essential again, forcing the phase inversion of the amphiphilic film.

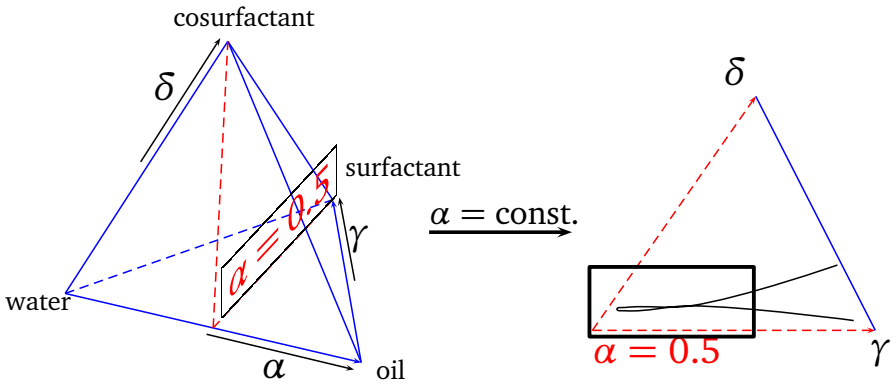

Figure 3.5: Schematic phase tetrahedron of a quaternary microemulsion system consisting of water, oil, surfactant and cosurfactant. At a constant oil to water ratio α (here α = 0.5), a cut through the phase tetrahedron leads to the pseudo-ternary triangle shown on the right side. The black box indicates the usual region of interest in this work at low δ and γ values.

The phase tetrahedron

Employing an auxiliary component changes the depiction of the temperature independent phase behaviour to the phase tetrahedron shown in figure 3.5.

As seen before for the ternary systems, the investigation of the phase behaviour is performed using perpendicular cuts through the phase tetrahedron. At schematic section through the phase tetrahedron at a constant oil to water ratio α is shown in figure 3.5 on the rigth side. This $\delta(\gamma)$-sections are usually taken by a series of pseudo binary compositions with a constant α value and an increasing amount of surfactant γ. Phase inversion is achieved by titrating the samples with an increasing amount of co-surfactant δ.

As indicated by the black box in figure 3.5, in this work only a small region of the pseudo-ternary system is investigated. For easy handling the resulting $\delta(\gamma)$-sections are deformed (see figure 3.6), gaining an orthogonal coordinate system. With alcohol and surfactant contents below $\delta \leq 0.35$ und $\gamma \leq 0,35$ in the investigated systems, this deformation is acceptable as the resulting error is smaller than the experimental error resulting from the recording of the phase diagrams and taking into account that only a small part of the phase tetrahedron is scrutinized in this work.

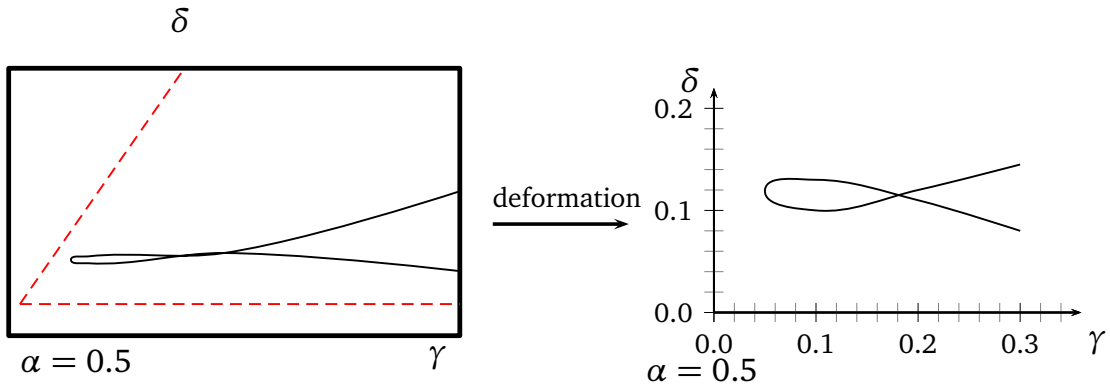

Figure 3.6: Deformation of the region of interest shown in figure 3.5 in detail. The conversion to an orthogonal coordinate system allows easy handling of the phase diagrams, but leads to a slight deformation of the "fish".

The quaternary microemulsion systems show the typical KAHLWEIT-fish, which has been explained for the ternary systems. Here, the co-surfactant takes over the role of the temperature as tuning parameter for the curvature of the amphiphilic film.

The role of the co-surfactant

Taking a closer look at the alkylpolyglycosides, each glucose unit offers six hydroxyl groups in the head. This leads to a huge hydrophilic head group with strong hydrogen bonds between the hydroxyl-groups of the glucose units and the water molecules of the solvent. For that reason they show no significant change in hydration and hence no phase inversion upon temperature changes in the experimentally relevant temperature range [99, 89]. As known for the ionic surfactants an additional co-surfactant is necessary to tune the phase behaviour.

Usually alcohols with medium or large alkyl chains are used as co-surfactants, for that reason the notation alcohol and co-surfactant are used synonymously in the following.

The added alcohol has two major effects. First, a part of the alcohol dissolves in the oil phase, increasing the hydrophilic character of the oil. And second, the amphiphilic alcohol becomes part of the interfacial layer. This leads to a change in the curvature of the interface, comparable to the temperature effect observed for the C_iE_j surfactants. Therefore, the phase behaviour can be explained with the sketch in figure 3.7, where the co-surfactant serves as tuning parameter. Hence, the content of co-surfactant δ is the ordinate. On the right hand side the increasing number of

alcohol molecules in the membrane is schematically shown. This changes the internal curvature H (see section 3.6 for a more detailed description of the behaviour of the internal film). KLUGE gave an elaborate description of this effect in his thesis [62].

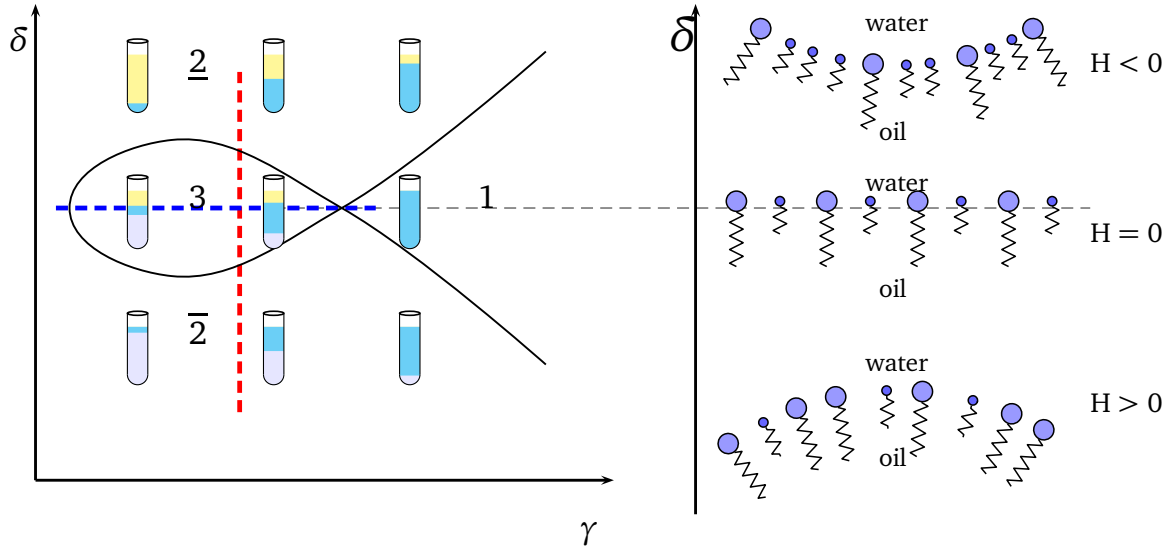

*Figure 3.7: Left: Schematic drawing of a phase diagram of a quaternary microemulsion system. The phase boundaries show the typical fish-shape. Following the dashed blue line, the formation of the microemulsion phase starts at low surfactant content γ and increases with rising γ until the **1**-phase region is reached. Again, the tubes are schemes of the coexisting phases, light blue denotes a water rich, yellow an oil rich and cyan the microemulsion phase. Right: Schematic drawing of the changes in curvature and composition of the interfacial film, following the dashed red line in the phase diagram on the left-hand side. At low co-surfactant content δ, the interfacial film is bend towards the oil phase (curvature H>0 by convention) and dominated by the large hydrophilic heads of the surfactant. Upon increasing the amount of co-surfactant, the internal curvature changes, as more alcohol molecules are embedded into the membrane. Further information in the text.*

3.3 Microemulsion additives

There is a wide variety of different additives described in the literature, which are applied to microemulsion systems with the goal to tune their phase behaviour and properties. The used additives can be distinguished according to their solubility into predominantly hydrophilic, lipophilic and amphiphilic components. The effects of the different components is summarized in the following:

Usual hydrophiles that occur in technical microemulsion systems are impurities carried in by some of the components. These are salts, short-chain alcohols, or reactants of the surfactant-synthesis, such as sugars. The most important are ionic impurities such as salts. Their influence on the phase behaviour has been widely studied in the past years [57, 53, 59].

In the case of salts, the empirical HOFMEISTER-Series [47] usually classifies the effect of the ion on macromolecules (proteins) in solution [10]. Here, the effect of the salt on the solubility of an oil in water is divided into two effects, it is well known that the influence of the anion is larger than the one of the cation [21, 19]. Along the HOFMEISTER-Series, which is depicted below, the solubility of an organic substance in water is reduced from the left to the right hand side.

The mechanism of the salting-out effect of so-called lyotrophic ions (such as SO_4^{2-} or Cl^-) is not entirely clear. In the case of surfactant molecules a reduction of the hydration of the surfactant head-group is expected, resulting in a shift of the Phase diagram to lower temperatures [53, 57]. The contrary effect, the salting-in, can be observed with later salts in the series such as I^- or SCN^-, which increase the solubility of organic compounds [109].

For microemulsion systems based on sugar surfactants C_nG_m the influence of salt is rather low [52]. Glycerol [56] or sugar show effects comparable to the lyotropic salts. HARWALL *et al.* [103, 2] reported the usage of alkyl naphthalene sulphonates. SÖDERMANN *et al.* used hydrophilic sugar surfactants, such as n-alkyl-β-D-maltosides (C_nG_m), as hydrophilic linkers to increase the hydrophilicity of a surfactant on the water side of the interfacial layer [18].

In the early work WINDSOR's first premise of an improved microemulsion system claimed for an increase of the size of both, the hydrophobic and the hydrophilic part of the amphiphile. But the solubility decreases with the size, especially in water, so that a hydrocarbon chain with more than

$$F^- \approx SO_4^{2-} > HPO_4^{2-} > Cl^- > NO_3^- > Br^- > ClO_3^- > I^- > ClO_4^- > SCN$$

Figure 3.8: The anions of the Hofmeister-Series [108]

18 carbon atoms leads to a loss of solubility [83]. Moreover, to keep the surfactant balanced, an enormous hydrophilic head group would be necessary. The problem was solved with the usage of lipophilic linkers, which are usually oils with a slightly polar group. Common examples are chlorinated oil, esters, ethers, long-chain alcohols such as dodecanol or ethyl oleate [34, 35]. These co-oils arrange in the oil phase close to the surfactant layer, oriented perpendicular to the hydrophobic surfactant chains. This segregation effect increases the interaction of the surfactant with the oil phase, producing a slightly polar zone close to the interfacial film [83].

Depending on the chain length, alcohols may act as hydrophilic (short chain) or lipophilic additives. The medium chain alcohols tend to be amphiphilic and therefore accumulate in the interfacial film. In the case of sugar surfactant microemulsions these so called co-surfactants are used to tune the system through phase inversion as discussed before in section 3.2.2.

3.4 Polymer-surfactant interaction

The combination of polymers with low molecular surfactants has been widely used. Polymeric additives in surfactant systems can be found in many technical applications, common examples are tertiary oil-recovery [100], cosmetics [17], detergents [81], coatings and pharmaceutical formulations [39].

Non amphiphilic polymers, often represented by homopolymers, are able to influence the surfactant film properties in microemulsions (see ALLGAIER [6]). KABALNOV *et al.* reported in 1994 the addition of an homopolymer to a three-phase microemuilsion system containing a bicontinuous phase with additional oil and water excess phase. The hydrophilic homopolymer leads to a decrease of the middle phase volume in favour of the aqueous phase [50]. The same group used hydrophobically modified ethyl hydroxyethyl cellulose and was able to show that the addition of these comb polymers to a stable balanced three phase microemulsion system results in a swelling of the middle phase [51].

Figure 3.9 shows the different architectures of amphiphilic polymers. In the comb polymers the oligomeric or polymeric units of one block are randomly attached to a backbone structure formed by the second monomer. The large group of the amphiphilic block copolymers (BCPs) usually used in these applications (see figure 3.9) the polymer chain consists of a block of one repeating hydrophilic monomer unit followed by at least a block of a different, hydrophobic monomer [19]. There is no strict separation between the classes of surfactant molecules and the amphiphilic polymers. Due to

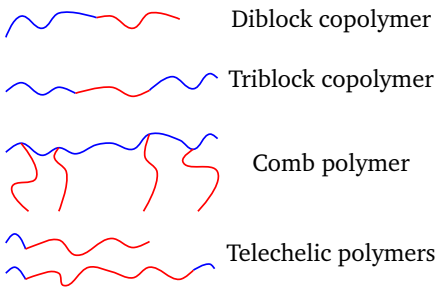

Figure 3.9: Architectures of different amphiphilic polymers. The two colors represent the hydrophilic and the lipophilic chains of the polymer.

the different solubility of their monomer-blocks, BCP show the formation of self-organized nano- and microstructures in selective solvents. This behaviour is comparable to low molecular weight surfactants [4]. The group of the telechelic polymers, which are usually prepolymers [67] , can be seen as the linker between the low molecular weight surfactants and the amphiphilic polymers. Starting from the C_iE_j surfactants, enlarging the poly(ethylene oxide) (PEO) chain leads to the telechelic polymer. An increase of the block lengths of both blocks leads to the diblock copolymers of the A-B type. Adding a third block leads to triblock copolymers of the A-B-C type. Often the two blocks A and C are polymerized from the identical monomer resulting in the A-B-A type. This is the case in the prominent group of the Pluronic polymers.

3.4.1 Efficiency boosting

The most striking effect of BCP on microemlusions may be the efficiency boosting effect which was discovered a decade ago by STREY and co-workers[49]. This improvement of the solubilisation was first studied for polymers of the PEP_x-PEO_y type, which have a hydrophobic poly(ethylene propylene) (PEP) block with a hydrophilic PEO head group [49]. Besides the branched hydrophobic block and the fact that the molecular weight of the hydrophilic and hydrophobic moieties are larger by factors of 10-300 [6], the polymers are similar to the used surfactant $C_{10}E_4$. Here, the role of the polymers is to increase the size of the amphiphilic layer. Following WINDSOR's premise, this should lead to an increase in solubilisation, which has been observed for a wide range of different systems [49, 23, 22, 69].

But instead of the rather small effect of surfactant mixtures, the total fraction of amphiphile needed to form a stable one-phase microemulsion is lower when a polymer-surfactant mixture is used in-

stead of the pure surfactant. Speaking in terms of the phase diagrams, this is equivalent to a shift of the Kahlweit-fish to lower γ-values. In many cases no significant change in the phase inversion temperature (for C_iE_j surfactants) is observed [48]. The second effect of polymer addition is the reduction of the size of the three phase region, the fish-body becomes smaller [28]. The enormous increase of emulsification capacity, the so-called *efficiency boosting effect*, appears already for small concentrations of the polymer and has been intensively studied during the last decade. In order to understand this effect, systematic studies of the influence of the polymer block size and composition [48], the surfactant and oil chain length [97, 33] and the polymer class [8] have been performed, using light scattering (SLS,DLS), SANS and NMR-self-diffusion experiments. A good overview over these issues is given in the early reviews by GOMPPER [33], ALLGAIER and FRIELINGHAUS [6].
The group of RICHTER compared the efficiency boosting effect of diblock copolymers with the corresponding homopolymers, which usually show a complementary effect [13, 14]. Recent developments introduce hydrophilic alcohol ethoxylates as efficiency boosters [27].

Efficiency boost factor

To compare the surfactant efficiency upon polymer addition in different systems, JAKOBS *et al.* introduced the *efficiency boost factor* f_B [49]:

$$f_B = \frac{\tilde{\gamma_0} - \tilde{\gamma}(1-\epsilon)}{\tilde{\gamma}\epsilon} \tag{3.6}$$

f_B is defined as the fraction of the amount of surfactant, needed to form a microemulsion saved by polymer addition ($\tilde{\gamma_0} - \tilde{\gamma}(1-\epsilon)$) divided by the amount of polymer ($\tilde{\gamma}\epsilon$) used. In the case of custom made amphiphilic diblock polymers, f_B values between 10 and 24 [49, 48] were reported.
Due to the fact that f_B depends on the efficiency of the base system (the less efficient the surfactant is, the higher is f_B) it is not suitable for inter system comparison. Here, it will be used to compare the influence of different additives on the same base system.

Efficiency boosting and sugar surfactants

Sugar surfactants are a favourable class of non-ionic surfactants. They are easy to obtain from renewable resources, are highly biodegradable and environmentally compatible. A limitation for the industrial usage is the medium efficiency they show as surfactants [80, 62, 99]. In microemulsion systems the X-point, which is an adequate measure for surfactant solubilisation capacity, sugar

surfactants reach $\tilde{\gamma}$ values in the region of $\tilde{\gamma} = 0.10 - 0.35$.

Therefore, they are ideal candidates to employ and exploit the efficiency boosting effect discovered by STREY and coworkers in 1999[49, 48]. The influence of large amphiphilic diblock copolymers is one of the most striking developments in microemulsion research. Upon addition of only small amounts of polymer a 10-fold increase in surfactant efficiency has been reported [99, 36].

JAKOBS showed that the polymer PEO_5-PEP_5 is able to penetrate the mixed amphiphilic film in the system water / n-octane / n-octyl-β-D-glycopyranoside (C_8G_1) / n-octanol. In this system besides the amount of surfactant C_8G_1 needed to form a thermodynamically stable microemulsion the cosurfactant n-octanol was reduced [48, 93]. In a comparative study of diblock copolymers and comb-polymers on the same microemulsion system, where the water phase was replaced with D_2O, NILSSON *et al.* were able to demonstrate that the enhancement of solubilisation capability can be achieved even with polymers with a branched or low hydrophobic part [71]. For C_iE_j surfactants, the efficiency boosting effect is known to reduce the amount of the surfactant by a factor of 10 [8]. But most of the effective Polymers reported up to date had to be laboriously synthesized in small amounts [13, 14, 7]. For technical or large scale applications, such as the decontamination process, a cheap and easily obtainable polymer is more desirable.

Concentrating on technically available polymers, NILSSON *et al.* were able to show the influence of a comb-polymer (Ketjenlube)as efficiency boosters [71].

The effect of poly(alkyleneoxide)-co-poly(ethyleneoxide) and Pluronic polymers on AOT (Dioctyl sodium sulfosuccinate) based microemulsion systems was studied by Mboumi, a member of the Strey group [101]. But to our knowledge, the influence of Pluronic polymers on sugar surfactant based microemulsion systems has not been investigated yet.

3.4.2 Pluronic polymers

However, for technical applications the usage of commercially available low-cost polymers is of high interest. The diblock copolymers of the PA-PEO type usually used for efficiency boosting are not available on industrial scale and have to be synthesized with a several step synthesis [7]. An important group of water soluble triblock copolymers of poly(ethylene oxide) (PEO) and poly(propylene oxide) (PPO) units, denoted as PEO_x-PPO_y-PEO_x are commercially available as Pluronics (BASF), Synperonic (ICI), or Genapol. For more than 60 years these so-called Poloxamers are produced as surfactants in large amounts and different compositions, which makes them a feasible component

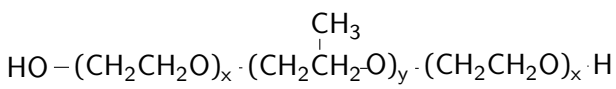

Figure 3.10: Pluronic polymers, chemical structure

for many technical applications [86, 66]. The structure of these polymers is shown in Figure 3.10.

Nomenclature

The PEO_x-PPO_y-PEO_x polymers are commercially available in several different molecular weights and PEO/PPO compositions. The nomenclature used in this work was developed by BASF (Pluronic) [84, 39]. The Pluronic grid shows the polymers characterized by the two important features, the molecular weight and the PEO/PPO ratio, as shown in Figure 3.11. Here, the copolymers along the horizontal lines have PPO blocks of the same size. Along the vertical grid lines the PEO/PPO ratio is constant [84, 39, 5]. The abbreviation of the Pluronic polymers consists of three parts: First a letter, containing information about the physical properties, the polymers are delivered as L (liquid), P (paste) or F (flakes). The letter is followed by two or three digits. The first one or two (in case of a three digit polymer) are a code for the size of the PPO block. The last digit multiplied by 10 is the PEO content given in wt%. For example P104 is a pasty polymer with an EO content of approximately 40 wt% and a PPO block with a molar mass of approximately $3250\,g \cdot mol^{-1}$.

Properties

In these polymers the amphiphilic characteristics depend on the composition of the poloxamer, the relevant parameters are the overall size given by the molecular weight and the PEO/PPO ratio and block length. Both parameters can easily be tuned in the synthesis by simply changing the amount of monomer, hence a range of PPO/PEO composition ratios and molecular weights are commercially available [85, 9, 70, 39]. In table 4.1 in the experimental section 4.1.4 some of the physical properties of the Pluronic polymers used in this work are given.

The self assembly of the Pluronic polymers in aqueous solution has been topic of a large number of investigations. The polymers self-assembly offers a wide variety of structures ranging from spherical micelles to elongated rods, pancake shaped micelles, even microemulsion structures are reported. The self assembly process depends on two key parameters, the critical micellization concentration (CMC) and the critical micellization temperature (CMT). For the CMC a decrease is observed with an increase of the PPO block size at constant temperature and PEO number. The similar effect is observed for the CMT at constant concentration [3]. A good summary of the dependency of physical

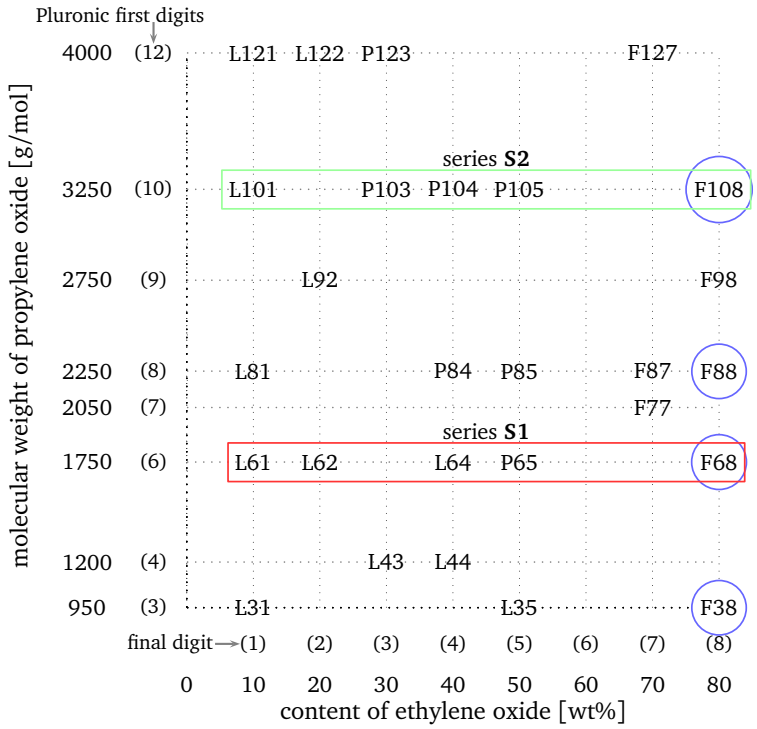

Figure 3.11: Pluronic grid: the length of the PPO block is plotted versus the overall PEO content in wt%. Further explanations are given in the text. The different series of Pluronic polymers applied to the microemulsions are indicated by frames. The low molecular weight polymers of series S1 in red, the high molecular weight polymers of series S2 in green. Series S3, with a constant EO content of 80 wt% is indicated by blue circles.

properties and micellization is given in the review of ALEXANDRIDIS and HATTON[5].

Due to their use in medical and pharmaceutical applications, the pluronic triblock copolymers are ideal candidates for efficiency boosting with regard to skin decontamination. Early work proposed e.g. the treatment of burnt tissues with F127 gels [84]. Their ability to enclose active ingredients in the micelles, made them ideal containers for drug delivery as seen by the increased number of studies concerning their biomedical use (see reviews by NEWMAN [70] and FUSCO [30].

3.5 Microstructure

Despite of their name, microemulsions are not microstructured. This name goes back to the early work of SCHULMAN *et al.* [88] and still produces a lot of misunderstandings. Meanwhile the knowledge is established that microemulsions offer different nano-scaled structures [98, 36]. These structures can be oil in water droplets or water in oil droplets (inverse microemulsion). The most fascinating microemulsion certainly is the bicontinuous phase, which was e.g. imaged by freeze-fracture electron microscopy (FFEM) or studied by small angle neutron scattering (SANS) [58, 95, 36].
Other phases like e.g. lamellar or cubic are not considered as microemulsions and will not be covered here.

3.6 Theory of microemulsion formation

The nanostructure is one of the major characteristics of the macroscopically homogeneous microemulsions. It can be described by the curvature of the amphiphilic film in between the water and oil domains, consisting of surfactant, co-surfactant, and, when applied, amphiphilic polymers.
For the description of microemulsion and sponge phases in dilute systems, many theoretical approaches were made.
Following the theory introduced by HELFRICH, the film is modelled as a thin surface. The relevant parameter controlling the structure of the microemulsion is the curvature free energy (or bending elastic energy) [15, 38].

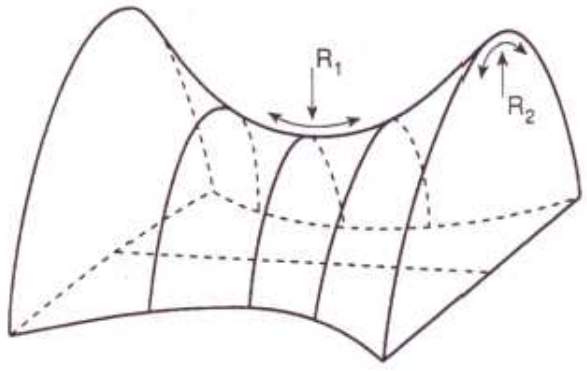

Figure 3.12: Definition of the curvature radii R_1 and R_2 according to a surfactant membrane.

The mean curvature H and the Gaussian curvature K of the amphiphilic film are computed from the mean curvatures $c_1 = \frac{1}{R_1}$ and $c_2 = \frac{1}{R_2}$ which depend on the local curvature radii R_1 and R_2:

$$\mathrm{H} = \frac{1}{2}(c_1 + c_2) \tag{3.7}$$

The gaussian curvature of the film is given by

$$K = c_1 c_2 \tag{3.8}$$

The curvature free energy is given by [41]:

$$F = \int_A \frac{1}{2}\kappa(C_1 + C_2 - 2C_0)^2 + \overline{\kappa} C_1 C_2 dA \tag{3.9}$$

Here, the integral over the film surface sums up the local properties at each point of the membrane [13]. Where c_1 and c_2 are the principal curvatures of the amphiphilic layer and c_0 is the spontaneous curvature, depending on the geometric shape of the surfactant molecules. κ and $\overline{\kappa}$ are the mean (splay) and the Gaussian (saddle-splay) bending elastic constants. In many cases $\kappa \simeq -\overline{\kappa}$. When c_0 changes the sign (= PIT for T-depending phase transition) no curvature is preferred, typical morphologies are the bicontinuous or the lamellar structures.

By definition positive curvatures are given if the amphiphilic film is concave towards the oil phase and negative towards the water phase. As shown in figure 3.12, positiv values of H lead to the formation of oil in water droplet microemulsions. An increase of the co-surfactant concentration changes the curvature of the internal film. Passing a planar structure at $\mathrm{H} = 0$, the structure changes to water in oil droplets when H reaches negative values. Depending on the curvatures c_1 and c_2 and the resulting curvatures H and K, the following structures are obtained:

$c_1 = c_2 = R^{-1};$	$H = r^{-1};$	$K > 0$	spheres with radius R
$c_1 = 0; c_2 = R_2^{-1};$	$H = \frac{1}{2}c_2;$	$K = 0$	cylindrical structures
$c_1 = -c_2;$	$H = 0;$	$K < 0$	bicontinuous structures
$c_1 = c_2 = 0;$	$H = 0;$	$K = 0$	lamellar structures

The actual structure is influenced by many other contributions so that it has to be clarified by suitable characterization methods.

3.7 Scattering techniques for microemulsion characterization

The internal structure of microemulsion systems was extensively examined during the last 30 years. The first attempt of a description of the bicontinuous structure was published by SCRIVEN in 1976 [90]. Amphiphiles in solution are able to form a large variety of different meso structures. From spherical micelles, cylindrical, disk-like, worm-like isosomes and so on are reported in the literature [95, 36, 107, 46]. A lot of information is gained due to the improvement of the experimental characterisation techniques and theory during the last decades. For microemulsions the most prominently up to date methods are direct imaging techniques, such as freeze fracture transmission electron microscopy [58, 95] or the cryogenic freeze-fracture direct imaging technique [40]. Nevertheless, scattering techniques are more relevant providing unambiguous information about the average structure. Various papers deal with the results the small angle scattering (SAS) methods. SAS methods include small angle neutron (SANS), X-ray (SAXS) and static light scattering (SLS).

Common for each of the SAS techniques is the elastic scattering of radiation by a sample followed by an analysis of the scattering pattern to gain information about the size, shape and dynamics of the sample. While SAXS and SANS provide time-average structural information, dynamic information about the motion in the microemulsion is gained by photon correlation spectroscopy (PCS) and neutron spin echo (NSE) experiments. Additionally, NSE offers a direct access to the bending rigidity of the surfactant films [104].

An overview is given by HELLWEG [40] and GRADZIELSKI [36].

The scattering process is schematically shown in figure 3.13.

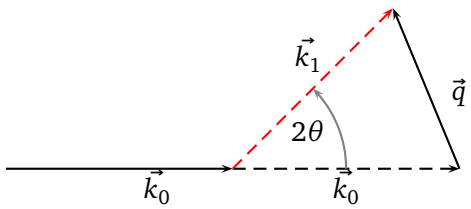

Figure 3.13: Scattering principle. The incident beam $\vec{k}_0$ is scattered at the particle.

Usually scattering patterns are presented as functions of the scattering vector q instead of the scattering angle θ. As shown in figure 3.13, q is connected to θ and the irradiated wavelength λ by

equation 3.10, resulting in a unit of a reciprocal length ($[q] = [\frac{1}{nm}]$).

$$q = |\vec{q}| = \frac{4\pi n_0}{\lambda} \sin\frac{\theta}{2} \tag{3.10}$$

with: n_0: refractive index of the solvent, λ: wavelength of the scattered light, θ: scattering angle. For SAXS and SANS n_0 is close to unity.

3.7.1 Photon correlation spectroscopy

Dynamic light scattering (DLS) or photon correlation spectroscopy (PCS) is routinely used for the investigation of colloidal systems, to determine particle or micelle size and polydispersity. Also microemulsion systems can be investigated by PCS [44, 76, 16].

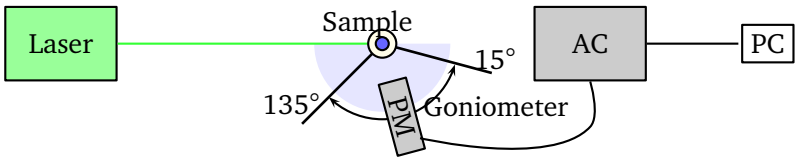

Figure 3.14: Example for the set-up of the PCS experiment, here ALV-5000 Photon Correlation Spectroscopy.

In figure 3.14 the setup of an PCS-experiment is shown. A monochromatic light source, usually LASER light, is focussed on the sample. Interaction of the electromagnetic radiation with the molecules of the sample introduces dipole oscillation resulting in elastic or quasi-elastic scattering. The change in the momentum of the radiation leads to a scattering pattern depending on the scattering angle θ. Light scattering is caused by local variations of the refractive index n. Here, only the outer electrons are polarized. Detection of the scattered light in different angles θ, usually between 30 and 150 ° is performed by a photomultiplier mounted on a goniometer.

Using the real time (i.e. Brownian) motion of the particles information about the dynamics are gained. This motion gives rise to a Doppler effect, which leads to time-dependent fluctuations in the scattering intensity I(q,t).

In an typical PCS experiment the real time fluctuations of the scattering intensity I(q,t) are monitored and analysed by an intensity time auto correlation function $g^2(q,t)$. Usually the scattered intensity I is measured time- and q-dependent.

The resulting time-averaged intensity correlation function (ICF) is shown in equation 3.11. Here, the intensity of the scattered light at time t is compared with the intensity at time $t+\tau$, the time dependency of the scattering intensity is given by the autocorrelation function $g^2(q,t)$.

$$g^2(q,t) = \frac{< I(q,0)I(q,\tau) >}{< I(q,0) >^2} \tag{3.11}$$

The normalised electric field autocorrelation function (see equation 3.13) containing information about the system dynamics is now available, as it is connected to the ICF by the SIEGERT relation [11, 79]:

$$g^2(q,t) = 1 + C|g^1(q,t)|^2 \tag{3.12}$$

where C is a coherence factor depending on instrumental conditions and background scattering (baseline parameter).

The normalised electric field auto correlation function $g^1(q,t)$ is given by

$$g^1(q,t) = \frac{< E^*(q,t)E(q,t+\tau) >}{< E(q,0) >} \tag{3.13}$$

where E^* is the complex conjugated of E

In an ideal, mono disperse solution of spherical particles, $g^1(q,t)$ is represented by a single exponential function containing the translational diffusion coefficient D:

$$g^1(q,t) = \exp(-\Gamma\tau) = \exp(-Dq^2\tau) \tag{3.14}$$

with Γ: relaxation rate.

The resulting diffusion coefficient D describes the motion of the particle through the observed medium, no information about the shape of the particle is gained. For spherical particles (such as droplet micelles), the hydrodynamic radius r_H can be calculated from the STOKES - EINSTEIN relation:

$$D = \frac{kT}{6\pi\eta r_H} \tag{3.15}$$

with: k: Boltzmann constant, T: temperature, η: viscosity of the solvent

In general, microemulsion systems at least apparently contain a distribution of structural sizes. In the case of these poly-disperse samples, a distribution function $G(\Gamma)$ has to be introduced. Equation 3.13 changes to:

$$g^1(q,t) = \int_0^\infty G(\Gamma)\exp(-\Gamma\tau)d\Gamma \tag{3.16}$$

with

$$\int_0^\infty G(\Gamma)d\Gamma = 1 \tag{3.17}$$

For data analysis of the resulting function of $g^1(q,t)$, two major ways are possible. Either the method of cumulants [12] is applied, or an inverse Laplace transformation [72]. For the inverse Laplace transformation PROVENCHER developed the FORTRAN program CONTIN [77, 78]. The output of CONTIN is a value of Γ_j, which depends on q. For bicontinuous microemulsions, the diffusion coefficient of the collective motion can be calculated from Γ_j by linear regression when Γ is plotted versus q^2 according to equation (3.18).

$$\Gamma = Dq^2 \tag{3.18}$$

By measuring at different angles θ, meaning different values of q, D can be obtained from the slope of the Γ-q^2 plot.

3.7.2 Small angle X-ray and neutron scattering

Scattering methods provide information on the structure sizes on nanometer scale and allow the determination of the radii of droplet structures in microemulsion systems [36].

Differences in X-ray and neutron scattering, contrast variation

In contrast to PCS, SAXS and SANS provide time-average structural information about the sample. SAXS and SANS offer the same q-range, depending on the experimental set-up.

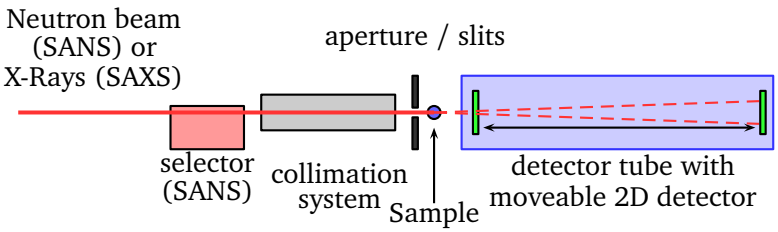

Figure 3.15: Simplified setup of a SAXS or SANS experiment.

Nevertheless both methods often complement one another which is related to the different contrast conditions.

X-rays are electromagnetic rays with a typical wavelength between 0.01 nm and 1 nm [60] corresponding to an energy range between ≈ 1 keV and 100 keV. A high and monochromatic flux is offered by synchrotron radiation (for example: ESRF, ID 01) or X-ray tubes with copper anodes, using the CuK_α-line ($\lambda = 0.154\,nm$). The q-range connected with Bragg law $\lambda = 2d\sin\theta$ leads to observeable dimensions of $d \approx \frac{2\pi}{q}$ [37]. Keeping in mind that X-rays are scattered at electrons, X-ray scattering only occurs if there are inhomogeneities in the electron density of the sample [31].

Also Neutrons are well suited for the non-destructive investigation of matter, as they offer a large penetration depth mainly caused by their vanishing electric charge. Furthermore neutrons possess a magnetic dipole moment (spin $\frac{1}{2}$), which makes them sensitive to magnetic fields. In addition, the scattering power of a neutron at an atomic nucleus depends on the spin of the atomic nuclei in a sample, allowing contrast variation by isotopic substitution of H for D [1]. The energy of a neutron is given by:

$$E_{neutron} = k_B T = \frac{1}{2} m v^2 \tag{3.19}$$

with the neutron mass m, the temperature T, the velocity v. k_B is the Boltzmann constant.

The wavelength of the neutron is given by the de-Broglie relation

$$\lambda = \frac{h}{mv} \tag{3.20}$$

where h is the Planck constant.

In neutron scattering cold ($E = 0.1 - 10\,meV, T \propto 1 - 120\,K, \lambda \approx 2\,to\,30$ Å), thermal and hot neutrons can be used with a wavelength of 0.1 Å to 1000 Å.

Scattering theory

Usually the scattering intensity I(q) is plotted versus the scattering vector q, which is given by equation 3.21. The scattering intensity I(q) depends on the number of particles per Volume N, the form factor $P(q)$ and the structure factor $S(q)$:

$$I(q) = NP(q)S(q) \tag{3.21}$$

The form factor $P(q)$ contains information about the size and structure of the particles and is proportional to the square of the difference of the scattering length densities $(\Delta\phi)^2$ of the particle and the surrounding solvent. The structure factor $S(q)$ reflects the inter-particle scattering. In ideal dilute solutions, where no interference of the scattering of neighbouring particles occurs, the structure factor $S(q) = 1$.

For monodisperse dilute systems ($S(q) = 1$), the scattering intensity for N identical particles depends on the scattering amplitude E_1(q) of a single particle.

$$I(\vec{q}) = N < |E_1(\vec{q})|^2 >= N I_1(\vec{q}) \tag{3.22}$$

Here, $E_1(\vec{q})$ is the single particle scattering amplitude which is the scattered field resulting from integration over the particle volume dV_p containing ϕ(r)V$_p$ electrons (SAXS) or nuclei (SANS). The resulting amplitude is the Fourier transform of the scattering length density ϕ(r) of the particle. The intensity is achieved using the conjugate complex E_1^*(q)

$$E_1(\vec{q}) = \int_V \Delta\phi(\mathrm{r}) e^{-i\vec{q}\vec{r}} d\mathrm{r} \tag{3.23}$$

$$|E_1(\vec{q})|^2 = E_1(\vec{q}) \cdot E_1^*(\vec{q}) = \int_V \int \Delta\phi(\vec{r}_1)\Delta\phi(\vec{r}_2) e^{-i\vec{q}(\vec{r}_1 - \vec{r}_2)} dr_1 dr_2 \tag{3.24}$$

The two kinds of radiation are sensitive to different physical properties of the scattering particles. While for SAXS the scattering length density ϕ(r) is directly connected to the electron density, which is easily connected to the number of electrons, the scattering length density for SANS is a complex function of the atomic number.

Introducing an autocorrelation function (ACF) $\gamma(\vec{r})$ with a constant r = r$_1$ - r$_2$, $\gamma(\vec{r})$ is the convolution square of the density fluctuations:

$$\gamma(\vec{r}) \equiv \Delta\tilde{\phi}^2 = \int_V \Delta\phi(\vec{r}_1)\Delta\phi(\vec{r}_1 - \vec{r}) d\mathrm{r}_1 \tag{3.25}$$

Equation 3.25 is the so-called Patterson function which is widely used in cristallography [75].

$$I(q) =< |E_1(\mathrm{q})|^2 > = < \int_V \Delta\tilde{\phi}^2(\mathrm{r}) e^{-i\mathrm{qr}} d\mathrm{r} > \tag{3.26}$$

$$= 4\pi \int_0^\infty \gamma(r) r^2 \frac{sinqr}{qr} dr \tag{3.27}$$

This is the most general formula for the diffraction of a statistically isotropic system without long range order[75].

Teubner Strey approximation

For bicontinuous microemulsions, the scattering pattern shows a broad peak in the I(q)-q-plot. A simplified description of the structure as a system of two volume fractions Φ_A and Φ_B with different scattering length density leads to a scattering intensity $I(q)$ according to equation 3.28.

$$I(q) = 4\pi \cdot \Phi_A \cdot \Phi_B \cdot (\Delta\phi)^2 \int_0^\infty \gamma(r) r^2 \frac{sinqr}{qr} dr \tag{3.28}$$

Here the following expression for the correlation function $\gamma(r)$ according to DEBYE is used:

$$\gamma(r) = \frac{\sin(k \cdot r)}{(k \cdot r)} \cdot \exp\left(-\frac{r}{\xi_{\mathrm{TS}}}\right) \tag{3.29}$$

with $k = 2\pi/d_{\mathrm{TS}}$.

Insertion of eq. (3.29) in eq. (3.28) yields the scattering intensity distribution described by the correlation length ξ_{TS} and the domain size d_{TS}:

$$I(q) = \frac{8\pi/\xi_{\mathrm{TS}} < \mu^2 > c_2}{a_2 + c_1 q^2 + c_2 q^4} (+I_{\mathrm{bkg}}) \tag{3.30}$$

with the average fluctuation of the scattering length density $< \mu^2 >= \Phi_A \cdot \Phi_B \cdot (\Delta\phi)^2$. In literature the expression (3.30) is called the TEUBNER-STREY (or abbreviated TS) formula. It is derived using the expansion of an empirical Ginzburg-Landau free energy equation [40, 104, 102]. It was used throughout this work to fit the resulting scattering patterns of bicontinuous microemulsions received in SAXS and SANS experiments.

From the parameters a_2, c_1 and c_2 in eq. (3.30) the two length scales d_{TS} and ξ_{TS} can be calculated according to:

$$\xi_{\mathrm{TS}} = \left(\frac{1}{2}\left(\frac{a_2}{c_2}\right)^{1/2} + \left(\frac{c_1}{4c_2}\right)\right)^{-1/2} \tag{3.31}$$

$$\frac{d_{\mathrm{TS}}}{2\pi} = \left(\frac{1}{2}\left(\frac{a_2}{c_2}\right)^{1/2} - \left(\frac{c_1}{4c_2}\right)\right)^{-1/2} \tag{3.32}$$

Knowing the volume v_c and the area a_c of the surfactant molecule, the persistence length of the film is obtained (3.33):

$$\frac{\xi_\kappa}{\delta} = \exp\left(\frac{4\pi\kappa_0}{3kT}\right) \tag{3.33}$$

With $\delta = v_c/a_c$ and κ_0 is the bending rigidity. At higher q-values in the Porod region, in several cases the scattering pattern can not be described by the TS-formula any longer. Here, the experimental scattering curves are shifted to higher intensities due to undulations in the real systems [40].

3.7.3 Neutron spin echo

Neutron spin echo (NSE) experiments offer an elegant way of measuring the dynamic of large molecules, such as polymers or biomolecules. Here, nanometer length scales correspond to correlation / relaxation times taking place in the range of 100 ps to 0.5 μs. Also thermally excited fluctuations of the interfaces in droplet and bicontinuous microemulsion samples can be studied directly without perturbation of the samples [43, 69, 26, 45, 105]. As neutrons are involved, contrast variation due to deuteration is possible. NSE provides access to the normalized intermediate scattering function in the pico- to nanosecond time window, typically in a q-range of 10^{-2} Å^{-1} up to a few Å^{-1}.

The Neutron spin echo technique is based on the Lamor precession of polarized neutrons in a magnetic field [68]. The schematic setting of an NSE-experiment is shown in figure 3.16. Here, two antiparallel magnetic fields, B1 and B2 (with the respective length L1 and L2) are located before (B1) and after (B2) the sample. After selection of the neutron wavelength with the velocity selector,

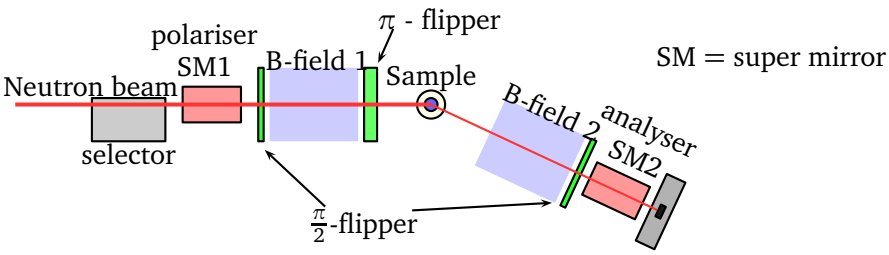

Figure 3.16: Schematic setup of a NSE experiment at beamline IN15 in reference to the ILL [1].

the monochromatic neutron beam is polarized in flight-direction by a supermirror polariser (SM1). The spin of the neutrons is then rotated by 90 degree at the first $\frac{\pi}{2}$-flipper and now perpendicular to the magnetic field. Here, the Larmor precession is initiated, another π-flipper transforms the precession angle from ϕ to $-\phi$. At the sample the neutrons are either scattered elastically without modification of the neutron spin or inelastically, which leads to an alteration of the spin. The Larmor precession is finally stopped at the second $\frac{\pi}{2}$-flipper and analysed. As the field integrals on each side of the π flipper are equal, the difference in the precession angle gives a measure of the inelasticity of the scattering process.

A neutron with the spin aligned perpendicular to the magnetic field coming from the source (left side in fig. 3.16) is influenced by the first field. Assuming a homogenous B-field, the phase of the

neutron spin can then be rewritten as :

$$\phi_1 = w_L t = \gamma B_1 t = \gamma B_1 \frac{L1}{v} = \gamma B_1 L_1 \lambda_1 \frac{m}{h} \tag{3.34}$$

with the gyromagnetic ratio $\gamma = 183.25 MHz/T$, the Lamor frequency w_L and the total time t the neutron spends in the B-field. The resulting polarization in x-direction for polychromatic neutrons with a distribution of neutron wavelengths ($f(\lambda)d\lambda$), P_x is given by

$$P_x = \int cos(\phi) f(\lambda) d\lambda = \int cos(\gamma B_1 L_1 \lambda_1 \frac{m}{h}) f(\lambda) d\lambda \tag{3.35}$$

After passing the second B-field B_2, which is identical to B_1, the overall phase of the neutrons can be written as:

$$\phi = \phi_1 + \phi_2 = \frac{\gamma m}{h} (B_1 L_1 \lambda_1 - B_2 L_2 \lambda_2) \tag{3.36}$$

For elastic scattering ($\lambda_1 = \lambda_2$) with homogeneous anti-parallel B-Fields ($B_1 L_1 = -B_2 L_2$), the total phase of the neutrons vanishes $\phi = 0$ and leads to a polarization of $P_x = 1$. In the case of inelastic or quasi-elastic scattering, the loss of kinetic energy leads to a change in the velocity and wavelength of the neutrons. Assuming an energy transfer $\hbar w$ and momentum transfer $\hbar q$, the scattering of the neutrons by the sample is described by a scattering function $S(q, w)$.

When the spin echo condition is fulfilled, the change in the precession angle $d\phi$ only depends on the fluctuations in the energy transfer $\hbar w$ from its deviation $\hbar w$.

Therefore $d\phi$ can be written as:

$$d\phi = \frac{\gamma m^2 \hbar}{h^3} \bar{\lambda_1}^3 BL dw_s = \tau dw_s \tag{3.37}$$

with the spin echo time τ:

$$\tau = \frac{\gamma m^2 \hbar}{h^3} \bar{\lambda_1}^3 BL = \frac{\gamma \hbar}{m} \frac{BL}{\bar{v_1}^3} \tag{3.38}$$

The final polarization P_{NSE} is given by equation (3.39):

$$P_{NSE} = P_S \frac{\int S(q,w) \cos(\tau w) \mathrm{d}w}{\int S(q,w) \mathrm{d}w} = \frac{S(q,\tau)}{S(q,0)} \tag{3.39}$$

Therefore, the NSE signal P_{NSE} is the Fourier transformation of $S(w)$.

Dynamics by NSE

In a typical NSE experiment the normalized intermediate scattering function $\frac{S(q,\tau_{NSE})}{S(q,0)}$ versus the spin echo time τ_{NSE} is obtained for a series of different q-values. To obtain information about the collective motion of the whole bicontinuous structure, the data is fitted with an empirical approach described in [105]. At short length scales $l \gg \epsilon$ the membrane is assumed to be described by the Zilman Granek approach [111, 110] , which uses the Zimm type dynamics of a set of free standing membrane plaquettes. In this model the normalized intermediate scattering function $\frac{S(q,\tau_{NSE})}{S(q,0)}$ is given by a stretched exponential fit according to (3.40).

$$\frac{S(q,\tau_{NSE})}{S(q,0)} = \exp(-\Gamma_{col}\tau)(A + (1-A)\exp(-(\Gamma_u\tau)^{\beta}). \tag{3.40}$$

As for the Zimm polymer dynamics, a stretching exponent of $\beta = \frac{2}{3}$ was used. The decay rate Γ_u, describing the thermal undulations of the membrane, is expected to be proportional to q^3.

Therefore, in a plot of Γ_u versus q^3, the bending elastic constant κ is received from a linear fit according to:

$$\Gamma_u = 0.025\gamma_\kappa \left(\frac{k_B T}{\kappa}\right)^{\frac{1}{2}} \frac{k_B T}{\eta_{eff}} q^3 \tag{3.41}$$

where η_{eff} is the effective solvent viscosity of the dispersion medium. The pre-factor γ_κ depends on κ and $\gamma_\kappa \to 1$ for $\frac{\kappa}{k_B T} \gg 1$.

Usually, the bending elasticity constant is in the range of 1 $k_B T$ for membranes in microemulsions [96, 92, 105].

3.8 References

[1] URL: http://www.ill.eu/science-technology/the-neutron/.

[2] E. Acosta et al. “The role of the hydrophilic linker”. In: *J. Surfactants Detergents* 5 (2002), pp. 151–157.

[3] P. Alexandridis, J.F. Holzwarth, and A.T. Hatton. “Micellization of PEO-PPO-PEO Triblock Copolymers in Aqueous Solutions: Thermodynamics of Copolymer Association”. In: *Macromolecules* 27 (1994), pp. 2414–2425.

[4] P. Alexandridis and B. Lindman. *Amphiphilic Block Copolymers: Self-Assembly and Applications*. Studies in Surface Science & Catalysis. Elsevier Science, 2000.

[5] P. Alexandridis, T. Nivaggioli, and A.T. Hatton. “Temperature Effects on Structural Properties of Pluronic P104 and F108 PEO-PPO-PEO Block Copolymer Solutions”. In: *Langmuir* 11.5 (1995), pp. 1468–1476.

[6] J. Allgaier and H. Frielinghaus. “Microemulsion”. In: ed. by C. Stubenrauch. Wiley VCH, 2009. Chap. 4 Effects of Polymers on the Properties of Microemulsions, pp. 122–147.

[7] J. Allgaier et al. “Synthesis and Characterization of Poly[1,4-isoprene-b-(ethylene oxide)] and Poly[ethylene-co-propylene-b-(ethylene oxide)] Block Copolymers”. In: *Macromolecules* 30.6 (1997), pp. 1582–1586.

[8] Jakobs B, Sottmann T, and Strey R. “Efficiency boosting with amphiphilic block copolymers: a new approach to microemulsion formulation.” In: *Tenside Surf Det* 37 (2000), pp. 357–364.

[9] P. Bahadur and G. Riess. “Block Copolymers”. In: *Tenside Surf. Det.* 28 (1991), p. 173.

[10] R.L. Baldwin. “How Hofmeister Ion Interactions Affect Protein Stability”. In: *Biophysical Journal* 71 (1996), pp. 2056–2063.

[11] B.J Berne and R. Pecora. *Dynamic Light Scattering*. John Wiley & sons, Inc., New York, 1976.

[12] J. C. Brown, P. N. Pusey, and R. Dietz. “Photon correlation study of polydisperse samples of polystyrene in cyclohexane”. In: *The Journal of Chemical Physics* 62.3 (1975), pp. 1136–1144.

[13] D. Byelov et al. “Microemulsion Efficiency Boosting and the Complementary Effect. 1. Structural Properties”. In: *Langmuir* 20 (2004), pp. 10433–10443.

[14] D. Byelov et al. “SANS studies of polymer efficiency boosting in microemulsions - diblock copolymers versus homopolymers.” In: *Physica B,* 350 (2004), pp. 931–933.

[15] P.B. Canham. “The minimum energy of bending as a possible explanation of the biconcave shape of the human red blood cell.” In: *Journal of Theoretical Biology* 26 (1970), pp. 61–81.

[16] A. M. Cazabat and D. Langevin. “Diffusion of interacting particles: Light scattering study of microemulsions”. In: *The Journal of Chemical Physics* 74.6 (1981), pp. 3148–3158.

[17] C. Co, L. Huang, and A. Lips. *Skin care cosmetic compositions and methods for microemulsification of sebum on contact*. WO Patent App. PCT/EP2004/008,660. 2005.

[18] C. von Corswandt, C. Olsson, and O. Soedermann. “Microemulsions Based on Soybean Phosphatidylcholine and Isopropylmyristate - Effect of Addition of Hydrophilic Surfactants”. In: *Langmuir* 14 (1998), pp. 6864–6870.

[19] H. Wennerström D. Fennell Evans. *The colloidal domain: where physics, chemistry, biology and technology meet*. Ed. by D.F. Evans. 2nd edition. Wiley-VCH, 1999.

[20] B. Danielsson I.; Lindman. “The definition of microemulsion”. In: *Colloids Surfaces* 3 (1981), pp. 391–392.

[21] H.-D. Dörfler. *Grenzflächen- und Kolloidchemie*. VCH Verlagsgesellschaft mbH, 1994.

[22] H. Endo et al. “Effect of amphiphilic block copolymers on the structure and phase behavior of oil-water-surfactant mixtures”. In: *The Journal of Chemical Physics* 115.1 (2001), pp. 580–600.

[23] H. Endo et al. “Membrane Decoration by Amphiphilic Block Copolymers in Bicontinuous Microemulsions”. In: *Phys. Rev. Lett.* 85 (1 2000), pp. 102–105.

[24] B. Fabry. “Aktuelle Aspekte auf dem Gebiet fettchemischer Tenside”. In: *Fat. Sci. Technol.* 7 (1990), pp. 287–291.

[25] B. Fabry. “Tenside - Eigenschaften, Rohstoffe, Produktion, Anwendungen”. In: *Chemie in unserer Zeit* 4 (1991), pp. 214–222.

[26] B. Farago and M. Gradzielski. “The effect of the charge density of microemulsion droplets on the bending elasticity of their amphiphilic film”. In: *The Journal of Chemical Physics* 114.22 (2001), pp. 10105–10122.

[27] C. Frank et al. “Hydrophilic Alcohol Ethoxylates as Efficiency boosters for Microemulsions.” In: *Langmuir* 20 (2008), pp. 6036–6043.

[28] C. Frank et al. “Influence of Amphiphilic Block Copolymers on Lyotropic Liquid Crystals in Water-Oil-Surfactant Systems”. In: *Langmuir* 21.20 (2005), pp. 9058–9067.

[29] S. Friberg. In: *Journal of Dispersion Science and Technology* 15 (1984), p. 611.

[30] S. Fusco, A. Borzacchiello, and P.A. Netti. “Perspectives on: PEO-PPO-PEO Triblock Copolymers and their Biomedical Applications.” In: *J. Bioactiv. Compat. Polymers* 21 (2006), p. 149.

[31] O. Glatter and O. Kratky. *Small Angle X-ray Scattering*. Academic Press, London, 1982.

[32] O. Glatter et al. “Nonionic Micelles near the Critical Point: Micellar Growth and Attractive Interaction”. In: *Langmuir* 16.23 (2000), pp. 8692–8701.

[33] G. Gompper, D. Richter, and R. Strey. “Amphiphilc block copolymers in oil-water-surfactant mixtures: efficiency boosting, structure, phase behaviour and mechanism.” In: *J Phys Condens Matter* 13 (2001), pp. 9055–9074.

[34] A. Graciaa et al. “Improving solubilization in microemulsions with additives - Part 1: The lipophilic linker role”. In: *Langmuir* 9 (1993), pp. 669–672.

[35] A. Graciaa et al. “Improving solubilization in microemulsions with additives - Part 2: Long chain alcohols as lipophilic linkers”. In: *Langmuir* 9 (1993), pp. 3371–3374.

[36] M. Gradzielski. “Recent developments in the characterisation of microemulsions”. In: *Curr. Opin. Colloid Interface Sci.* 13 (2008), pp. 263–269.

[37] A. Guinier and Fournet G. *Small angle scattering of x-rays.* John Wiley & Sons, New York, 1955.

[38] W. Helfrich. “Elastic properties of lipid bilayers: Theory and possible experiments.” In: *Zeitschrift für Naturforschung* 28c (1973), pp. 693–703.

[39] T. Hellweg. “Block Copolymer Surfactant Mixtures in Aqueous Solution: Can we Achieve Size and Shape Control by Co-Micellization?” In: *Self Organized Nanostructures of Amphiphilic Block Copolymers II*. Ed. by Axel H.E. Mueller and Oleg Borisov. Vol. 242. Advances in Polymer Science. Springer Berlin Heidelberg, 2011, pp. 1–27.

[40] T. Hellweg. “Microemulsions”. In: ed. by C. Stubenrauch. Wiley VCH, 2009. Chap. 2. Scattering Techniques to Study the Microstructure of Microemulsions, pp. 48–83.

[41] T. Hellweg. “Microemulsions: A Versatile Carrier for Decontamination Agents”. In: *Decontamination of Warfare Agents*. Ed. by A. Richardt and M.-M. Bum. Wiley-VCH, Weinheim, 2008.

[42] T. Hellweg. “Phase structures of microemulsions”. In: *Current opinion in colloid & interface science* 7.1 (2002), pp. 50–56.

[43] T. Hellweg, A. Brulet, and T. Sottmann. “Dynamics in an oil-continuous droplet microemulsion as seen by quasielastic scattering techniques”. In: *Physical Chemistry Chemical Physics* 2.22 (2000), pp. 5168–5174.

[44] T. Hellweg and R. von Klitzing. “Evidence for polymer-like structures in the single phase region of a dodecane-C12E5-water microemulsion: a dynamic light scattering study”. In: *Physica A: Statistical Mechanics and its Applications* 283.3-4 (2000), pp. 349–358.

[45] T. Hellweg et al. “Shape fluctuations of microemulsion droplets: a neutron spin-echo study”. In: *Colloids and Surfaces A: Physicochemical and Engineering Aspects* 183-185 (2001), pp. 159–169.

[46] J. P. Hill et al. “Self-Assembly: From Amphiphiles to Chromophores and Beyond”. In: *Molecules* 19.6 (2014), pp. 8589–8609.

[47] F. Hofmeister. “Zur Lehre von der Wirkung der Salze. Zweite Mittheilung.” In: *Archiv für experimentelle Pathologie und Pharmakologie* 24.4-5 (1888), pp. 247–260.

[48] B. Jakobs. *Amphiphile Blockcopolymere als ’Efficiency Booster’ für Tenside: Entdeckung und Aufklärung des Effektes*. Cuvillier Verlag Goettingen, 2001.

[49] B. Jakobs et al. “Amphiphilic Block Copolymers as Efficiency Boosters for Microemulsions”. In: *Langmuir* 15.20 (1999), pp. 6707–6711.

[50] A. Kabalnov, U. Olsson, and H. Wennerstroem. “Polymer Effects on the Phase Equilibrium of a Balanced Microemulsion”. In: *Langmuir* 10.7 (1994), pp. 2159–2169.

[51] A. Kabalnov et al. “Polymer Effects on the Phase Equilibrium of a Balanced Microemulsion: Adsorbing versus Nonadsorbing Polymers”. In: *Langmuir* 10.12 (1994), pp. 4509–4513.

[52] M. Kahlweit, G. Busse, and B. Faulhaber. “Preparing Microemulsions with Alkyl Monoglycosides and the Role of n-Alcohols”. In: *Langmuir* 11 (1995), pp. 3382–3387.

[53] M. Kahlweit, E. Lessner, and R. Strey. “Phase behavior of quaternary systems of the type water-oil-nonionic surfactant-inorganic electrolyte. 2”. In: *The Journal of Physical Chemistry* 88.10 (1984), pp. 1937–1944.

[54] M. Kahlweit and R. Strey. “Phase behavior of quinary systems: tracing the three-phase body”. In: *The Journal of Physical Chemistry* 91.6 (1987), pp. 1553–1557.

[55] M. Kahlweit and R. Strey. “Phase Behavior of Ternary Systems of the Type H2O - Oil - Nonionic Amphiphile (Microemulsions)”. In: *Angewandte Chemie International Edition in English* 24.8 (1985), pp. 654–668.

[56] M. Kahlweit, R. Strey, and G. Busse. “Microemulsions: a qualitative thermodynamic approach”. In: *The Journal of Physical Chemistry* 94.10 (1990), pp. 3881–3894.

[57] M. Kahlweit et al. “General patterns of the phase behavior of mixtures of water, nonpolar solvents, amphiphiles, and electrolytes. 2”. In: *Langmuir* 5.2 (1989), pp. 305–315.

[58] M. Kahlweit et al. “How to study microemulsions”. In: *Journal of Colloid and Interface Science* 118.2 (1987), pp. 436–453.

[59] M. Kahlweit et al. “Phase behavior of ternary systems: water-oil-nonionic surfactant as a near-tricritical phenomenon”. In: *Langmuir* 1.3 (1985), pp. 281–288.

[60] G.M. Kalvius. *Physik IV*. Ed. by G.M. Kalvius. 5., vollstaendig ueberarbeitete Auflage. De Gruyter Oldenbourg (Verlag), 1999.

[61] P. K. Kilpatrick et al. “Patterns of phase behavior in ethoxylated alcohol-n-alkane-water-sodium chloride mixtures”. In: *J. Phys. Chem.* 90 (1986), pp. 5292–5299.

[62] K. Kluge. *Der Schlüssel zum Verständnis von Mikroemulsionen aus Zuckertensiden: Die interne Grenzfläche, Dissertation*. Logos Verlag Berlin, 2000.

[63] B. M. Knickerbocker et al. “Patterns of three-liquid-phase behavior illustrated by alcohol-hydrocarbon-water-salt mixtures”. In: *The Journal of Physical Chemistry* 86.3 (1982), pp. 393–400.

[64] E.-M. Kutschmann et al. “Interfacial tension of alkylglucosides in different APG-oil-water systems”. In: *Colloid and Polymer Science* 273.6 (1995), pp. 565–571.

[65] R.G. Laughlin. *The Aqueous Phase Behavior of Surfactants*. Ed. by R.G. Laughlin. Colloid Science. Academic Press, 1996.

[66] L.G Lundstedt and I.R. Schmolka. “The synthesis and properties of block copolymer surfactants”. In: *Block and Graft Copolymerization*. Ed. by R.J. Ceresa. Wiley and Sons, London, 1976, pp. 1–111.

[67] A. D. McNaught and A. Wilkinson. *IUPAC. Compendium of Chemical Terminology, 2nd ed. (the Gold Book)*. Blackwell Scientific Publications, Oxford, 1997.

[68] F. Mezi. “Neutron Spin Echo: A new concept in Polarized Thermal Neutron Techniques”. In: *Z. Physik* 255 (1972), pp. 146–160.

[69] M. Mihailescu et al. “Dynamics of bicontinuous microemulsion phases with and without amphiphilic block-copolymers”. In: *Journal of Chemical Physics* 115 (2001), pp. 9563–9577.

[70] M. Newman, M. Balusubramanian, and C.W. Todd. “Development of adjuvant-active non-ionic block copolymers”. In: *Advanced Drug Delivery Reviews* 32.3 (1998), pp. 199–223.

[71] M. Nilsson, O. Soedermann, and I. Johansson. “The effect of polymers on the phase behaviour of balanced microemulsions: diblock-copolymer and comb-polymers.” In: *Colloid Polym Sci* 284 (2006), pp. 1229–1241.

[72] N. Ostrowsky et al. “Exponential Sampling Method for Light Scattering Polydispersity Analysis”. In: *Optica Acta: International Journal of Optics* 28.8 (1981), pp. 1059–1070.

[73] H. T. Davis P. K. Kilpatrick and L. E. Scriven. “Thermodynamic modeling of quaternary systems: oil-brine-surfactant-alcohol”. In: *Soc. Pet. Eng. Journal* 25 (1985), pp. 330–342.

[74] M. Podzimek and S. E. Friberg. “O/W Microemulsions”. In: *Journal of Dispersion Science and Technology* 1.3 (1980), pp. 341–359.

[75] G. Porod. “General Theory”. In: *Small Angle X-ray Scattering*. Ed. by O. Kratky O.Glatter. Academic Press, London, 1982.

[76] L.M. Prince. *Microemulsions, Theory and Practice*. Academic Press, New York, 1977.

[77] S.W. Provencher. "A constrained regularization method for inverting data represented by linear algebraic or integral equations." In: *Comput. Phys. Com.* 27 (1982), pp. 213–217.

[78] S.W. Provencher. "Contin: A general puirose constrained regularization program for inverting noisy linear algebraic and integral equations." In: *Comput. Phys. Com.* 27 (1982), pp. 229–242.

[79] P. N. Pusey and W. van Megen. "Dynamic light scattering by non-ergodic media." In: *Physica A* 157 (1989), pp. 705–741.

[80] W. von Rybinski and K. Hill. "Alkyl Polyglycoside - Properties and Applications of a new Class of Surfactants". In: *Angewandte Chemie International Edition* 37.10 (1998), pp. 1328–1345.

[81] W. von Rybinski, M. Hlouche, and I. Johansson. "Microemulsion". In: ed. by C. Stubenrauch. Wiley VCH, 2009. Chap. 8 Microemulsions in Cosmetics and Detergents, pp. 230–258.

[82] H. Saito and K. Shinoda. "The solubilization of hydrocarbons in aqueous solutions of nonionic surfactants". In: *Journal of Colloid and Interface Science* 24.1 (1967), pp. 10–15.

[83] J.L. Salager et al. "Microemulsions". In: ed. by C. Stubenrauch. Wiley VCH, 2009. Chap. 3. Formulation of Microemulsions, pp. 84–117.

[84] I. R. Schmolka. "Artificial skin I. Preparation and properties of pluronic F-127 gels for treatment of burns". In: *Journal of Biomedical Materials Research* 6.6 (1972), pp. 571–582.

[85] I.R. Schmolka. "A review of block polymer surfactants". In: *J. Am. Oil Chem. Soc.* 54 (1977), pp. 110–116.

[86] I.R. Schmolka. "Polyalkylene oxide block copolymers." In: *Nonionic Surfactants.* Ed. by M.J. Schick. Marcel Dekker, New York, 1966, pp. 300–371.

[87] K.-V. Schubert, R. Strey, and M. Kahlweit. "A new purification technique for alkyl polyglycol ethers and miscibility gaps for water-CiEj". In: *Journal of Colloid and Interface Science* 141.1 (1991), pp. 21–29.

[88] J. Schulman, W. Stoeckenius, and L. Prince. "Mechanism of Formation and Structure of Micro Emulsions by Electron Microscopy". In: *The Journal of Physical Chemistry* 63.10 (1959), pp. 1677–1680.

[89] C. Schulreich et al. “Bicontinuous microemulsions with extremely high temperature stability based on skin friendly oil and sugar surfactant”. In: *Colloids and Surfaces A: Physicochemical and Engineering Aspects* 418 (2013), pp. 39–46.

[90] L. E. Scriven. “Equilibrium bicontinuous structure.” In: *Nature* 263 (1976), pp. 123–125.

[91] K. Shinoda and H. Saito. “The effect of temperature on the phase equilibria and the types of dispersions of the ternary system composed of water, cyclohexane, and nonionic surfactant”. In: *Journal of Colloid and Interface Science* 26.1 (1968), pp. 70–74.

[92] T. Sottmann and R. Strey. “Ultralow interfacial tensions in water-n-alkane-surfactant systems”. In: *J. Chem. Phys.* 106 (1997), p. 8606.

[93] T. Sottmann et al. “General Patterns of the Phase Behavior of Mixtures of H2O, Alkanes, Alkyl Glucosides, and Cosurfactants”. In: *Langmuir* 18.8 (2002), pp. 3058–3067.

[94] R. Stehle et al. “An enzyme containing microemulsion based on skin friendly oil and surfactant as decontamination medium for organo phosphates: Phase behavior, structure, and enzyme activity”. In: *Journal of colloid and interface science* 413 (2014), pp. 127–132.

[95] R. Strey. “Microemulsion microstructure and interfacial curvature”. In: *Colloid and Polymer Science* 272.8 (1994), pp. 1005–1019.

[96] R. Strey. “Phase behavior and interfacial curvature in water-oil-surfactant systems”. In: *Current Opinion in Colloid & Interface Science* 1.3 (1996), pp. 402–410.

[97] R. Strey et al. “Efficiency boosting by amphiphilic block copolymers in microemulsions: Dependence on surfactant and oil chain length”. In: *Proceedings of the International Conference on Colloid and Surface Science 25th Anniversary of the Division of Colloid and Surface Chemistry, The Chemical Society of Japan*. Ed. by Noboru Oyama Yasuhiro Iwasawa and Hironobu Kunieda. Vol. 132. Studies in Surface Science and Catalysis. Elsevier, 2001, pp. 39–44.

[98] C. Stubenrauch, ed. *Microemulsions*. Wiley VCH, 2009.

[99] C. Stubenrauch. “Sugar surfactants - aggregation, interfacial, and adsorption phenomena”. In: *Current Opinion in Colloid & Interface Science* 6.2 (2001), pp. 160–170.

[100] K. Taugbol, T.V. Ly, and T. Austad. “Chemical flooding of oil reservoirs 3. Dissociative surfactant-polymer interaction with a positive effect on oil recovery”. In: *Colloids and Surfaces A: Physicochemical and Engineering Aspects* 103.1-2 (1995), pp. 83–90.

[101] L.J. Tchekountieu Mboumi. “Technisch relevante amphiphile Blockcopolymere in Mikroemulsionen”. Phd Thesis. Universität zu Köln, 2010.

[102] M. Teubner and R. Strey. “Origin of the scattering peak in microemulsions”. In: *The Journal of Chemical Physics* 87.5 (1987), pp. 3195–3200.

[103] H. Uchiyama et al. “Supersulibilization on chlorinated hydrocarbon microemulsions: Solubilization enhancement by lipophilic and hydrophilic linkers.” In: *Ind.Eng.Chem.Res* 39 (2000), pp. 2704–2708.

[104] S. Wellert et al. “Structure of biodiesel based bicontinuous microemulsions for environmentally compatible decontamination: A small angle neutron scattering and freeze fracture electron microscopy study”. In: *J.Colloid Interf.Sci.* 325.1 (2008), pp. 250–258.

[105] S. Wellert et al. “Temperature dependence of the surfactant film bending elasticity in a bicontinuous sugar surfactant based microemulsion: a quasielastic scattering study”. In: *Physical Chemistry Chemical Physics* 13.8 (2011), pp. 3092–3099.

[106] P.A. Winsor. *Solvent Properties of Amphiphilic Compounds*. Butterworth Scientific: London, 1954.

[107] A. Yaghmur, L. de Campo, and O. Glatter. “Formation and Characterization of Emulsified Microemulsions”. In: *Microemulsions - Properties and Applications*. Ed. by M. Fanun. CRC Press, 2008.

[108] Z. Yang. “Hofmeister effects: an explanation for the impact of ionic liquids on biocatalysis”. In: *Journal of Biotechnology* 144.1 (2009), pp. 12–22.

[109] Y. Zhang and P.S. Cremer. “Interactions between macromolecules and ions: The Hofmeister series”. In: *Current Opinion in Chemical Biology* 10.6 (2006), p. 65863.

[110] A. G. Zilman and R. Granek. “Membrane dynamics and structure factor”. In: *Chemical Physics* 284.1-2 (2002), pp. 195–204.

[111] A. G. Zilman and R. Granek. “Undulations and Dynamic Structure Factor of Membranes”. In: *Phys. Rev. Lett.* 77 (23 Dec. 1996), pp. 4788–4791.

Chapter 4

Experimental section

4.1 Used chemicals

4.1.1 Surfactants

The pure sugar surfactants n-decyl-β-D-maltoside ($C_{10}G_2$) and n-decyl-β-D-glucopyranoside ($C_{10}G_1$) were purchased from Glycon (Luckenwalde, Germany).

The technical surfactants were supplied by the following manufacturers: Simulsol SL55 (Seppic, Paris, France) is a $C_{12/14}G_{1.3}$ alkylglucoside, with a medium size alkyl chain length varying between 12 and 14 carbon atoms with a glycosidic head group with an average of 1.3 glucose units.

Glucopon 220 ($C_{8/10}G_{1.3}$, Henkel, Düsseldorf, Germany), the alkyl chain is shortened by four CH_2 units, the glucoside/maltoside ratio of the head group is identical to the larger surfactant SL 55.

A set of Plantacare surfactants (Cognis, Düsseldorf, Germany) were tested as replacements for Glucopon 220, which was taken off the market. Plantacare 810 UP replaces Glucopon220 and according to Cognis should have similar properties.

The technical surfactants are usually delivered as aqueous solutions with a surfactant content of 53-57 wt.% for Simulsol SL55, 52-62 wt.% for Glucopon 220.

The water content of the used batch was determined by Karl-Fischer titration and taken into account in the calculation of the sample composition. All technical grade surfactants were used as received, only for the preparation of the samples for SANS experiments the water was removed by freeze-drying to a water content below 2 wt%.

4.1.2 Co-surfactants

The following chemicals were used without further purification as co-surfactants: 1-pentanol (≥ 98%, Merck, Darmstadt, Germany), benzyl alcohol (≥ 99%, Grüssing, Filsum, Germany) and eugenol (99 %) (Aldrich, Feuchtwangen, Germany).

4.1.3 Solvents

Water phase

For the formulation of microemulsions water from a Milli Q (Millipore, U.K.) purification system was used.

Oil phase

For the experiments with the pure sugar surfactants cyclohexane (> 99.7%, Sigma-Aldrich, Schnelldorf, Germany) was utilized as oil phase. In case of the technical grade surfactants the hydrophobic phase was cyclohexane (technical grade, 99 %, Aldrich, Feuchtwangen, Germany), Synative ES ME TI 05 (BASF Personal Care and Nutrition GmbH, Düsseldorf, Germany) as well as Lanol 99 (Seppic), ethyl laurate (≥ 98%) and ethyl caprate (≥ 98%) (both Aldrich) were used.

Synative ES ME TI 05 is a fatty acid methyl ester (FAME), consisting mainly of oleic acid. Lanol99 is an isononyl isononate, which is used as an emollient in many cosmetic products due to its skin compatibility. Ethyl laurate is used as a fatty additive in food industry and cosmetics industry. Ethyl caprate is an odour additive in the synthesis of flavours.

Deuterated solvents

In the SANS and the NSE experiments deuterated solvents were used, to prepare bulk and film contrast samples. Phase diagrams and samples were prepared using deuterated cyclohexane C_6D_{12} with an isotopic purity >99.5 % D and deuterated water D_2O (Isotopic puritiy >99.95 % D). Both solvents were purchased from Deutero (Kastellaun, Germany). For the SANS experiments performed at the FRM II in Garching, Munich, Germany, the water phase was replaced with D_2O with an isotopic purity >99.9 % D_2O obtained from Eurisotop (Gif-sur-Yvette, France).

4.1.4 Pluronic polymers

The triblock copolymers added to the microemulsion systems belong to the Pluronic Series from BASF (Düsseldorf, Germany). These block copolymers are PEO_x-PPO_y-PEO_x applied in three different series with x in the range of 2 and 133 and y between 16 and 60.
The molecular characteristics of the block copolymers used in this study are presented in table 4.1, for further information and nomenclature see section 3.4.2 in chapter 3.

Table 4.1: Properties of the Pluronic PEO_x-PPO_y-PEO_x copolymers. According to Figure 3.10, y and 2x are the average number of PO-units and EO- units respectively. [a] average molecular weight M and hydrophilic-lipophilic balance HLB: information provided by manufacturer; [b] calculated from M and the PEO-content provided by the manufacturer.

Polymer name	M[a] g/mol	y [b]	2x [b]	HLB-value[a]	Series S1	S2	S3
L61	2000	31.0	4.5	3	S1		
L62	2500	34.4	11.3	7	S1		
L64	2900	30.0	26.3	15	S1		
P65	3400	29.3	38.5	17	S1		
F68	8400	28.9	152.4	29	S1		S3
F38	4700	16.2	85.3	31			S3
F88	11400	39.3	206.8	28			S3
L101	3800	58.9	8.6	1		S2	
P103	4950	59.7	33.7	9		S2	
P104	5900	61.0	53.5	13		S2	
P105	6500	56.0	73.7	15		S2	
F108	14600	50.3	264.9	22		S2	S3

4.2 Sample preparation

This section treats the procedure for the preparation of microemulsion samples. The order of the component addition depends on practical experience and reduces the formation of highly viscous meso phases hindering the homogenisation of the samples.

The technical surfactants G220, SL55 and UP810 are used as aqueous solutions. Here, the optimal procedure found was to start with the surfactant solution, then adding the remaining amount of water calculated with the known water content of the surfactant batch. After intense mixing the binary surfactant-water composition, the oil phase is added. For the pure surfactants the order of the components is similar. In contrast to the technical surfactant solutions the mixing has to be performed after addition of the oil phase. Otherwise stable water-surfactant meso phases are formed. These phases are hardly soluble and highly viscous, leading to a time consuming homogenisation process for the sample preparation. In some cases this homogenisation required addition of co-surfactant up to $\delta = 0.05$ and took several days of forceful stirring and moderate heating to about 50 °C.

The polymer containing samples were prepared from stock solutions of technical surfactant and polymer. The dry mass of polymer and the respective surfactant solution are weighed into a screw cap glass bottle equipped with a stirring magnet and homogenized for several days. Due to the fact that some of the polymers tend to sediment in the ternary water surfactant polymer mixture, the stock solutions have to be remixed before every weighing. A low stirrer speed is necessary to avoid foam formation.

The pure sugar surfactants are white, hygroscopic solids. The production of stock solutions containing pure surfactant and polymer with a relatively low water content failed due to formation of long term stable water - surfactant phases. Hence, the samples were prepared by weighing first the polymer and then the sugar surfactant into a test tube equipped with a screw cap. The water and oil are added subsequently.

All samples were homogenised by intense stirring and shaking for several hours. Especially the pure surfactants with medium length alkyl chains starting from dodecyl and glucose headgroup show a low solubility in water. These samples often have to be gently heated to 50 °C to dissolve the residue. In some cases after three days of stirring undissolved precipitate of surfactant or polymer remained. Here, addition of small amounts of co-surfactant (up to $\delta = 0.1$) made homogenisation possible.

For the samples with defined co-surfactant content δ, the procedure is identical. The alcohol is

added as the last compound with a microliter pipette. Usually homogenisation of these samples could be performed rather quick and with a low potential of forming disturbing meso phases. The amount of alcohol pipetted to the mixture was calculated from the desired δ value and the resulting mass using the density of the alcohol.

4.3 Phase behaviour

A precise knowledge of the phase boundaries of the systems is essential for the use of microemulsions in decontamination processes. In this section the basics for the understanding of the phase behaviour of microemulsion systems are explained and the procedure for gaining these informations is illuminated. Usually phase diagrams are taken from pseudo-binary systems, where the ratio of two components is kept constant. This correlates with a cut through the phase tetrahedron, in our case usually at constant oil to water ratio of $\alpha = 0.5$. The phase diagram is recorded by preparing a series of samples with increasing content of the third component, here the surfactant amount γ was varied in the range of $0.025 \leq \gamma \leq 0.40$. Depending on the used surfactant, the overall sample size varied between 1 – 2 g for pure sugar surfactants and 5 g for the technical grade surfactants. All components except the co-surfactant were weighed into a scaled glass tube with screw cap and homogenized according to the procedures described in section 4.2.

Recording phase boundaries

The determination of the phase boundaries is the most time consuming step in the inverstigation of the microemulsion behaviour based on sugar surfactants. The phase inversion can not be achieved by a simple temperature variation experiment as in the case of the C_iE_j surfactants [11, 12, 13, 16]. Hence, the phase behaviour is tuned by stepwise titration with the co-surfactant, changing the curvature of the amphiphilic film. In most cases the chosen cut through the phase tetrahedron is the "Kahlweit-fish" (see e.g. figure 4.1).

As co-surfactants usually a short or medium chain alcohol is used [13, 16, 17]. The influence of the co-surfactant on the internal film is described in section 3.2.2 and shown in figure 3.7. Starting at $\delta = 0$, usually the alcohol content is increased in steps of $\Delta\delta = \delta_{\text{new}} - \delta_{\text{old}} = 0.05$ until the upper phase boundaries are reached. That is when the three or one phase region (**3** or **1**) became the $\overline{2}$. The added mass of alcohol is calculated by (4.1), with $m_{\text{w+s+o}}$ being the overall weight of the

sample without the alcohol (usually $m_{\mathrm{w+s+o}} = 5\,\mathrm{g}$ for SL 55).

$$\Delta m_{\mathrm{alcohol}} = \frac{\delta_{\mathrm{new}} * m_{\mathrm{w+s+o}}}{1-\delta_{\mathrm{new}}} - \frac{\delta_{\mathrm{old}} * m_{\mathrm{w+s+o}}}{1-\delta_{\mathrm{old}}} \tag{4.1}$$

With the specific density of the alcohol the related volume determined and added to the sample using a microliter pipette. After each co-surfactant addition the sample is homogenized with a vortex mixer and afterwards equilibrated in a thermostated water bath until complete phase separation appeared. This step is the most time consuming in the recording of the phase behaviour, as some samples take several days for the phase separation, especially when polymers are involved.

Here, the samples are visually inspected in transmitted and scattered light. The samples are kept at a constant temperature of 20 °C by a thermostated water bath. After an adequate equilibration time, the phases are distinguished as follows: The bicontinuous microemulsion phase **1** is an optical isotropic and clear solution in transmitted light. Scattered light is in the systems with greater length scales of a pale blue. This phase remains clear upon shaking or stirring. In contrast the phase separated samples are of turbid, milky appearance during shearing or mixing. After phase separation the two and three phase systems can easily be differentiated. In the polymer containing systems the equilibration time is minimum 8 hours, in some systems up to several days due to a meta stable phase. Here, one has to be careful not to obtain wrong-three phase results. To distinguish the two 2-phase systems $\underline{2}$ and $\overline{2}$, the microemulsion phase has to be identified. This can be done by observing the scattering of coherent light, a simple laser pointer is sufficient for that task. The internally structured phase scatters the laser light. In some systems an optical matching appears. Here, the phase boundaries are hard to detect due to the similar refractive indices of the phases. Carefully shearing or mixing (by soft tapping the glass tube) leads to the formation of cords at the contact surface of the two phases. With the same method systems with two or more phases with one dominant phase, as they appear close to the X-point, can be distinguished from single phase systems. Soft tapping leads to cords, bicontinuous systems stay completely clear.

Lamellar phases (L_α) are optically anisotropic phases. They can be identified due to their static birefringence using crossed polarizers [13, 15, 16].

Pure versus technical surfactants

As the technical grade sugar surfactants are usually a mixture of sugar surfactants with varying headgroup size (glucoside or maltoside) and different chain length, the observed phase diagrams

differ from those of pure sugar surfactants.

The comparision of Glucopon 220, which is a mixture with approximately $C_{8\cdots10}G_{1.3}$, and n-octyl-α-glycoside (C_8G_1) is shown in figure 4.1. Here, the usually observed behaviour can be explained. The pure surfactants show smaller **3** and **1** phase regions, often with extended lamellar phases. In some cases the **1** region is completely suppressed by the formation of the lamellar phases, as the identical chain length of the surfactant tends to form the more ordered structure. Additional higher amounts of cosurfactant are needed to change the curvature of the amphiphilic film. The technical grade surfactants with their variety of different surfactant structures are able to stabilize larger amounts of oil and water (broader **3** and **1**) and lower $\tilde{\gamma}$ values. Often only small lamellar regions appear at higher γ values. On the other hand, the properties of the technical grade surfactants may vary from batch to batch, slightly changing the borders of the phase diagrams.

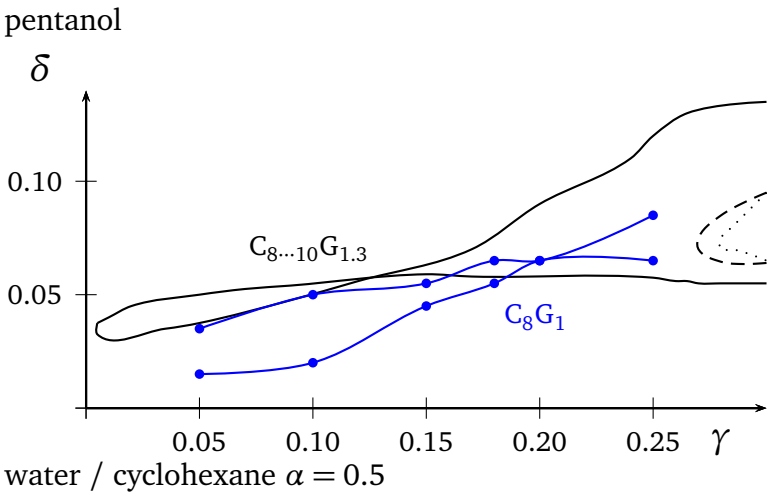

Figure 4.1: Cut through the phase tetrahedrons of the system water / cyclohexane / surfactant / n-pentanol with pure sugar surfactant n-octyl-α-glycoside (C_8G_1) in blue and the technical grade surfactant Glucopon 220 $C_{8\cdots10}G_{1.3}$ in black at a constant oil-water ratio of $\alpha = 0.5$ and 293 K. Further explanation see text.

Determination of the X-point according to Kunieda

The influence of the polymers on a microemulsion system can easily be tested by observing the change in the bicontinuous (microemulsion) phase in a three phase system[4, 6]. Preparing the samples in small glass cuvettes this method works fine utilizing temperature sensitive surfactants, where the phase transition can be achieved by a simple change of the temperature. For sugar surfactants a co-surfactant is needed to tune the phase behaviour and therefore a fourth component has to be added stepwise in small amounts. This makes larger sample volumes necessary to reduce the addition failures. Close to the X-point the determination of the different phases was inaccurate.

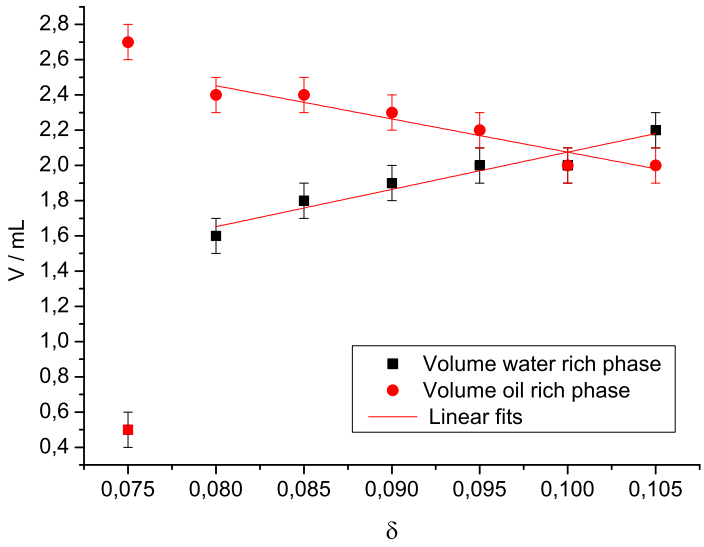

Figure 4.2: Determination of V_{middle} in the system Water / Lanol 99 / Simulsol SL55 / pentanol as the connection point of the linear fits of the changes in the volumes of the upper (oil rich) and the lower (water rich) phase in the three phase region upon increasing δ. Example shown for a sample containing 5% F108 at $\gamma = 0.05$.

Hence, we used the method derived by KUNIEDA *et al.* [5, 18, 14] to determine the location of the X-point. Following the blue line in the three phase region (see 3.7, section 3.2.2), the lower and the upper phase are in an equilibrium with the middle phase. The more surfactant is added, the more oil and water can be stabilized in the microemulsion (middle) phase, so this phase is growing while the other two are reduced. The equilibrium state is reached, when the volume of the upper

(oil-rich) and the lower (water rich) phase are equal. Therefore the change of the volumes was observed upon increasing the cosurfactant content δ, as shown exemplary for $\gamma = 0.05$ in the system water/lanol 99/ SL55 (5% F108)/pentanol in figure 4.2. As the equilibrium point often is located in between the δ steps, it was identified by linear fits. Hence, the resulting volume fraction of the middle phase in the three phase body $V_{\text{middle}}/V_{\text{total}}$ was measured as a function of the surfactant content γ. When the three phase body evolves and the volume fraction V_{middle} increases with rising γ until the X-point is reached at $V_{\text{middle}}/V_{\text{total}} = 1$. As shown in Figure 4.3, the $\tilde{\gamma}$ value can be easily determined by linear fitting. The X-point in the example was calculated to $\tilde{\gamma} = 0.152$, which fits well to the recorded phase diagram shown in figure 5.5.

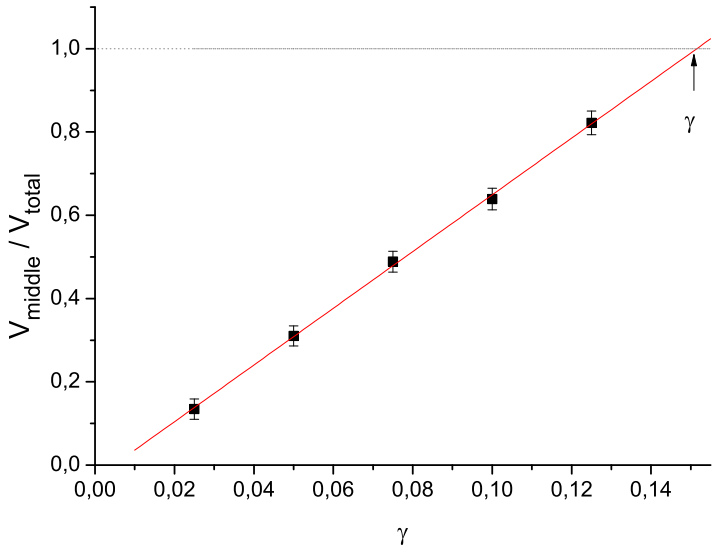

Figure 4.3: Determination of the X-point ($\tilde{\gamma}$) by linear fitting the swelling of the middle phase V_{middle}/V_{total} plotted versus γ. The example is taken from the system Water / Lanol 99 / Simulsol SL55 (5% F108) / pentanol.

4.4 PCS experiments

The samples for the PCS experiments were prepared by the method described above. The overall sample weight without the cosurfactant content was usually 1 g for the pure sugar surfactants and 5 g for technical grade sugar surfactants.

To avoid scattering from dust particles, approximately 1 mL of the sample was transferred into 10 mm glass cuvettes in a laminar flow box. The cuvettes were cleaned with ethanol before use.

Measurements were performed with the ALV Goniometer setup (ALV-Laservertriebsgesellschaft, Langen, Germany), using an argon ion laser (Spectra Physics, Santa Clara, USA) with 100 mW at $\lambda =$ 514,5 nm as light source. After adjustment of the laser intensity to a count rate of $\approx 60 - 120$ kHz over the whole angular range, the correlation function was recorded with an ALV-5000/E multiple-τ digital correlator.

Measurements were performed at constant temperatures of 20 °C, (22 °C and 26 °C for the samples used in the NSE-experiments), using decaline as matching bath. After an equilibration time of 45 min the correlation function was recorded three times for 60 s at different angles Θ in the range of 30 ° and 120 ° in steps of 15 °.

The obtained autocorrelation function was treated with the program Contin, using the method of the inverse Laplace transformation[7, 8].

By plotting the resulting mean values of Γ in a $\Gamma(q^2)$ plot (q calculated from Θ), the diffusion coefficient D can be obtained by a linear fit according to 3.18 (see section 3.7.1).

4.5 SAXS experiments

X-rays are scattered at electrons, therefore X-ray scattering occurs if there are inhomogeneities in the electron density distribution within the sample. In microemulsions, the contrast between water and oil phase is sufficient. Therefore, all samples were prepared as described in section 4.2 without addition of heavy atoms.

In this work different X-ray sources were used. The Ganesha system uses a copper (Cu-K_α) rotating anode, Synchrotron radiation is used as X-ray source at the ESRF beamlines ID01 and ID02. In the case of microemulsions, the scattering intensity I(q) plotted versus the scattering vector q shows a broad peak if bicontinuous phases are present. Here, the model introduced by TEUBNER and STREY was used for fitting with the Qtiplot software utilising the Nelder-Mead simplex or Levenberg-Marquardt algorithm.

Ganesha system:

The SAXS measurements of the water / Lanol 99 / Simulsol SL55 / n-pentanol system were performed with an inhouse system of the Förster group (Universität Bayreuth, PC 1). Here, the mi-

croemulsion samples were transferred with syringes to mark tubes with a diameter of 1 mm and measured at 20 °C.

This SAXSLAB Ganesha instrument the X-rays are focused with a pinhole collimation system. The high resolution 2D-Pilatus 300k detector (Dectris, Baden, Switzerland) can be moved in a vacuum vessel, allowing sample-detector distances in the range of 0.35 m and 2.00 m. After masking the beamstop and defects, the detected 2D intensity was radially averaged to obtain I(q). According to the method described by GLATTER et al., the scattering intensity of water was used to obtain absolute intensities[3].

4.6 SANS experiments

SANS measuements were carried out at the Laboratoire Léon Brillouin (LLB, Saclay, France) using the PAXY instrument at the research reactor Orphée.

The bulk contrast samples were prepared as described before in section 4.2. Bulk contrast here means that all water was replaced by D_2O. At least 6 hours prior the measurement the samples were transferred into 1 mm quartz cells (Hellma) to avoid multiple scattering [10] and inspected visually before and after the measurement to ensure homogeneity.

The estimated scattering length density of the sugar surfactant SL55 is $\rho_s = 3.7 \times 10^9 cm^{-2}$ [15].

The measurements were performed at a constant wavelength of $\lambda = 6$ with a distribution of $\Delta\lambda/\lambda = 0.1$ and three different sample - detector distances of 1,06 m, 3,06 m and 6,7 m. The measurements were performed in a temperature range between 261 K and 343 K using a thermostated holder. To avoid condensation of water on the quartz cells at temperatures below room temperature, an additional cap flushed with nitrogen was placed over the sample holder. Each temperature change was followed by an equilibration time of minimum 30 minutes.

The data collection was performed with a BF_3 filled XY multi detector of 15500 cells of $5 \times 5 mm^2$ resulting in an overall size of $64 \times 64 cm^2$.

Data treatment was performed with the programs provided by the LLB [2, 1]. The incoherent scattering of water was used to correct the detector intensity and the data was brought to absolute scale using the method described by COTTON [2].

The corresponding data sets were joined together and overlapped without further adjustment. Data analysis was performed with Qtiplot and Origin by fitting the TS-equation with a Levenberg-Marqwardt

algorithm.

4.7 NSE experiments

NSE experiments were carried out with the IN15 instrument at the Institut Laue-Langevin (ILL), Grenoble [9]. Among all the NSE instruments worldwide, the IN15 currently provides the highest Fourier times available. The samples were prepared as film contrast samples, using deuterated C_6D_{12} as oil and D_2O as water phase. The co-surfactant and the F68 were used in the protonated form as usual. After transferring the samples to $40 \times 40 \times 1$ mm quartz cells (Hellma), they were stored at 22 °C. Measurement was performed in a thermostatic holder at 22 ± 0.1 °C, at a wavelength of 10 Å and 16 Å at q-values in the range from 0.020 $^1/_{Å}$ to 0.138 $^1/_{Å}$. As the deuterated sample f68p0 was turbid at 22 °C, the measurements were performed at 26 °C, where the microemulsion was stable for more than 24 h. The wavelength distribution in all cases had a full width at half maximum (FWHM) of $\Delta\lambda/\lambda = 0.15$, the data collection was performed with a ^{3}He and CF_4 filled detector at a distance of 4.6 m from the sample, offering a 32×32 cm^2 area (pixel size 1 cm^2).

4.8 References

[1] A. Brulet et al. “Improvement of data treatment in small-angle neutron scattering”. In: *J. Appl. Cryst.* 40 (2007), pp. 165–177.

[2] J.P Cotton. *Initial data treatment. In:Neutron, X-ray and light scattering.* Ed. by P. Lindner and T. Zemb. Elsevier Science Publishers B.V., 1991.

[3] O. Glatter et al. “Sugar-Ester Nonionic Microemulsion: Structural Characterization”. In: *Journal of Colloid and Interface Science* 241 (2001), pp. 215–225.

[4] B. Jakobs. *Amphiphile Blockcopolymere als ’Efficiency Booster’ für Tenside: Entdeckung und Aufklärung des Effektes*. Cuvillier Verlag Goettingen, 2001.

[5] H. Kunieda and M. Yamagata. “Mixing of Nonionic Surfactants at Water-Oil Interfaces in Microemulsions”. In: *Langmuir* 9 (1993), pp. 3345–3351.

[6] M. Nilsson, O. Soedermann, and I. Johansson. “The effect of polymers on the phase behaviour of balanced microemulsions: diblock-copolymer and comb-polymers.” In: *Colloid Polym Sci* 284 (2006), pp. 1229–1241.

[7] S.W. Provencher. “A constrained regularization method for inverting data represented by linear algebraic or integral equations.” In: *Comput. Phys. Com.* 27 (1982), pp. 213–217.

[8] S.W. Provencher. “Contin: A general puirose constrained regularization program for inverting noisy linear algebraic and integral equations.” In: *Comput. Phys. Com.* 27 (1982), pp. 229–242.

[9] P Schleger et al. “The sub-neV resolution NSE spectrometer IN15 at the Institute Laue Langevin”. In: *Physica B: Condensed Matter* 266.12 (1999), pp. 49–55.

[10] J.A. Silas and E.W. Kaler. “Effect of multiple scattering on SANS spectra from bicontinuous microemulsions”. In: *J.Colloid Interface Sci.* 257 (2003), pp. 291–298.

[11] R. Strey. “Microemulsion microstructure and interfacial curvature”. In: *Colloid and Polymer Science* 272.8 (1994), pp. 1005–1019.

[12] R. Strey. “Phase behavior and interfacial curvature in water-oil-surfactant systems”. In: *Current Opinion in Colloid & Interface Science* 1.3 (1996), pp. 402–410.

[13] C. Stubenrauch. “Sugar surfactants - aggregation, interfacial, and adsorption phenomena”. In: *Current Opinion in Colloid & Interface Science* 6.2 (2001), pp. 160–170.

[14] C. Stubenrauch, B. Paeplow, and G. H. Findenegg. “Microemulsions Supported by Octyl Monoglucoside and Geraniol. 1. The Role of the Alcohol in the Interfacial Layer”. In: *Langmuir* 13.14 (1997), pp. 3652–3658.

[15] S. Wellert et al. “Structure of biodiesel based bicontinuous microemulsions for environmentally compatible decontamination: A small angle neutron scattering and freeze fracture electron microscopy study”. In: *J.Colloid Interf.Sci.* 325.1 (2008), pp. 250–258.

[16] S. Wellert et al. “Temperature dependence of the surfactant film bending elasticity in a bicontinuous sugar surfactant based microemulsion: a quasielastic scattering study”. In: *Physical Chemistry Chemical Physics* 13.8 (2011), pp. 3092–3099.

[17] S. Wellert et al. “The DFPase from loligo vulgaris in sugar surfactant based bicontinuous microemulsions: Structure, dynamics and enzyme activity”. In: *European Biophys. J.* 40 (2011), pp. 761–774.

[18] S. Yamaguchi and H. Kunieda. “Determination of a Three-Phase Tie Triangle (Microemulsions-Lipophile Balance Plane) in a Composition Tetrahedron: Evaluation of the Composition of Adsorbed Mixed-Surfactant and the Monomeric Solubilities of Short-Chain Surfactant”. In: *Langmuir* 13.26 (1997), pp. 6995–7002.

Chapter 5

Efficiency boosting in application - Pluronic polymers and the SL 55 / L99 system

The widely known and used triblock copolymers of the ABA type, here denoted as PEO-PPO-PEO, Poloxamers or by their trade name Pluronic (BASF), are used for about 60 years in lots of industrial applications [8]. They are also available in pharmaceutical purity, sold under the trade name Lutensol, which makes them interesting in terms of the skin decontamination application treated in chapter 7.

In this chapter the systematic screening of the efficiency boosting effect performed with three series of pluronic polymers is shown. Their influence on the phase behaviour, internal structure and parameters of the studied microemulsions is compared with the well known microemulsion system water / Lanol 99 / Simulsol SL55 ($C_{12/14}G_{1.3}$) / n-pentanol. [1]

5.1 Initial system water / Lanol 99 / Simulsol SL 55 / n-pentanol

The microemulsion system used as a starting point to investigate the influence of different poloxamers was developed as a skin friendly variation of the technical decontamination system based on bio-diesel as hydrophobic phase [13, 14].

[1] The results of this section were published in Tenside, Surfactants, Detergents.

The quaternary system consists of water, Lanol 99 as oil and Simulsol SL55 as surfactant. To tune the phase behaviour, n-pentanol was used as co-surfactant.

Compared with the Glucopon 220 ($C_{8-10}G_{1.3}$) surfactant originally used in the biodiesel system [15], the hydrophobic group is enlarged, increasing the balance of the surfactant. Due to the usage of n-pentanol as co-surfactant this system still has to be taken as a model system, further improvements on the composition are presented and discussed in later parts of this work (see chapter 7).

In figure 5.1 a cut through the phase tetrahedron [10, 11] at a constant oil/water ratio of $\alpha = 0.5$ as a function of γ and δ of the quaternary system is shown. The coexistence curves show the expected "fish"-shape. Phase inversion was achieved by stepwise addition of n-pentanol and the result is comparable with the bio-diesel system reported before by WELLERT *et al.* [15].

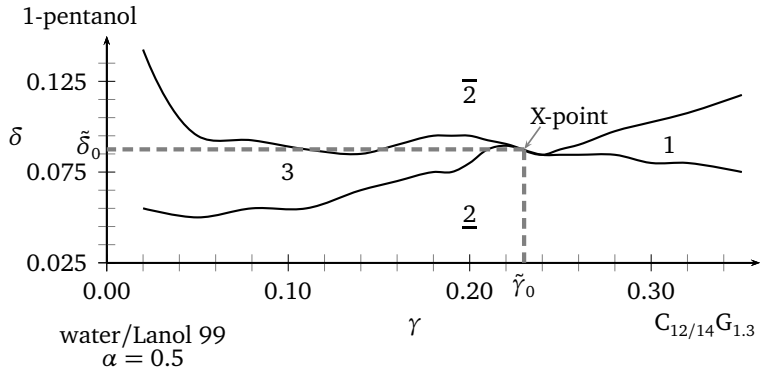

Figure 5.1: Cut through the phase tetrahedron of the system water / Lanol 99 / $C_{12/14}G_{1.3}$ / n-pentanol at a constant oil-water ratio of $\alpha = 0.5$ and 293 K.

At low δ a microemulsion of the o/w type coexists with an excess oil phase (denoted with $\underline{2}$). Upon addition of further co-surfactant at low surfactant mass fractions, below $\tilde{\gamma}$, the three phase body appears (3). In this region an upper oil excess phase coexists with microemulsion middle phase and a lower water excess phase. At higher surfactant mass fractions of $\gamma \geq \tilde{\gamma}$ the one phase region occurs (denoted by 1). At high δ a microemulsion of the w/o type coexists with excess water ($\overline{2}$).

The X-point is located at the transition from the three phase body to the one phase tail. At this point the minimum amount of surfactant needed to form a bicontinuous microemulsion is given by $\tilde{\gamma}$, and the amount of co-surfactant by $\tilde{\delta}$. For the pure system ($\tilde{\gamma_0}$, $\tilde{\delta_0}$) the X-point is located at $\tilde{\gamma_0} = 0.23$ and $\tilde{\delta_0} = 0.0875$, as shown in Figure 5.1.

5.2 Influence of the Pluronic polymes on the phase behaviour

The influence of the different PEO-PPO-PEO polymers on the phase behaviour of the microemulsion system water / Lanol 99 / Simulsol SL55 / n-pentanol was investigated by $\delta(\gamma)$-cuts through the phase tetrahedron. All cuts were performed at a constant water to oil ratio of $\alpha = 0.5$. In all systems the X-Point was determined using the method according to KUNIEDA described in section 4.3.

5.2.1 Pluronic polymers

The triblock copolymers of the PEO_x-PPO_y-PEO_x type used in this work were Pluronic polymers produced by BASF.

Three different series were applied: Two of them with a variation in the PEO/PPO content at comparable weight of the PPO backbone. For further information see table 4.1 in section 4.1.4 in the experimental chapter.

Series **S1** at intermediate polymer size, consisting of the Pluronics L61, L62, L64, P65 and F68. The second series **S2** was chosen with higher molecular weight, including L101, P103, P104, P105 and F108.

In the last series **S3**, the size effect of the most efficient polymers from series **S1** and **S2** were investigated, using polymers with a PEO content of 80 wt% and increasing the PPO backbone size from F38, F68, F88 to F108.

5.2.2 Effect of the polymer fraction

To investigate the influence of the polymer content, we focussed on F68. As shown later in this work, it is the smallest (MW $= 8400\,g{\cdot}mol^{-1}$) of the highly effective polymers in Series 3 and the closest to the overall median of $M = 5920\,g{\cdot}mol^{-1}$ in the polymers listed in table 4.1.

As mentioned in the sample preparation (see section 4.2), the method presented by JAKOBS [9] is not feasible for sugar surfactants due to the continuing addition of co-surfactant. Due to the ongoing addition of a fourth component to induce the phase inversion instead of simply increasing the temperature, the recording of the phase diagram can't be performed in small glass cuvettes. So the complete cut through the phase tetrahedron at a constant $\alpha = 0.5$ is taken for γ values between 0.05 and 0.25. By sequentially replacing the surfactant by polymer, the influence of the polymer on the phase behaviour can be observed. Starting with a polymer content of $\epsilon = 0.01$, the phase

diagrams of the system Lanol 99 - water - $C_{12/14}G_{1.3}$(F68) - 1-pentanol at a constant $\alpha = 0.5$ were taken. The results for $\epsilon = 0.01, 0.025, 0.05, 0.075$ and 0.10 are shown in Figure 5.2 and summarized in table 5.1. Upon addition of even small amounts of polymer a dramatical shift in the phase diagram can be observed. The Kahlweit-fish is moving towards smaller γ values, corresponding to an increase of the solubilisation capacity of the utilized surfactant system. Addition of $\epsilon = 0.01$, which is 1 wt% polymer relating to the surfactant mass or 0.21 wt% compared to the system at the X-point, reduces the necessary surfactant amount to $\gamma = 0.21$. This is a reduction of the needed surfactant amount by 8.7 %. Compared to the base system the size of the microemulsion phase in the three phase body is increased. A swelling of the one phase body close to the X-point is also observed, as shown in figure 5.2. This effect leads to a higher long time stability of the samples prepared closely behind the X-point. Some of the samples prepared in 2009 were still stable after 4 years.

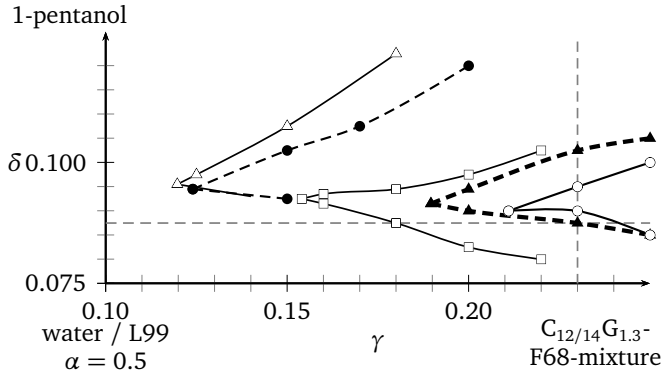

Figure 5.2: Shift of the X-point in the system water / Lanol 99 / SL55 (F68) / n-pentanol upon increasing F68 concentration in the amphiphile mixture. The F68-content rises from 1% (open circles), 2.5% (triangles), 5% (squares), 7.5% (filled circles) up to 10% (open triangles). The dashed vertical line indicates the position of the X-point in the base system.

Further rise of the polymer amount fortifies this effect. The bicontinuous microemulsion phase **1** is shifting to lower γ values, the minimal surfactant amount is reached employing 10 wt% F68. Here only 10.1 wt% surfactant are needed to solubilize equal amounts of water and oil. This corresponds to a reduction of 48 % compared with the base system.

The correlation between ϵ and $\tilde{\gamma}$ is shown in a $\epsilon(\tilde{\gamma})$-plot in Fig. 5.3. At low polymer amounts one might assume a linear behaviour, as described by the dashed line. At high polymer content a saturation effect appears, when ϵ is increased above $\epsilon = 0.075$. The expected $\tilde{\gamma}$ value for $\epsilon = 0.10$

should be at $\tilde{\gamma}_{\text{calculated}} = 0.08$, experimentally a value of $\tilde{\gamma}_{10\,\%\,\text{F68}} = 0.112$ has been found. This can be seen in the resulting efficiency boosting factors, which reach their maximum at $\epsilon = 0.075$ and decrease at $\epsilon = 0.100$.

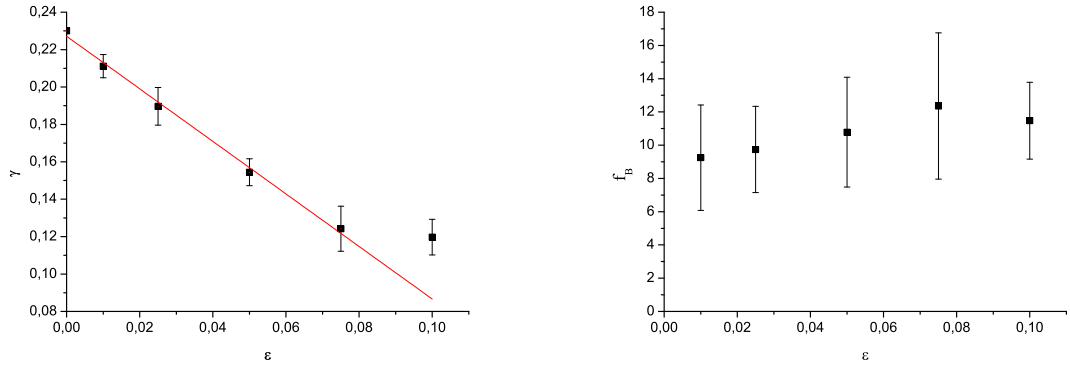

Figure 5.3: Effects of increasing the amount of surfactant replaced by polymer F68 in the system water/L99/SL55/pentanol. Left: Shift of the X-point ($\tilde{\gamma}$) versus ϵ. Up to $\epsilon = 0.075$ a linear behaviour of γ can be assumed, indicated by the red lines. At $\epsilon = 0.15$ no bicontinuous microemulsion phase occurred. Right: Resulting boost factors f_B plotted versus ϵ. f_B does not show any significant change upon changing ϵ.

In the systems with $\epsilon = 0.150$ and $\epsilon = 0.200$, the microemulsion structure collapsed in the investigated region. No bicontinuous region appeared in the range of $\delta = 0$ to $\delta = 0.25$.
This saturation effect is not known for the C_iE_j - surfactants and diblock copolymers, where the polymer in the polymer-surfactant mixture was applied up to 52 wt% [9].
Due to the limitation of the solubilisation capacity of the surfactant observed at polymer contents above $\epsilon = 0.10$, a standard value of $\epsilon = 0.05$ was chosen for the further investigation of the influence of the poloxamers on the phase behaviour in this work.

5.2.3 Variation of PEO/PPO ratio

The Pluronic polymers are available in a wide variety of compositions. With their properties depending on the size of the polymer and the PEO/PPO ratio, two different series with approximately common PPO backbone size and a variation of the PEO content were chosen.
The two series of Pluronics applied to the SL55 system correspond to a variation of the PEO content in the composition of the Pluronic polymers. According to the Pluronic grid (see Figure 3.11), the

Table 5.1: Position of the X-Points in the system water / Lanol 99 / $C_{12/14}G_{1.3}$(F68) / n-pentanol at different F68 concentrations. The last column contains the calculated boosting factors.

polymer content (wt.%)	$\tilde{\gamma}$	$\tilde{\delta}$	f_B
0.0	0.23	0.0875	-
1.0	0.211	0.0900	9.63
2.5	0.190	0.0915	9.74
5.0	0.154	0.0925	10.78
7.5	0.124	0.0945	12.36
10	0.112	0.0955	11.47
15	no bicontinuous phase		

mass of the PPO remains nearly constant in the series **S1** (M(PPO) = 1750 g·mol^{-1}, first digit = 6) and **S2** (M(PPO) = 3250 g·mol^{-1}, first digits = 10) . The PEO-content of the polymer increases from 10 wt.% (last digit = 1) up to 80 wt.% (last digit = 8) corresponding to an increase of the hydrophilic character of the polymers.

From the preliminary experiments performed with F68 a Pluronic concentration of 5 wt% of the total surfactant dry mass has been estimated to be useful for the efficiency boosting experiments.

Series S1

In Figure 5.4 the phase diagrams of the **S1** polymer containing systems at constant oil-to-water ratio of $\alpha = 0.5$ are shown. As described before, in each of the systems 5 wt.% of the SL55 mass was replaced by polymer, starting from L61 to F68. The basic shape of the phase boundaries is in all cases similar to the base system, showing the typical fish-shape. The resulting shift of the X-point compared to the microemulsion without polymer (dotted line in Fig. 5.4) follows the polymer composition. In the case of the polymers with a low amount of PEO, such as L61 (10 wt.% EO), L62 (20 wt.% EO) and L64 (40 wt.% EO), a shift to higher $\tilde{\gamma}$ values is observed. Simply replacing 5 wt.% of the surfactant by a surface inactive filling material leads to a calculated X-point of $\tilde{\gamma} = 0.2421$.

Hence, the polymers with a low PEO-content decrease the solubilisation capacity of the surfactant, leading to a shift of the X-point in the phase diagram to higher $\tilde{\gamma}$ values. RICHTER *et al.* [1, 2]

reported this *anti boosting effect* upon the addition of homopolymers.

The reduction effect clearly changes when a more balanced polymer structure is reached. Pluronic L64 with an EO content of about 40 wt.% increases from $\tilde{\gamma_0} = 0.23$ to $\tilde{\gamma}_{L64} = 0.245$. Thus about 1.2 % more surfactant are needed to solubilize equal amounts of oil and water.

A rise in the hydrophilic character by usage of P65 (EO-content 50 wt.%) leads to a small efficiency boosting effect ($\tilde{\gamma}_{P65} = 0.199$), which corresponds to a saving of 17.8 % surfactant. Further increase of the PEO content improves the effect, in the case of F68 the X-point is located at $\tilde{\gamma}_{F68} = 0.165$. This corresponds to a saving of approximately 32 % surfactant.

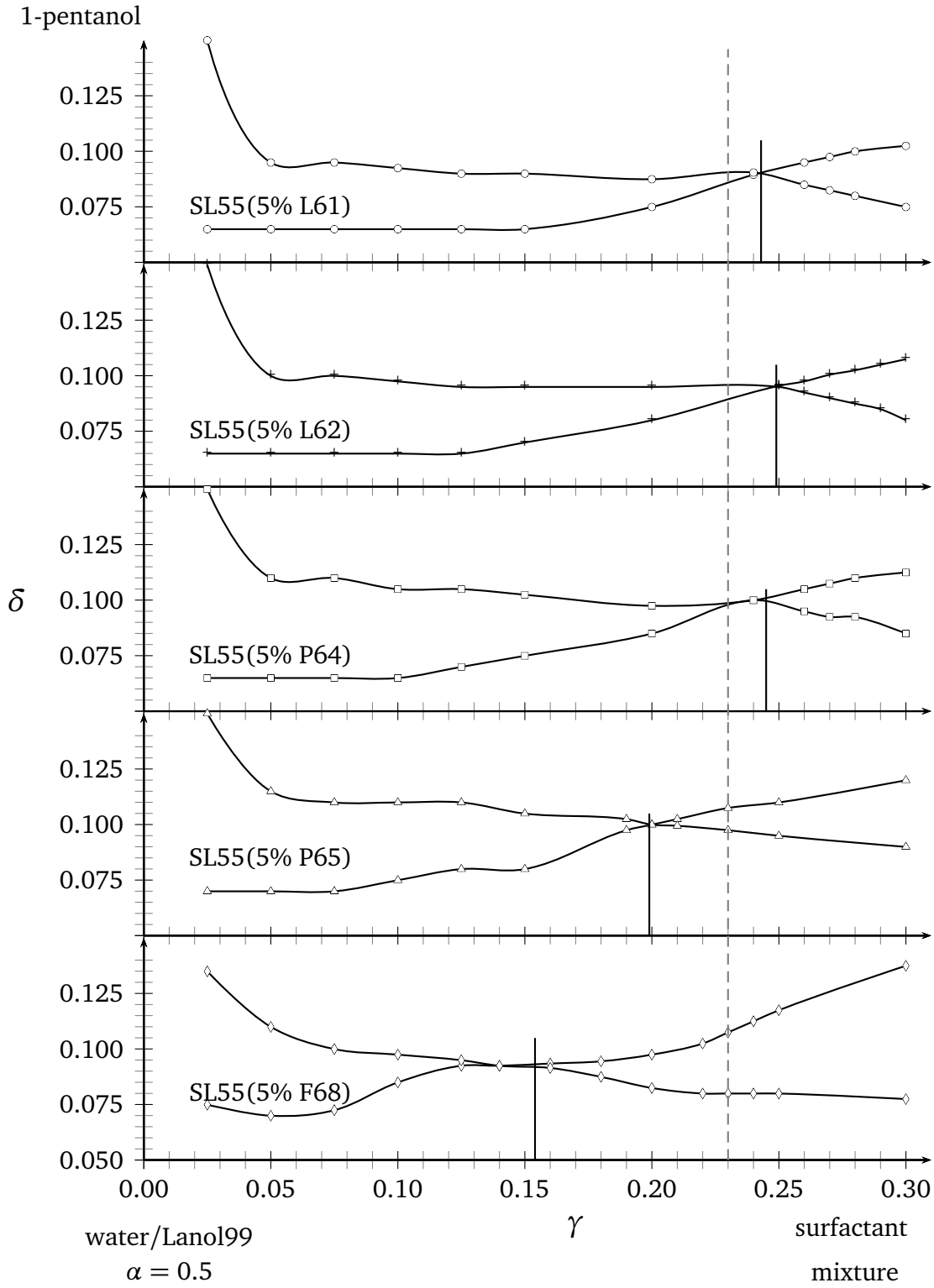

*Figure 5.4: Resulting phase diagrams in the system water / Lanol 99 / SL55(**S1**) / n-pentanol at $\alpha = 0.5$. The dashed line marks the position of the X-point in the base system with pure SL55. The straight lines show the position of the X-points estimated by the method of Kunieda (see section 4.3 for details). Further information in the text.*

Series S2

With the second series **S2** of higher molecular mass a comparable behaviour is found for the highly hydrophobic polymer L101 (see Figure 5.5). Here, the surfactant efficiency is reduced and the X-point is shifted to $\tilde{\gamma}_{L101} = 0.26$.

All other polymers of this series decrease the necessary amount of surfactant to form a bicontinuous microemulsion phase, shifting the X-point to lower $\tilde{\gamma}$ values.

Comparing the results of the phase behaviour of **S1** and **S2** shows that an increase of the overall polymer size at constant PEO contents shifts the X-point to lower $\tilde{\gamma}$ values. On the other hand the formation of large lamellar phases is forced with F108 at $\gamma > 0.28$.

This is displayed in Figure 5.6, where the calculated f_B is compared with the EO-content. For the larger polymers of **S2** a linear increase of the boost factor is observed. In polymer series **S1** an EO-content of more than 40 wt.% is needed to reach $\tilde{\gamma}$ values below $\tilde{\gamma}_0 = 0.23$.

While P64 still shows a decrease of the X-point position to $\tilde{\gamma}_{P64} = 0.245$, the surfactant efficiency is increased if 5 wt.% of SL 55 are replaced by P65 with a PEO content of 50 wt.%, leading to $\tilde{\gamma}_{P65} = 0.199$ or $f_B = 4,06$, respectively. The results, including the calculated efficiency boost factors, are summarized in table 5.2.

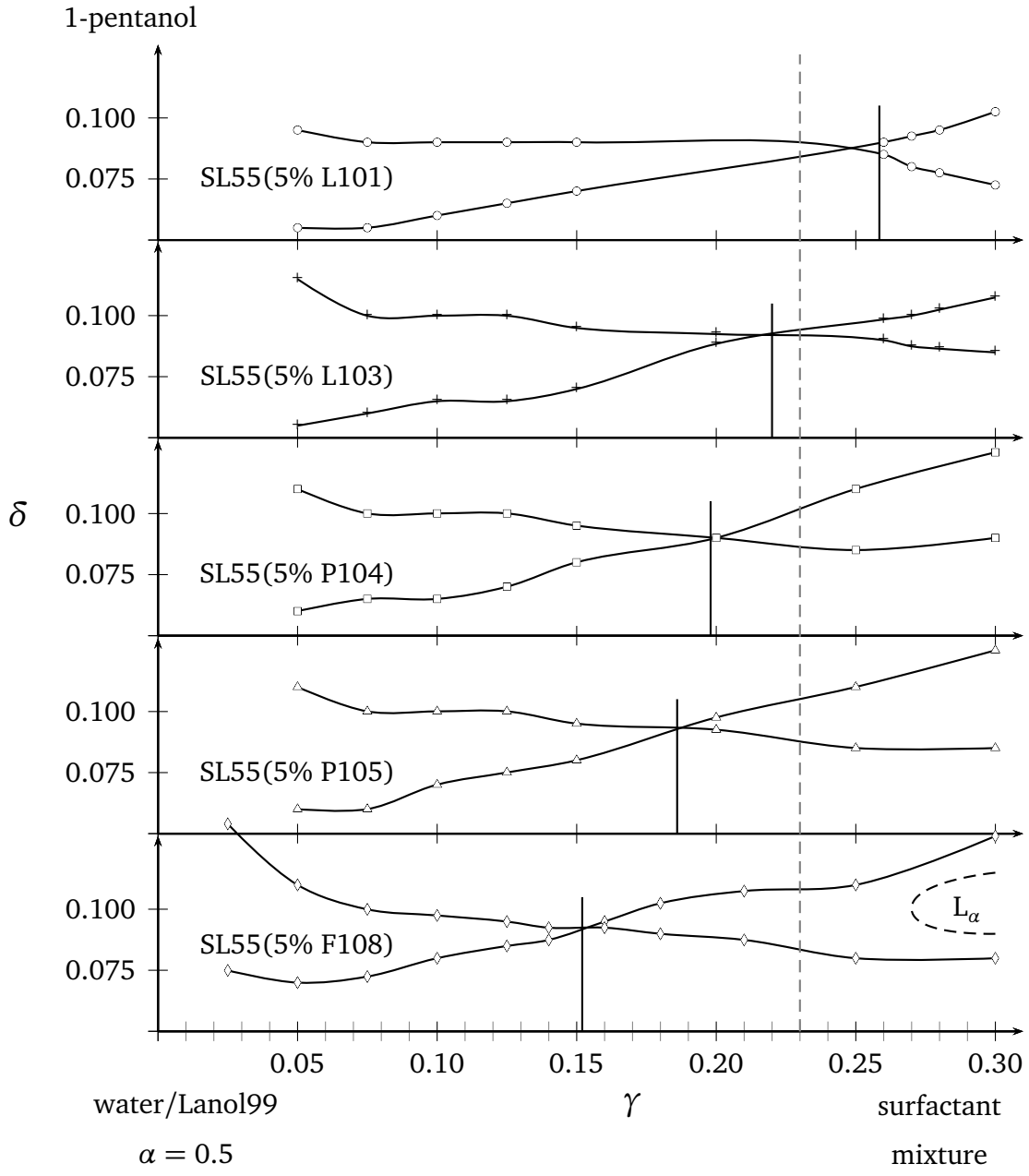

*Figure 5.5: Resulting phase diagrams in the system water / Lanol 99 / SL55(**S2**) / n-pentanol at $\alpha = 0.5$. The dashed line marks the position of the X-point in the base system with pure SL55. The straight lines show the position of the X-points estimated by the method of Kunieda (see section 4.3 for details). Further information in the text.*

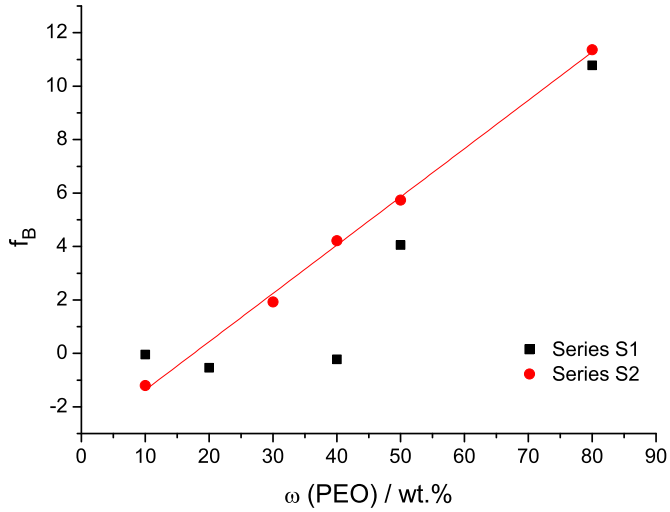

*Figure 5.6: Effects of the Series **S1** and **S2** polymers in the system water / Lanol 99 / SL55 / n-pentanol. Here, the calculated efficiency boost factor f_B is plotted versus the PEO content ω(PEO) of the polymers used in Series 1 and Series 2.*

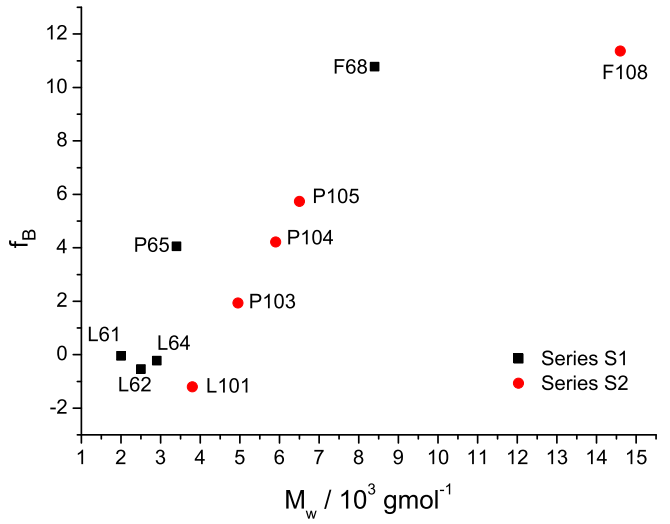

*Figure 5.7: Effects of the Series **S1** and **S2** polymers in the system water/L99/SL55/pentanol. Resulting boost factors f_B plotted versus the average molecular weight.*

Effect of the polymer size

Focussing on the Pluronic polymers with the strongest effect, the influence of the polymer size was investigated. The series **S3** (circles in Figure 3.11) consists of four polymers with an average PEO-content of 80 wt.%. Starting with F38, the size of the PPO block increases from m(PPO) = 950 g·mol^{-1} to 3250 g·mol^{-1} in F108. In Figure 5.8 the corresponding sections of the phase tetrahedron at constant $\alpha = 0.5$ are shown.

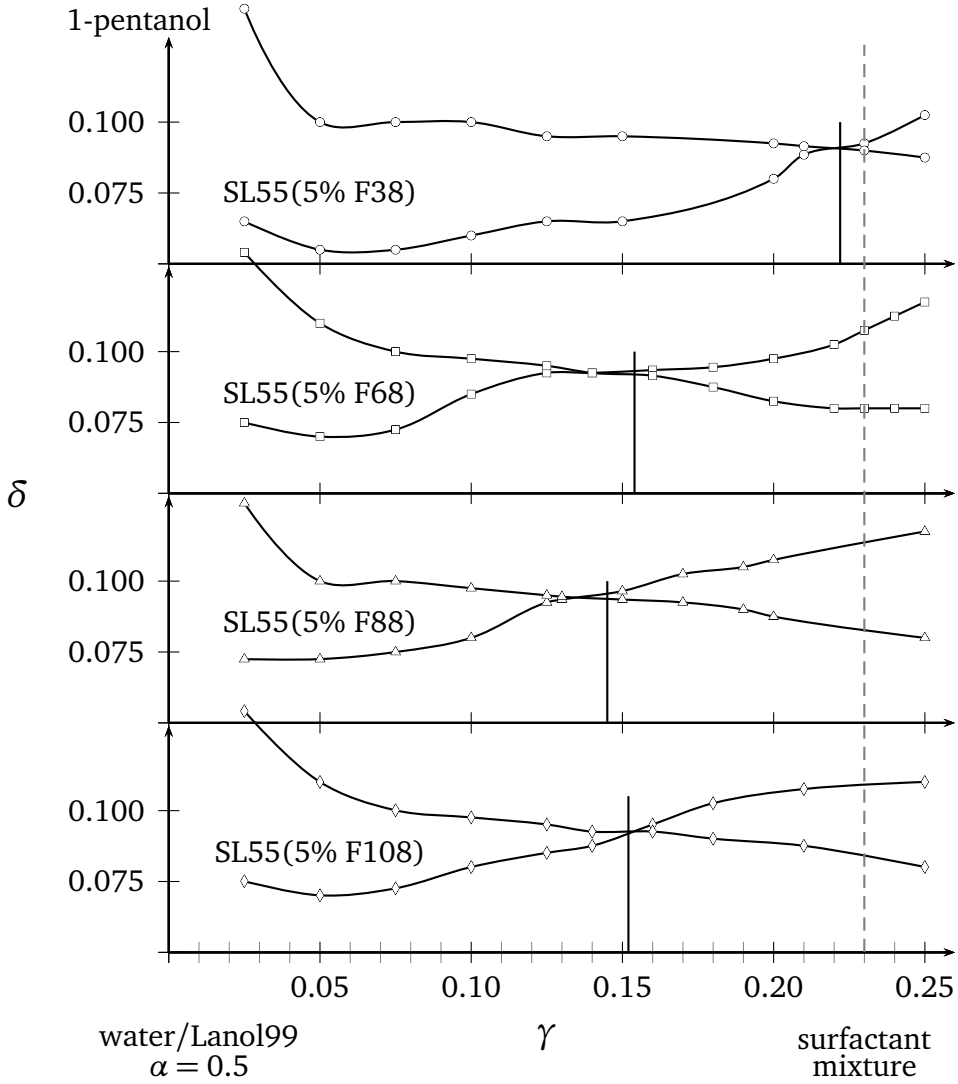

*Figure 5.8: Resulting phase diagrams in the system water / Lanol 99 / SL55(**S3**) / n-pentanol at* $\alpha = 0.5$. *The dashed line marks the position of the X-point in the initial system with pure SL55. The straight lines show the position of the X-points estimated by the method of Kunieda (see section 4.3 for details). Further information in the text.*

Assuming a constant ratio of 80 wt.% PEO in the Pluronics F38, F68, F88 and F108 the relation between the increasing molecular weight of the polymers and the resulting efficiency boost factor is shown in Figure 5.9. The smallest Pluronic F38 has a significant lower effect than the larger polymers, increasing the size above F68 shows only small variations in the effect. F88 and F108 allow the formation of bicontinuous microemusion phases at slightly lower $\tilde{\gamma}$-values as F68, as $\tilde{\gamma}_{F88} = 0.145$ and $\tilde{\gamma}_{F108} = 0.152$ compared to $\tilde{\gamma}_{F68} = 0.154$. At higher surfactant concentrations, this advantage is dramatically reduced, as extended lamellar phases occur. In the case of F108, at $\gamma = 0.30$ the L_α is found in the range of $\delta = 0.08 - 0.105$ by a microemulsion phase in a range of $\delta = 0.075 - 0.12$. Comparable behaviour is observed at $\gamma = 0.35$ in the case of F88, while F68 generates an extended bicontinuous microemulsion phase in the same range.

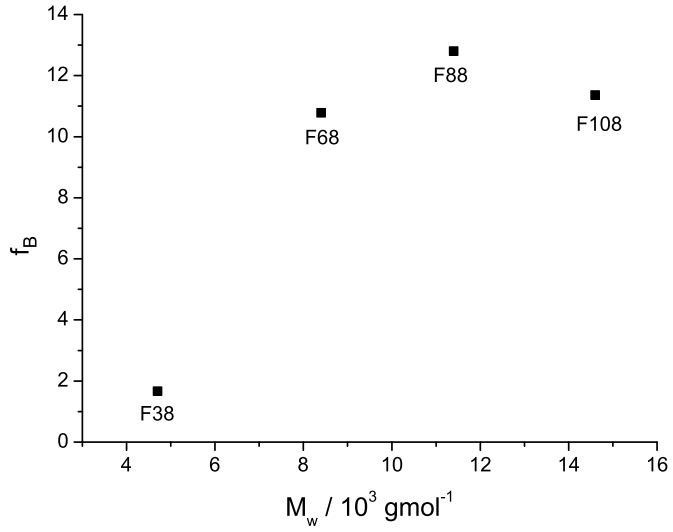

*Figure 5.9: Effects of the **S3** Pluronic polymers in the system water/L99/SL55/pentanol. Calculated boost factor f_B plotted versus the average molecular weight. The larger polymers show comparable effects.*

5.2.4 Comparison of the results for all three series

In all systems with pluronics, a higher amount of co-surfactant is needed to form a bicontinuous phase compared to the pure system with $\tilde{\delta} = 0.0875$. This is shown in figure 5.10, where the position of the X-point of all pluronic containing microemulsion systems is plotted with respect to the experimental error. The position of the pure water / Lanol 99 / $C_{12/14}G_{1.3}$ / n-pentanol microemulsion is indicated by the dashed lines. Four Pluronics polymers (L61, L62, L64 and L101) even reduce the efficiency of the surfactant. The efficiency boosting effect of the Pluronic polymers is, in our opinion, connected with the number of PEO units and therefore the solubility of the polymer in the aqueous phase and the size of the polymer (see figure 5.12). The average number of PPO units has no significant influence on the shift of the X-point in the microemulsion system, as shown in figure 5.12.

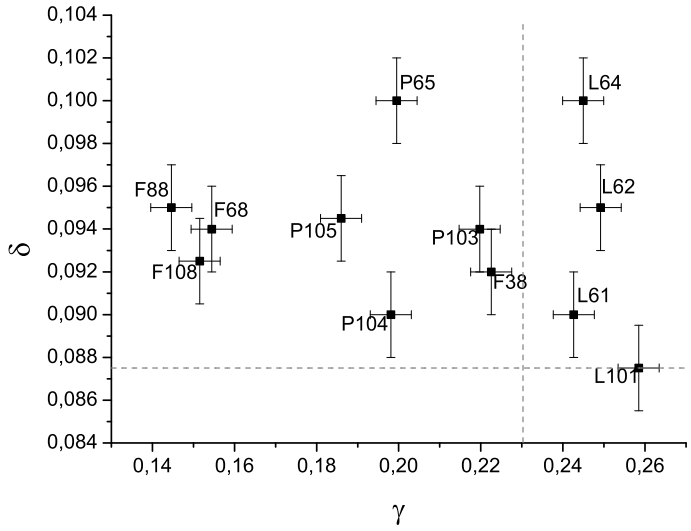

Figure 5.10: Position of the X-points in the system water / Lanol L99 / Simulsol SL55 / 1-pentanol with different pluronic polymers. The dashed lines show the position of the X-point in the system water / Lanol 99 / Simulsol SL55 / n-pentanol without addition of polymers.

As shown in figure 5.12, relating the effect of the polymers to the overall molar mass of the molecules, an increase of the molar weight leads to an increasing boosting effect. But it is not the PPO middle block of the polymers that correlates with this effect. Referring to Figure 5.12, there is a clear connection of the number of the EO units in the molecule and the boost factor.

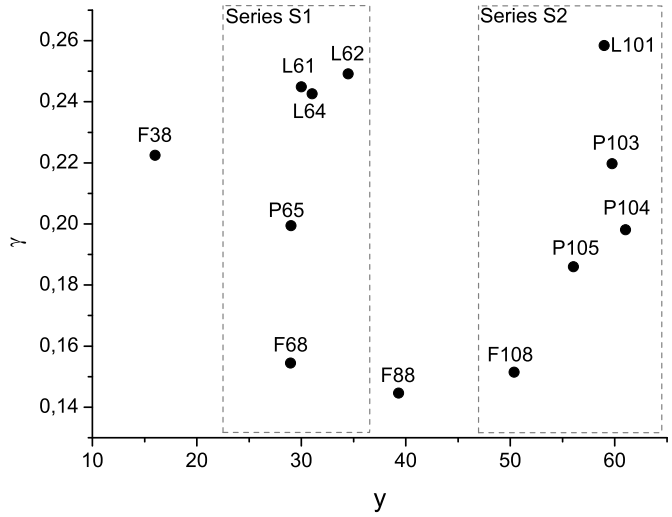

*Figure 5.11: Effects of the Pluronic polymers in the system water / Lanol L99 / Simulsol SL55 / 1-pentanol. No significant correlation between $\tilde{\gamma}$ and the average number of PPO units (y) of the polymer is observed. The dashed boxes indicate the two series **S1** and **S2**.*

An overview of the X-points of all systems examined in this survey is given in table 5.2 and shown in figure 5.10.

The lowest $\tilde{\gamma}$ value reached at $\epsilon = 0.05$ was $\tilde{\gamma}_{F88} = 0.145$, which corresponds to a $f_B = 12.8$. This is quite impressive for a technical grade system, as the amount of surfactant needed to form a bicontinuous microemulsion is reduced by 63 % upon an addition of only 0.725 wt.% of polymer compared to the pure microemulsion system.

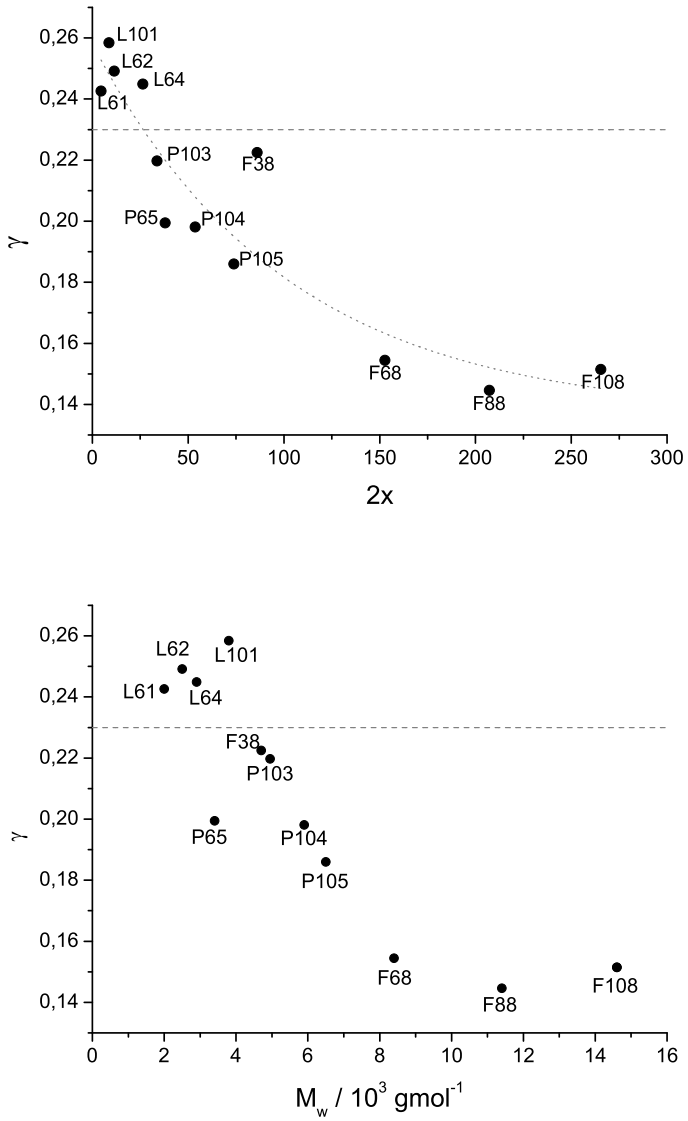

Figure 5.12: Effects of the Pluronic polymers in the system water/L99/SL55/pentanol. Top: $\tilde{\gamma}$ plotted versus the average number of EO units (2x) of the polymer. Upon increase of the overall PEO-chains, the amount of surfactant needed to form a bicontinuous microemulsion is reduced. The dashed line indicates $\tilde{\gamma}$ of the pure system. Bottom: $\tilde{\gamma}$ plotted versus the average molecular weight.

Table 5.2: Position of the X-points in the system water / Lanol 99 / $C_{12/14}G_{1.3}$ (Pluronic) / n-pentanol and the calculated efficiency boost factors f_B.

polymer name	M (g·mol^{-1})	ω(PEO) wt.%	ϵ	$\tilde{\gamma}$	f_B
L61	2000	10	0.05	0.243	-0.04
L62	2500	20	0.05	0.249	-0.54
L64	2900	40	0.05	0.244	-0.22
P65	3400	50	0.05	0.199	4.06
F68	8400	80	0.05	0.154	10.78
L101	3800	10	0.05	0.258	-1.20
P103	4950	30	0.05	0.220	1.93
P104	5900	40	0.05	0.198	4.22
P105	6500	50	0.05	0.186	5.74
F108	14600	80	0.05	0.152	11.36
F38	4700	80	0.05	0.222	1.67
F88	11400	80	0.05	0.145	12.81

5.3 Influence of the polymer on the internal structure of the microemulsion

Depending on the polymer, the addition of Pluronic polymers has a dramatic effect on the macroscopic phase behaviour of the microemulsion system. To identify the influence on the internal structure several different samples were prepared and investigated with a SAXSLAB Ganesha [3] inhouse SAXS system.

Samples composed with Pluronic polymers from series **S2** and series **S3** were investigated. Therefore three different γ values of $0.25, 0.30$ and 0.35 at constant $\alpha = 0.5$ and $\delta = 0.0875$ were investigated. Three sets of samples with increasing surfactant content were prepared for every series. All samples of one γ set were prepared from the same stock solution by adding the respective polymer.

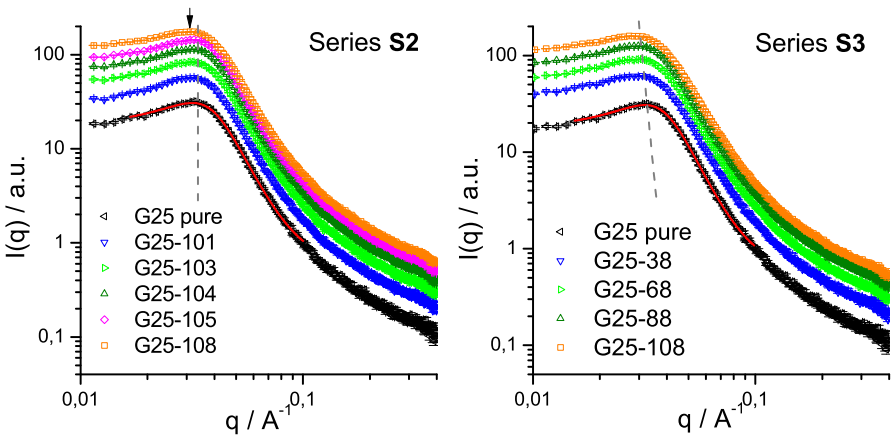

*Figure 5.13: SAXS measurements of **S2** left and **S3** right. All samples were composed at $\alpha = 0.5$, $\gamma = 0.25$ and $\delta = 0.0875$. The red line shown exemplarily for the pure system (G25-rein) represents the fit according to the TS approximation. The gray lines are just a guide to the eyes, indicating the shift of q_{max}: for **S2** q_{max} does not shift significantly for L101 to P105, only in the case of F108 q_{max} is at lower q-values (arrow). For **S3** q_{max} is reduced with an increase of the polymer size. The intensities I(q) of the samples containing polymer (G25-101 to G25-108 for **S2** and G25-38 to G25-108 for **S3**) were shifted for clarity reasons with respect to each other.*

Exemplary double logarithmic I(q)-q-plots for the **S2** - samples composed at $\alpha = 0.5, \gamma = 0.25$ and $\delta = 0.0875$ are shown in figure 5.13. In every scattering pattern the typical structure peak described for the bicontinuous structure of microemulsions [12, 5] is observed. For the pure system the red

line is a fit according to the TEUBNER-STREY approximation. The scattering patterns of the polymer containing microemulsions are shifted to higher I(q) values for clarity. As can be seen in figure 5.13, neither the position of the maximum q_{max} nor the general shape of the peak is influenced significantly by the added polymers of **S2** except F108.

The results of the data analysis using the TEUBNER-STREY approximation of the resulting scattering intensities is given in table 5.4 for **S2** and in table 5.5 for **S3**. As described before, in the polymer containing samples a polymer content of $\tau = 0.05$ was chosen. The domain size d remains almost constant for the observed samples at $\gamma = 0.25, 0.30$ and 0.35. For F108 only one sample was measured at $\gamma = 0.25$, higher surfactant content leads to the formation of lamellar phases. For the correlation length a slight increase with increasing PEO content of the polymer at higher γ values can be assumed. In the case of F108 the ξ value is reduced to $\xi_{SAXS} \approx 4.8\,\text{nm}$.

For the pure microemulsion system at $\alpha = 0.5$, $\delta = 0.0875$ and γ in the range of $\gamma = 0.25$ to 0.35, domain sizes of $d = 11.1 - 17.7nm$ and correlation length of $\xi = 5.5 - 6.7nm$ were calculated from fits with the TS-formula. As shown in table 5.3, these parameters are in the typical range for sugar surfactant based microemulsion systems.

Table 5.3: Comparision of the results of the TS-Analysis in the system water / Lanol 99 / $C_{12/14}G_{1.3}$ / n-pentanol at constant $\alpha = 0.5$ and $\delta = 0.0875$ with examples of sugar surfactant based microemulsions using n-pentanol as cosurfactant found in the literature. [a] *RME = rapeseed methyl ester;* [b] *SANS measurements, water replaced by D_2O;* [c] *Please note that in this work a different batch of $C_{12/14}G_{1.3}$ was used.*

system	α	γ	δ	ξ / nm	d / nm	ref.
Lanol 99 / $C_{12/14}G_{1.3}$	0.5	0.25 to 0.35	0.0875	6.7 to 5.5	17.7 to 11.1	
RME[a] / $C_{12/14}G_{1.3}$	0.5	0.299	0.07	4.7 to 4.4	14.4 to 14.1	[16]
RME / $C_{12/14}G_{1.3}$ [b]	0.5	0.29 to 0.30	0.07	4.7 to 4.4	13.4 to 12.8	[15]
C_6H_{12} / $C_{8/10}G_{1.3}$ [b]	0.5	0.15 to 0.23	0.06	7.9 to 6.5	22.2 to 13.5	[7]
Lanol 99 / $C_{12/14}G_{1.3}$ [b,c]	0.5	0.24 to 0.34	0.0825	5.6 to 4.7	18.6 to 9.7	[7]

Series 2

With respect to the error bars, the addition of the polymer only leads to small changes in the structural sizes of the microemulsions. Only F108, the largest polymer with an average molecular mass of approximately 14600 g·mol^{-1} differs significantly from the other samples. The domain size d of the pure microemulsion at $\gamma = 0.25$ is around 17.7 nm, the domain size upon addition of L101 - P105 is slightly increased, as the amount of surfactant available is reduced. This effect is rather small, as the changes in d are within the error bars. Otherwise for F108 the domain size $d_{F108} =$ 20.2 nm.

*Table 5.4: Results of the TS-Analysis of the SAXS-data in the system water / Lanol 99 / $C_{12/14}G_{1.3}$(**S2**) / n-pentanol at constant $\alpha = 0.5$ and $\delta = 0.0875$.*

	$\gamma = 0.25$		$\gamma = 0.30$		$\gamma = 0.35$	
	d / nm	ξ / nm	d / nm	ξ / nm	d / nm	ξ / nm
pure	17.7	6.7	13.4	5.7	11.1	5.5
L101	18.0	6.4	13.9	6.2	11.5	5.8
P103	18.1	5.9	13.7	6.1	11.3	6.0
P104	17.8	6.5	13.6	6.5	11.3	6.3
P105	17.7	6.7	13.6	6.2	11.3	6.3
F108	20.2	4.8	lamellar			

This increase of the domain size in the F108 containing system is an indication of the change in the internal structure of the microemulsion. Further increase of the surfactant and the polymer amount to $\gamma \geq 30$ leads to the formation of lamellar structures, the bicontinuous phase is not longer observed. At $\gamma = 0.25$ ξ varies slightly around 6.5 nm, only for P103 lower values are reached. At higher γ values the addition of triblock copolymers leads to a slight increase of the correlation length. The effect is rather small, at $\gamma = 0.30$ and 0.35 the increase is in the range of 0.4 to 0.9 nm , with the tendency of a larger effect for the more hydrophilic polymers.

This effect, shown for $\gamma = 0.35$ in figure 5.14 is comparable to the results BYELOV *et al.* reported for microemulsion systems containing homo and diblock copolymers. For the diblock copolymers they observed an increase of ξ while the domain size d was not influenced [2].

The same observation is made for the bending rigidity κ_{TS}, calculated from the fit parameters of the

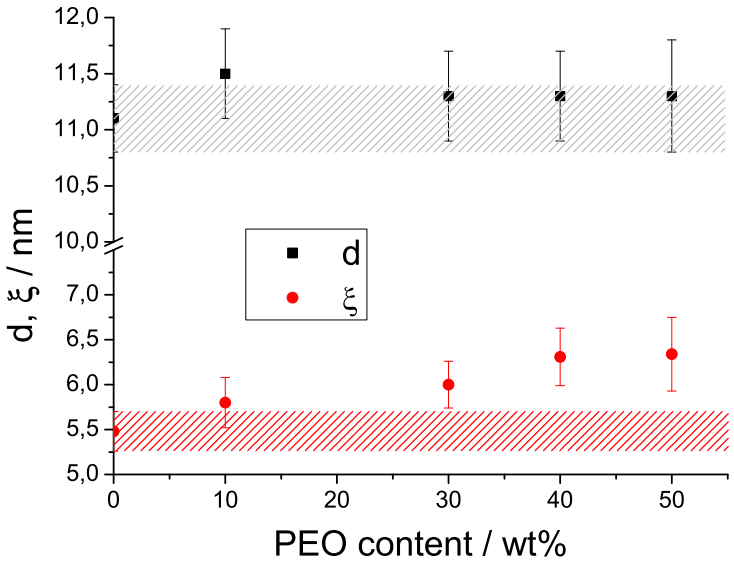

*Figure 5.14: d and ξ calculated from the scattering patterns in the system water / Lanol 99 / $C_{12/14}G_{1.3}$(**S2**) / n-pentanol at constant $\alpha = 0.5$, $\gamma = 0.35$, $\delta = 0.0875$ and $\epsilon = 0.05$. The resulting length scales are plotted versus the PEO content in the polymers. Upon addition of F108 lamellar phases occurred at $\gamma = 0.35$, therefore no sample containing F108 was measured. Within the error bars, d is not increased compared to the pure system, while ξ increases upon polymer addition.*

TS- approximation. Only for the samples with the highest surfactant content and hence the highest polymer content related to the overall mass, the bending rigidity is slightly increased.

Among the series **S2** polymers the composition of the polymers changes. Therefore the variation of the size of the PEO- and PPO-blocks changes the solubility of the polymer in the water and oil phase. These changing solubilities at $\gamma = 0.25$ lead to different polymer concentrations at the interface, resulting in larger variations in d and ξ. At higher surfactant and polymer concentration this effect is reduced as water and oil phase are saturated.

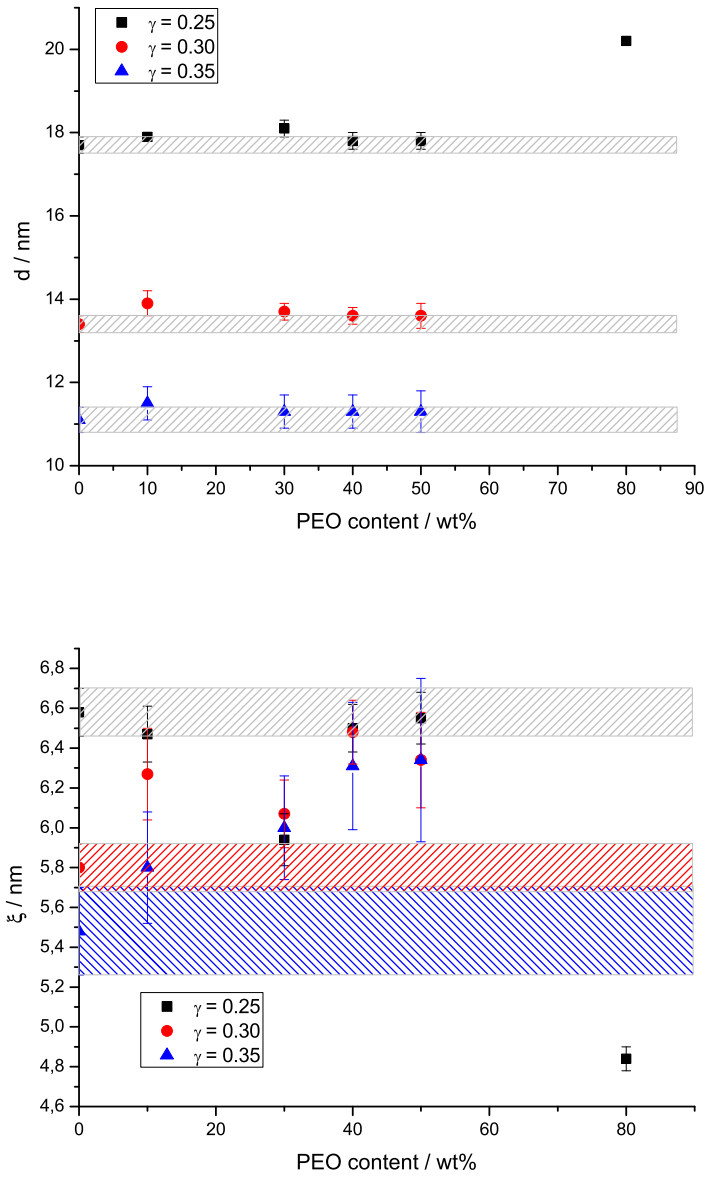

Figure 5.15: Results of the TS analysis for ***S2****: top domain size d plotted versus PEO content of the polymer (0 for pure system). Except F108 (80 wt% PEO), the domain size does not change within the error bars upon polymer addition. bottom: correlation length ξ plotted versus PEO content. At low γ values no clear trend is observed, with increase of γ, ξ rises with PEO content of the polymer. For F108 at γ = 0.25 the ξ value is significantly lowered.*

Series 3

Applying the highly effective polymers of the series **S3** changes the phase behaviour of the microemulsion systems dramatically. The SAXS experiments were again performed at $\gamma = 0.25, 0.30$ and 0.35. The F108 containing microemulsion shows an extended lamellar phase at γ values above $\gamma = 0.28$, so only the sample at $\gamma = 0.25$ was measured. For similar reasons no data is available for F88 at $\gamma = 0.35$.

*Table 5.5: Results of the TS-Analysis of the SAXS-data in the system water / Lanol 99 / $C_{12/14}G_{1.3}$ (**S3**) / n-pentanol at constant $\alpha = 0.5$ and $\delta = 0.0875$.*

	$\gamma = 0.25$		$\gamma = 0.30$		$\gamma = 0.35$	
	d in nm	ξ in nm	d in nm	ξ in nm	d in nm	ξ in nm
pure	17.7	6.7	13.4	5.7	11.1	5.5
F38	19.3	5.6	14.4	5.4	11.6	5.1
F68	18.7	6.2	14.4	5.5	11.6	4.9
F88	19.2	5.6	14.6	4.9	lamellar	
F108	20.2	4.8	lamellar			

The influence of the large hydrophilic polymers on the internal structure of the microemulsion is completely different compared to the observations with the less efficient polymers of series **S2**. While with **S2** the domain size did not show significant changes and only at high γ values ξ increased upon polymer addition. All of the **S3** polymers increase d and reduce ξ. This is a result of the Ḥ growing structure sizes, as 5% less surfactant is available to form the internal film. The same effect is observable within the series **S2**, but in case of the **S3** polymers the increase of d is constantly higher and dH rising from F68 to F108 at $\gamma = 0.25$. At higher γ values the overall surfactant content in the microemulsion is higher, reducing this effect. As shown in figure 5.16, among the highly efficient polymers (F68 to F108) d rises with the molecular weight of the polymer, while the correlation length ξ is reduced. In SAXS experiments we are only able to see the water domains and the polar headgroups of the sugar surfactants due to their higher electron densities compared to the oil phase [4]. This may be a result of a swelling of the water phase due to the large hydrophilic PEO chains. This effect might be superimposed by the rendering of the water domains by the soluble polymers. But as the effect is higher with the heavy polymers applied, which additionally show an extended

formation of lamellar phases at higher surfactant content, we expect the amphiphilic polymers being part of the internal surfactant film. Interestingly, the highest effects are reached with less molecules, as the mass fraction of the added polymer remains equal while the molecular mass increases from 8400 g/mol for F68 to 14600 g/mol in case of F108.

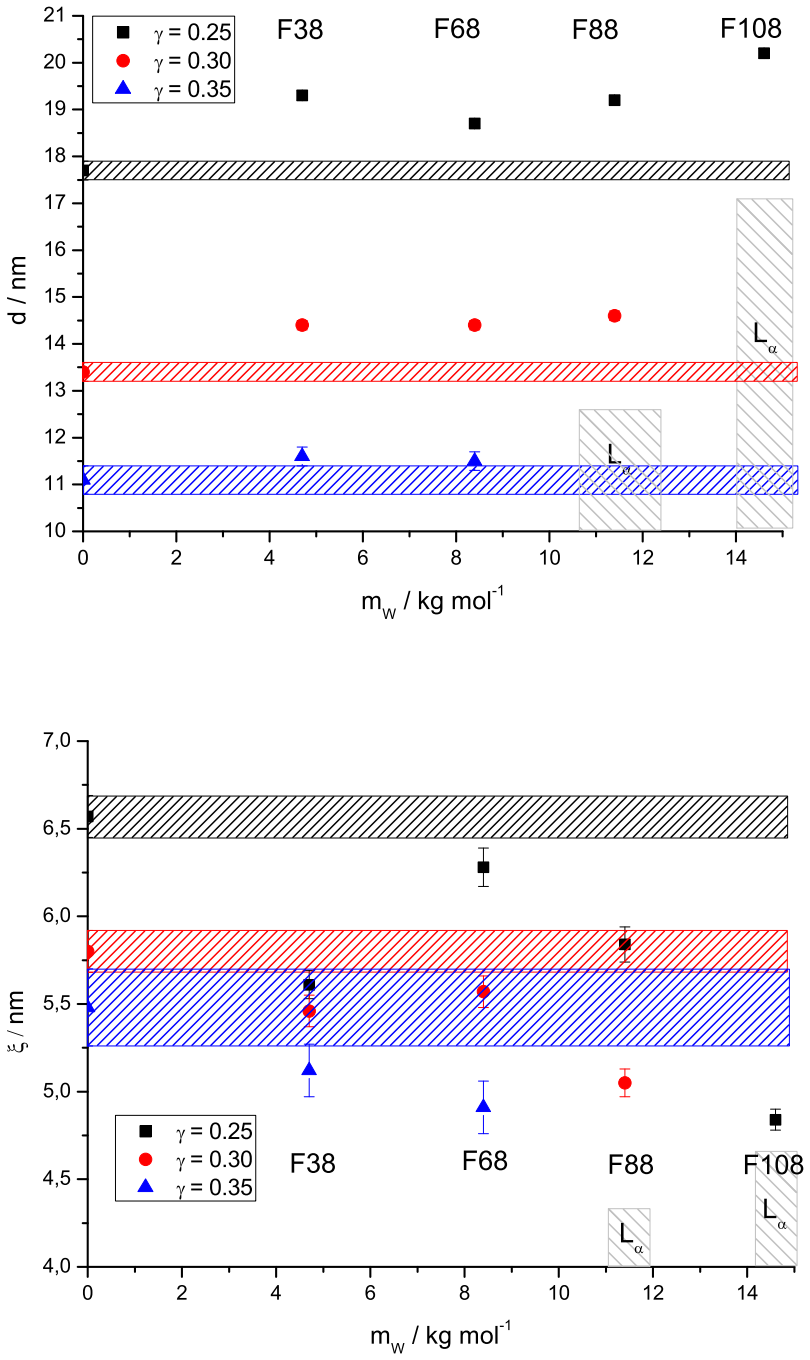

*Figure 5.16: Results of the TS analysis for series **S3**. top: Domain size d plotted versus the mass m_W of the Pluronic polymer. In all cases the polymers increase the domain size compared to the pure system. bottom: Correlation length ξ plotted versus the molar mass m_W of the used Pluronic polymer. The correlation length of the samples containing Pluronics is shorter than in the pure system.*

5.4 Microemulsion dynamics: results of the PCS experiments

The center of mass diffusion of droplet structures, the more complex dynamics of worm-like micelles, and also the collective motion of bicontinuous microemulsions can be studied by DLS [6]. This so called breathing mode is a result of the overall motion of the oil and water domains. As no droplet structures occur, the Stokes-Einstein equation cannot be applied to calculate a length scale. In the present case the change in the collective diffusion coefficient D of the bicontinuous phases was studied as a function of the polymer architecture.

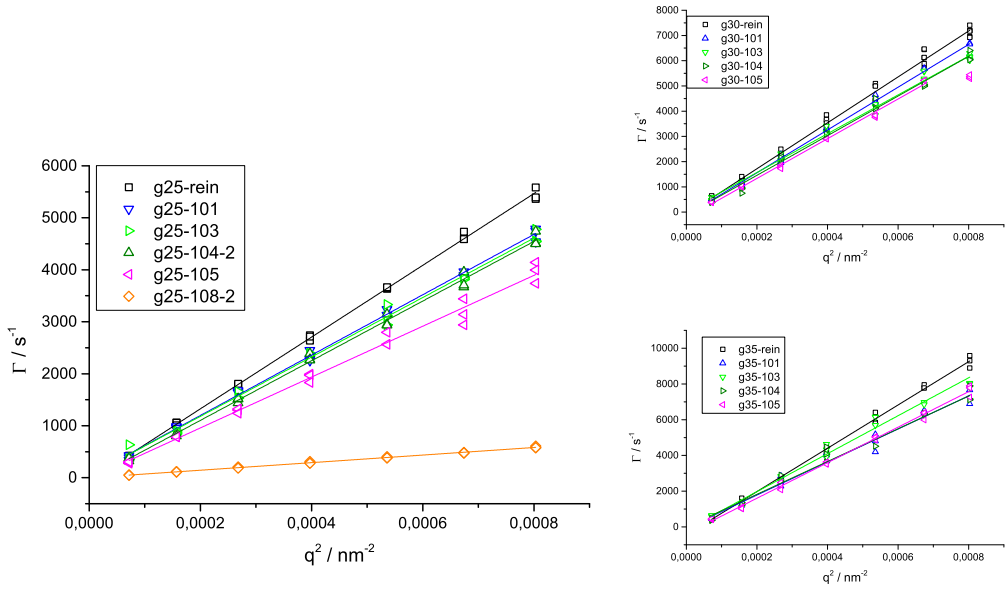

Figure 5.17: Results of the CONTIN analysis of the PCS measurements at 293.25 K of series ***S2****. Plots of the mean relaxation mode* Γ *versus the squared scattering angle* q^2*. All samples were composed at* $\alpha = 0.5$ *and* $\delta = 0.0875$*.* γ *is increased from* $\gamma = 0.25$ *(left side), the right side shows the results at* $\gamma = 0.30$ *(top) and* $\gamma = 0.35$ *(bottom). Solid lines are linear fits to the data. The linear relationship indicates purely Fickian diffusion as the dominant collective dynamics of the bicontinuous samples.*

First of all it can be observed that all polymers reduce the mean relaxation rates Γ. In figure 5.17, where the results of the CONTIN analysis are plotted versus q^2 resulting from the scattering angle the reduction of the collective diffusion coefficient as the slope of the linear fit is evident. As shown in figure 5.18, this effect is small for the inefficient polymers of series **S2**. Here, the collective diffusion coefficient is plotted versus the EO-content of the polymer for three different γ-values of

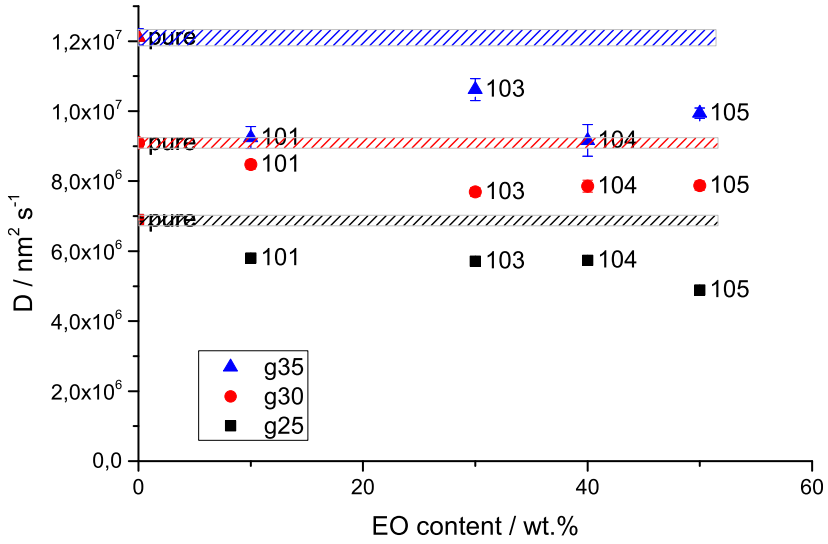

*Figure 5.18: Collective diffusion coefficients D for the series **S2** Pluronics - Simulsol sytem at $\gamma = 0.25, 0.30$ and 0.35 plotted versus the Pluronic PEO-content. The range of the dynamic correlations increases with growing PEO content of the used polymer.*

$\gamma = 0.25, 0.30$ and 0.35.

The **S3** polymer series, with a PEO content of 80 wt%, lead to a stronger reduction of the mean relaxation rate at q^2 (see figure 5.19). By increasing the amount of interfacial film structural sizes inside a bicontinuous microemulsion are decreased. This also applies to the range of the dynamic correlations which cause the decay of the DLS intensity correlation functions. Hence, D increases with γ.

In figure 5.20 the resulting collective diffusion coefficients at $\gamma = 0.25$ of the **S2** polymer series in comparison with the highly efficient polymers of series **S3** are shown. The decrease of the diffusion coefficients with increasing polymer size indicate an increase of the dynamic correlation length. Here, the **S3** polymers have a larger influence on D. That is, most likely, a result of their stronger interaction with the amphiphilic film. The polymers are embedded as a part of the internal film and dramatically reduce the motion due to the enlarged coils. This effect is closely connected to the size of the polymer, which is shown in figure 5.21, where D is plotted versus the molecular weight of the polymers.

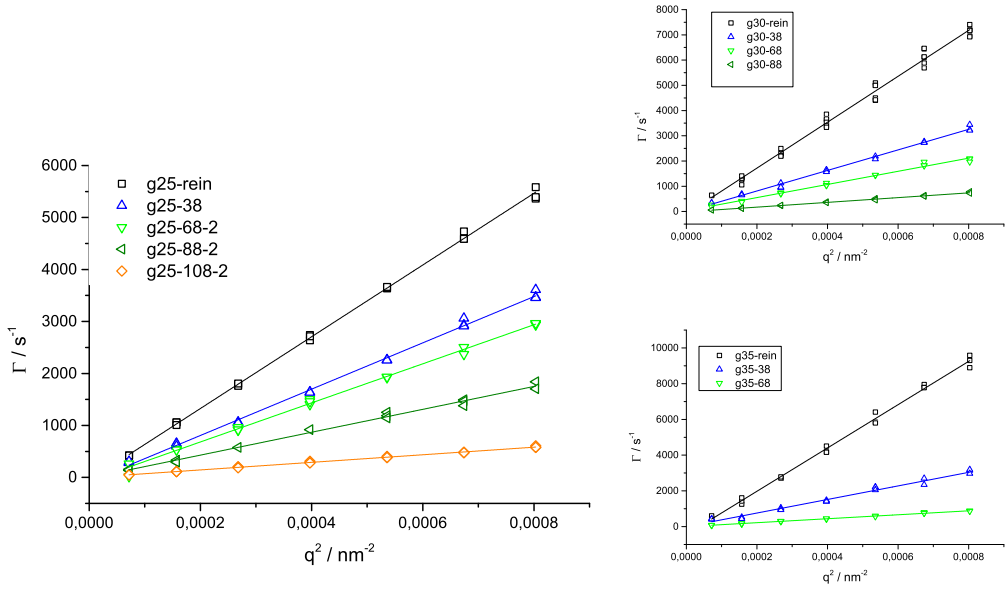

*Figure 5.19: DLS measurements of series **S3**, plots of* Γ *versus* q^2*. All samples were composed at* $\alpha = 0.5$ *and* $\delta = 0.0875$*.* γ *is increased from* $\gamma = 0.25$ *(left side), the graphs on the right side show the results at* $\gamma = 0.30$ *(top) and* $\gamma = 0.35$ *(bottom). In case of F108 the samples with* $\gamma \geq 0.30$ *and for F88 the samples with* $\gamma \geq 0.35$ *are lamellar and therefore not measured. Again purely Fickian diffusion is observed.*

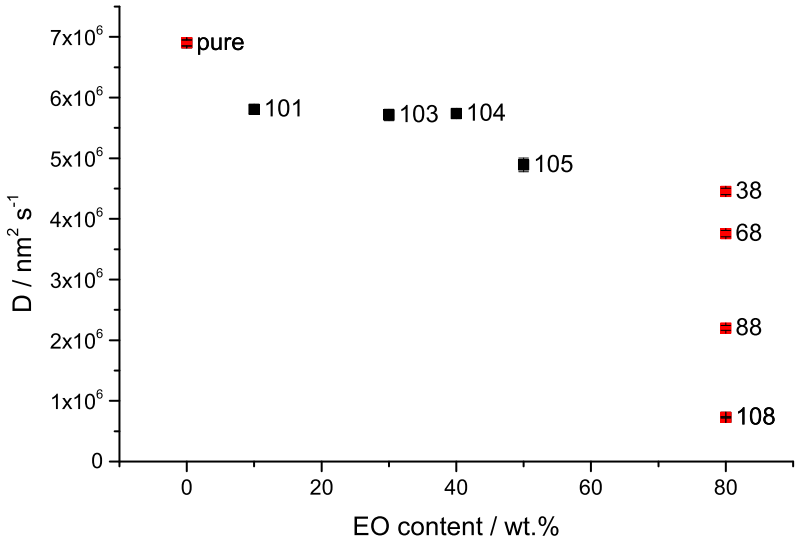

*Figure 5.20: PCS diffusion coefficients D of the Simulsol system at $\gamma = 0.25$ for the series **S2** and **S3** Pluronics plotted versus the Pluronic PEO-content. For all Pluronics containing 80 wt.% EO, the resulting dynamic correlations grows stronger with the increasing molar mass of the used polymer at constant PEO content in series **S3**.*

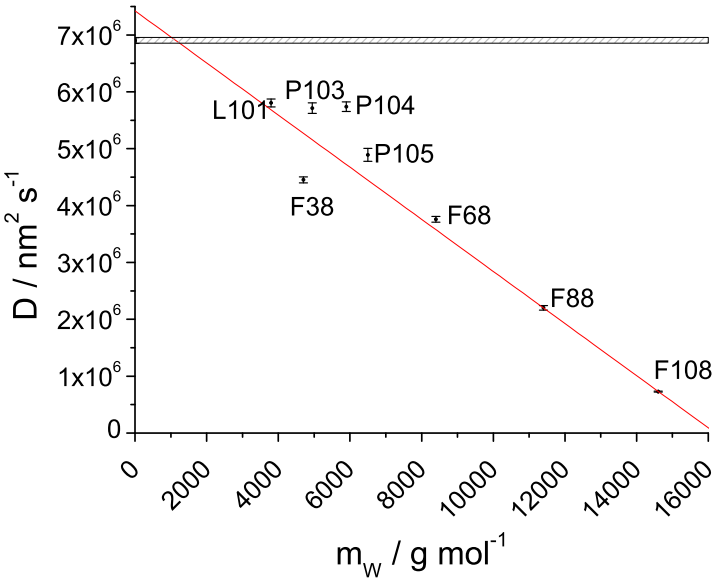

*Figure 5.21: Collective diffusion coefficients D of the Simulsol based system at $\gamma = 0.25$ for the series **S2** and **S3** Pluronics plotted versus the average molecular mass m_W of the polymers. The decrease of D is linearly connected to the size of the Pluronic polymer, as indicated by the red line.*

5.5 Conclusion

In the technical microemulsion system water / Lanol 99 / Simulsol SL55 / n-pentanol the usage of Pluronic polymers offers an interesting possibility to tune the phase behaviour and the size of the structures. All of the applied polymers showed an influence on the phase behaviour of the investigated microemulsion system. The PEO-content of the polymer and the molar mass of the polymer were the parameters identified as relevant for the shift of the X-point. The Pluronic polymers with a low PEO content decrease the efficiency of the surfactant, and therefore lead to a shift in $\tilde{\gamma}$ to higher values. In the series **S1** and **S2** the change in the polymer composition to a higher amount of PEO had a stimulating effect on the surfactant efficiency. The $\tilde{\gamma}$ values shifted to lower values, the best results were obtained for the polymers with a PEO-content of 80 wt.%. Regarding the polymer size, an increase of the overall polymer size usually leads to a higher surfactant efficiency. In all cases the amount of co-surfactant needed to form a bicontinuous structure was found at higher $\tilde{\delta}$ values compared to the pure system. Upon addition of the polymers with high EO-content (S3), the solubilisation capacity of the sugar surfactant is increased. Here, the lowest surfactant demand at the X-point $\tilde{\gamma}$ at $\epsilon = 0.05$ was reached upon addition of F88, where a bicontinuous microemulsion phase was formed with 63% less surfactant than in the pure system. This was achieved by addition of approximately 0.725 wt% polymer to the microemulsion. At high γ values, the larger polymers of series **S3** induce the formation of extended lamellar phases reducing the available bicontinuous region. Therefore the best results were archived upon addition of F68, which increases the surfactant efficiency comparable to F88 and F108, without the formation of extended lamellar phases.

The internal sizes, as estimated by SAXS experiments showed only a small influence upon polymer addition. The domain size d is slightly increased when the less efficient Pluronics of series **S2** are added, the correlation length ξ is increased. The series **S3** polymers increase d compared to the pure system, by a reduction of ξ. By the integration of the large polymers, the motion of the membranes is significantly reduced. The reduction of D can be connected to the mass of the polymer added to the microemulsion system.

These findings are interesting for application, as the tuning of the microemulsion system can be done by simply adding small amounts of Pluronic polymer. The resulting saving of sugar surfactant will lead to cost reduction on the one hand. On the other hand an increase of the microemulsion stability can be reached, when the composition is kept at constant γ values and polymer is added.

In all experiments the samples containing the series **S3** polymers showed an extended long time stability and some of the samples composed close to the X-point were still bicontinuous after several month up to a time scale of 4 years. In case of the usage of pre-mixed microemulsion systems for decontamination purposes this increase of the long time stability even of samples composed close to the phase boundaries is an important feature, as the storage time is one of the central requests for decontamination media.

Upon the results of the SAXS and PCS experiments one has to keep in mind that we are dealing with technical grade systems, exhibiting a wide variation in the composition of both, surfactant and polymer. According to our experience, the results differ from batch to batch, therefore the results presented in this work are based on experiments with the same batch. Differences are in the range of approximately 0.2 to 1.5 nm in the domain-size and correlation length, depending on the composition of the technical compounds. The borders of the phase diagrams may shift by 0.005 in δ and γ, all presented phase diagrams in this work were recorded at least twice.

5.6 References

[1] D. Byelov et al. “Microemulsion Efficiency Boosting and the Complementary Effect. 1. Structural Properties”. In: *Langmuir* 20 (2004), pp. 10433–10443.

[2] D. Byelov et al. “SANS studies of polymer efficiency boosting in microemulsions - diblock copolymers versus homopolymers.” In: *Physica B,* 350 (2004), pp. 931–933.

[3] *Ganesha - Small Angle X-Ray Scattering instrument.*

[4] O. Glatter et al. “Sugar-Ester Nonionic Microemulsion: Structural Characterization”. In: *Journal of Colloid and Interface Science* 241 (2001), pp. 215–225.

[5] T. Hellweg. “Microemulsions”. In: ed. by C. Stubenrauch. Wiley VCH, 2009. Chap. 2. Scattering Techniques to Study the Microstructure of Microemulsions, pp. 48–83.

[6] T. Hellweg and R. von Klitzing. “Evidence for polymer-like structures in the single phase region of a dodecane-C12E5-water microemulsion: a dynamic light scattering study”. In: *Physica A: Statistical Mechanics and its Applications* 283.3-4 (2000), pp. 349–358.

[7] T. Hellweg, R. Stehle, and C. Schulreich. *Herstellung von Struktur-Wirkungsbeziehungen für Mikroemulsionen zur Dekontamination*. 2009.

[8] T. Hellweg et al. “Shape fluctuations of microemulsion droplets: a neutron spin-echo study”. In: *Colloids and Surfaces A: Physicochemical and Engineering Aspects* 183-185 (2001), pp. 159–169.

[9] B. Jakobs. *Amphiphile Blockcopolymere als ’Efficiency Booster’ für Tenside: Entdeckung und Aufklärung des Effektes*. Cuvillier Verlag Goettingen, 2001.

[10] M. Kahlweit and R. Strey. “Phase Behavior of Ternary Systems of the Type H2O - Oil - Nonionic Amphiphile (Microemulsions)”. In: *Angewandte Chemie International Edition in English* 24.8 (1985), pp. 654–668.

[11] M. Kahlweit et al. “General patterns of the phase behavior of mixtures of water, nonpolar solvents, amphiphiles, and electrolytes. 2”. In: *Langmuir* 5.2 (1989), pp. 305–315.

[12] M. Kahlweit et al. “How to study microemulsions”. In: *Journal of Colloid and Interface Science* 118.2 (1987), pp. 436–453.

[13] C. Schulreich et al. “Bicontinuous microemulsions with extremely high temperature stability based on skin friendly oil and sugar surfactant”. In: *Colloids and Surfaces A: Physicochemical and Engineering Aspects* 418 (2013), pp. 39–46.

[14] R. Stehle et al. “An enzyme containing microemulsion based on skin friendly oil and surfactant as decontamination medium for organo phosphates: Phase behavior, structure, and enzyme activity”. In: *Journal of colloid and interface science* 413 (2014), pp. 127–132.

[15] S. Wellert et al. “Structure of biodiesel based bicontinuous microemulsions for environmentally compatible decontamination: A small angle neutron scattering and freeze fracture electron microscopy study”. In: *J.Colloid Interf.Sci.* 325.1 (2008), pp. 250–258.

[16] S. Wellert et al. “Temperature dependence of the surfactant film bending elasticity in a bicontinuous sugar surfactant based microemulsion: a quasielastic scattering study”. In: *Physical Chemistry Chemical Physics* 13.8 (2011), pp. 3092–3099.

Chapter 6

The influence of Pluronics on the dynamics of the amphiphilic film: The $C_{10}G_2$ system

For the better understanding of the influence of single components applied to the existing technical systems, a model system was investigated. Instead of a technical surfactant mixture with varying composition, the pure sugar surfactant n-decyl-β-D-maltoside ($C_{10}G_2$) was used. The oil phase was changed to cyclohexane, as it is available also as cyclohexane-d12, offering the possibility of applying film contrast for SANS and NSE experiments. In this chapter we focus on the model system water - cyclohexane - $C_{10}G_2$ - n-pentanol or partly deuterated variations thereof and the influence of different Pluronic polymers, showing high efficiency boosting in the technical system based on SL55.

6.1 Phase behaviour

Compared with the technical grade sugar surfactants, which are mixtures of APG with varying alkyl chain length and different glucosidical head groups, the phase behaviour of a pure sugar surfactant shows usually a smaller **1** phase region. This is shown exemplarily in chapter 3, figure 4.1, where the phase behaviour of $C_{12}G_1$ [1] is compared with technical grade SL 55 ($C_{12/14}G_{1.3}$). Here, both

[1] Phase diagram recorded in cooperation with R. Neubauer and C. Schulreich.

microemulsion systems contain water, cyclohexane as oil phase at $\alpha = 0.5$ and n-pentanol as co-surfactant, these differences are clearly visible. Due to the mixture of different surfactants, the technical grade surfactant mixture is more efficient, the X-point is located at $\tilde{\gamma}_{SL55} = 0.10$ and $\tilde{\delta}_{SL55} = 0.0175$, in case of the pure surfactant $\tilde{\gamma}_{C_{12}G_1} = 0.16$ and $\tilde{\delta}_{C_{12}G_1} = 0.04$. Comparable behaviour is observed by other pure sugar surfactants investigated in our group, they are less efficient and tend to exhibit extensive lamellar phases. For detailed information see the works of NEUBAUER and SCHULREICH [15, 18].

6.1.1 $C_{10}G_2$ system

Compared to the technical grade SL55, $C_{10}G_2$ is an efficient surfactant although it requires a high amount of co-surfactant. The X-point is located at $\tilde{\gamma}_{C10G2} = 0.08$ and $\tilde{\delta}_{C_{10}G_2} = 0.095$. For comparison, the X-point of the technical system water / cyclohexane / SL55 / 1-pentanol is located at $\tilde{\gamma}_{SL55} = 0.09$ and $\tilde{\delta}_{SL55} = 0.015$.

The size of the hydrophilic head group is increased, combined with the slightly reduced alkyl chain length. This results in a much better usability of the surfactant, which compared to $C_{12}G_1$ is easy to dissolve even at higher concentrations. But, as a result of the homogeneity of the surfactant molecules the **1** phase region comprises by an extended $L_{\alpha,2\Phi}$ phase, at $\gamma = 0.20$ a $L_{\alpha,1\Phi}$ appears in the middle of the $L_{\alpha,2\Phi}$. The resulting cut through the phase tetrahedron in the system water / cyclohexane / $C_{10}G_2$ / 1-pentanol at $\alpha = 0.5$ is given in figure 6.1.

6.1.2 Deuteration effects

As mentioned before, neutron scattering is a powerful tool for the investigation of nano-scale structures, as the contrast of the systems can easily be modified by deuteration of the components. Here, two different contrasts were applied. In the bulk contrast, water is replaced by D_2O, while the oil phase and the amphiphiles are used in their protonated form. In this case, the change in the scattering length density due to deuteration leads to an increase in the contrast between the D_2O phase on the one side and the amphiphilic film and the oil phase on the other. Therefore, the periodicity of the two major bulk phases in the microemulsion system can be detected. The second contrast is the film contrast, were H_2O is replaced by D_2O and the oil phase C_6H_{12} by C_6D_{12}. If the scattering length densities of the aqueous and the oil phase are comparable, the measured signal is correlated to the periodicity of the amphiphilic film consisting of the surfactant, co-surfactant, and the polymer

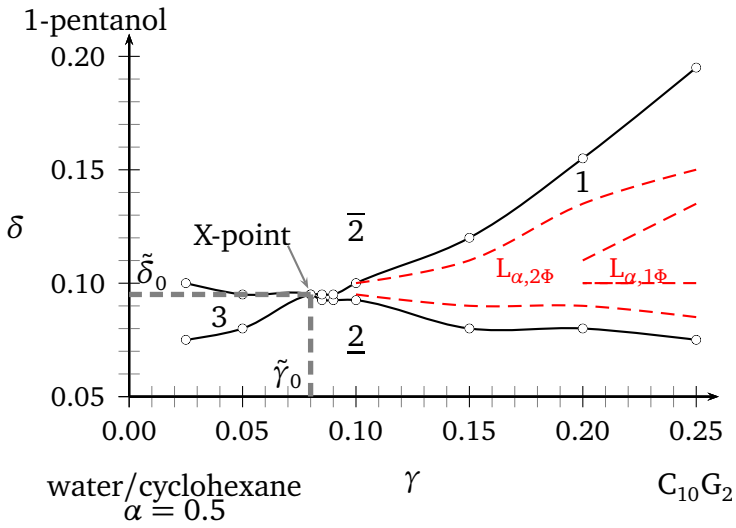

Figure 6.1: Cut through the phase tetrahedron of the system water/cyclohexane/$C_{10}G_2$/n-pentanol at a constant oil-water ratio of $\alpha = 0.5$ and 293 K.

molecules. One disadvantage of the H-D exchange is the change of the system composition and the resulting influence on the phase behaviour which we observed. The phase diagrams of the systems D_2O / cyclohexane / $C_{10}G_2$ / 1-pentanol and D_2O / C_6D_{12} / $C_{10}G_2$ / 1-pentanol are shown in figure 6.2 at a constant $\alpha = 0.5$. Here, two sets of cuts through the phase tetrahedrons are shown. On the left hand side the pure sugar surfactant, on the right hand side the surfactant consisting of 95% $C_{10}G_2$ and 5% Pluronic F68. In the following the phase boundaries of the pure systems containing water / cyclohexane / $C_{10}G_2$ / 1-pentanol are shown in gray. Replacement of water by D_2O increases the hydrophobicity of the surfactant [6, 20] and leads to the phase behaviour indicated by the blue lines. The overall co-surfactant amount needed to form a stable microemulsion is reduced, that means that the upper and the lower phase boundaries are shifted to lower δ values. For $\tilde{\gamma}$ a marginal increase is observed. This behaviour is comparable to the shift of the phase inversion temperature $\tilde{T}$ observed with C_iE_j-surfactants [6]. Usually these findings are described as an effect of the reduced number of water molecules and the change in the intermolecular forces, as in D_2O the strength of O-D bonds is higher than the one of O-H bonds. If the hydration number stays constant in water and D_2O, the distances between the D_2O molecules are significantly lowered, leading to a more dense packing and therefore a smaller hydration shell of the hydrophilic head group [23, 5, 4, 16]. Replacement of H_2O by D_2O has no significant influence on the large L_α region in the pure

system, as the lamellar region is already very large close to the X-point, as indicated by the scattered lines. In the system with F68 no lamellar phase occurs in the investigated region up to $\gamma = 0.10$, neither in the system with water nor in the D_2O-based one.

For SANS measurements in film contrast, the systems consist of D_2O / C_6D_{12} / amphiphile / 1-pentanol. The respective phase diagram of the polymer free system is shown in figure 6.2 (left). In figure 6.2, the relevant phase boundaries are indicated by the red lines. The right hand side of figure 6.2 shows the phase diagram for the film contrast sample in the presence of F68. The amount of cosurfactant $\tilde{\delta}$ is lowered again, which is more pronounced in the case of the F68-containing system. In the pure system the **1** phase region is again dominated by an extended $L_{\alpha,2\Phi}$. Therefore, only a small bicontinuous region is available for sample preparation close to the X-point. With 5% F68 only a small lamellar phase is formed at $\gamma = 0.10$. This is interesting, as the non-deuterated system shows an extended **1** phase region up to $\gamma = 0.15$. The resulting positions of the X-points are summarized in table 6.1.

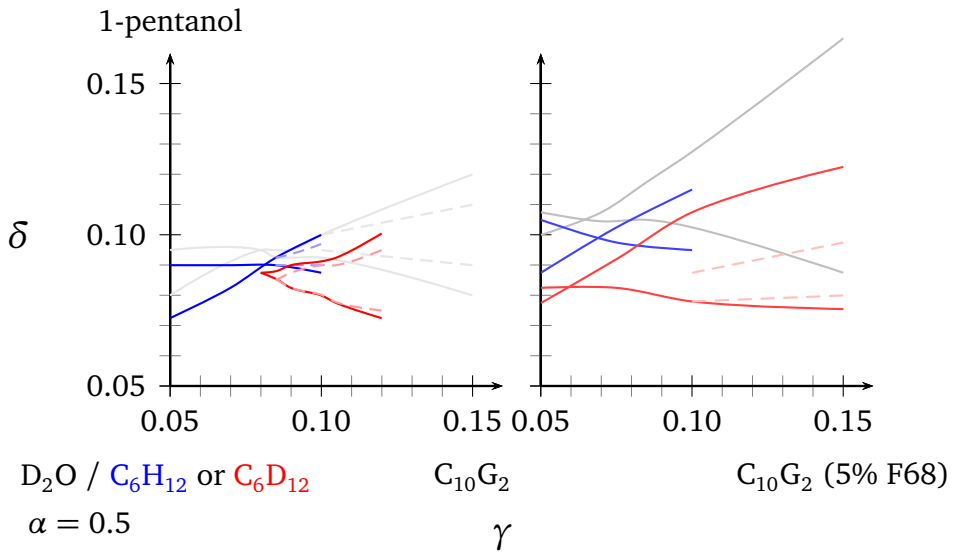

Figure 6.2: Effect of the usage of deuterated solvents on the phase behaviour shown in different cuts through the phase tetrahedron of the $C_{10}G_2$ - system at a constant $\alpha = 0.5$ and 293 K. The pure systems are shown in gray, for $C_{10}G_2$ on the left side, the system containing 5% F68 on the right. Bulk contrast (blue lines): Water phase is replaced by D_2O, the oil phase is C_6H_{12}. Film contrast (red lines): Oil and water phase deuterated, the systems consist of D_2O / C_6D_{12} / amphiphile / 1-pentanol.

Table 6.1: Influence of the deuteration of the solvents on the position of the X-Points in the pure $C_{10}G_2$ system and the system $C_{10}G_2$ (5%F68). The values for D_2O with C_6H_{12} are estimations, only few samples were used to investigate the phase behaviour.

surfactant	solvent	$\tilde{\gamma}$	$\tilde{\delta}$
$C_{10}G_2$	H_2O, C_6H_{12}	0.080	0.095
	D_2O, C_6H_{12}	0.082	0.090
	D_2O, C_6D_{12}	0.081	0.088
$C_{10}G_2$ (5%F68)	H_2O, C_6H_{12}	0.065	0.105
	D_2O, C_6H_{12}	0.069	0.099
	D_2O, C_6D_{12}	0.060	0.083

6.1.3 Effect of Pluronics

As shown in figure 6.1, the phase behaviour of the system water / cyclohexane / $C_{10}G_2$ / n-pentanol is dominated by extended lamellar phases. Here, the region of the fish tail is almost completely covered by an extensive $L_{\alpha,2\Phi}$ region, existing already at low γ values close to the X-point. At $\gamma \geq 0.20$, a $L_{\alpha,1\Phi}$ rises. Hence sample preparation close to the X-point is difficult, as the **1** phase bicontinuous microemulsion is only stable over a very limited δ and γ range. Polymer-addition is reported in the literature as a suppressant to lamellar phases [12, 14], this effect was as well observed in the present work.

In contrast to the phase diagrams of the technical surfactants, the phase diagrams taken with pure sugar surfactant were constructed by extrapolating the phase boundaries of a few samples. Usually between four to six samples were prepared in the γ range of $\gamma = 0.05$ and 0.20, were the X-point was expected. The phase boundaries in areas of higher interest, especially the **1** phase region close to the X-point were investigated more precisely by additionally prepared samples. This method gives a good overview of the phase boundaries and allows a quite precise estimation of the position of the X-point with a maximal error of $\Delta\gamma = \pm 0.005$ based on several samples.

Only Pluronic polymers, which previously showed efficiency boosting abilities were taken into account. Therefore series **S3** (F38, F68, F88 and F108) was investigated completely in the $C_{10}G_2$ based system , the resulting phase diagrams at $\alpha = 0.5$ are presented in figure 6.3. Series **S1** was omitted, and for series **S2** the low efficient polymers L101 and P103 were excluded.

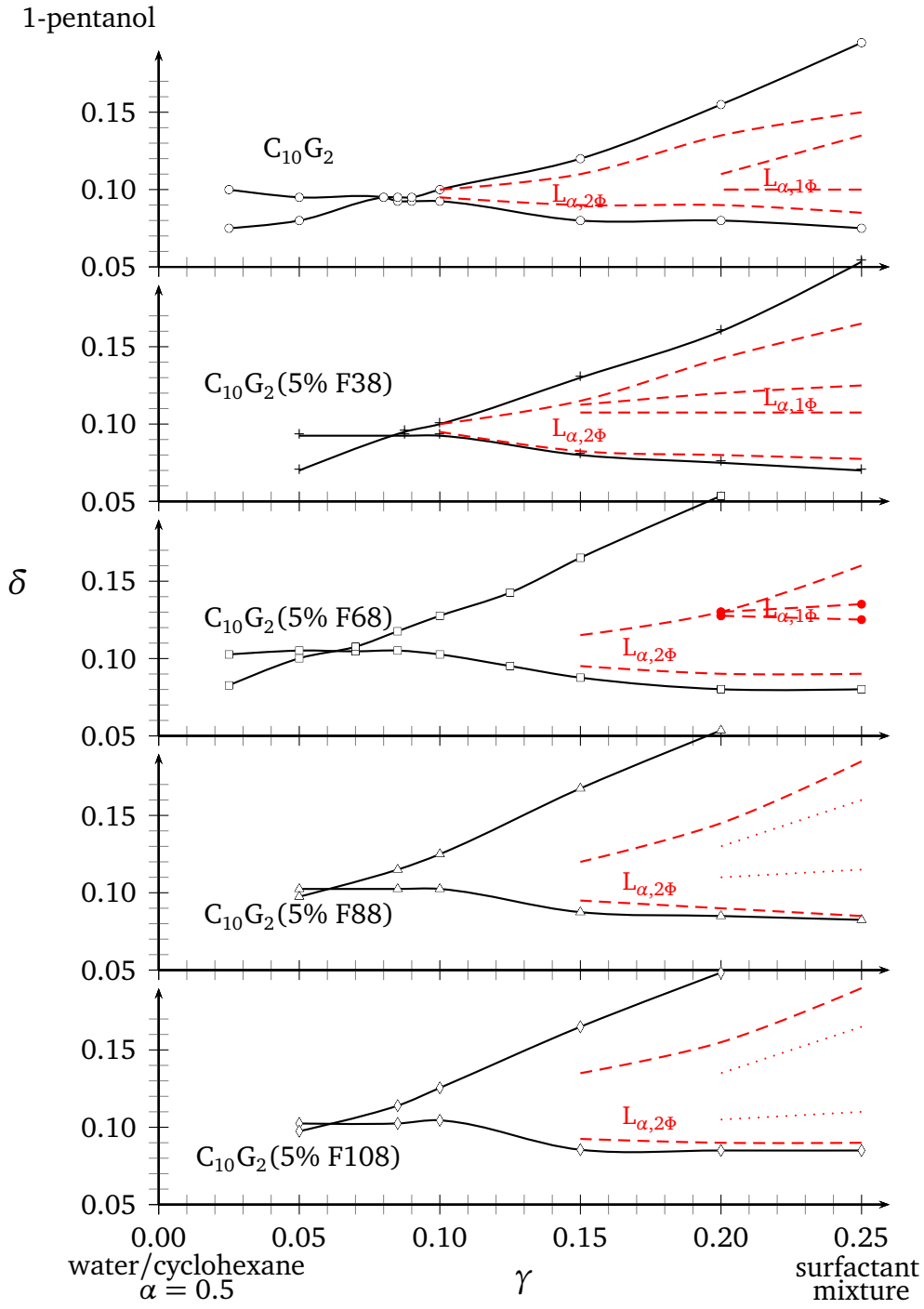

*Figure 6.3: Cut through the phase prism in the system water/cyclohexane/ $C_{10}G_2$/n-pentanol with the series **S3** Pluronics. The major difference is the suppression of the lamellar phases compared to the the pure system which is shown in the top panel. In case of F108 the position of a $L_{\alpha,1\Phi}$ could not be determined, as the samples showed separated regions of high viscosity. Therefore no separation or formation of a homogeneous single phase L_α was observed. The upper phase boundaries are not shown for $\delta > 0.2$.*

*Series **3***

As shown in figure 6.3 the series **S3** polymers all influence the phase behaviour of the pure surfactant $C_{10}G_2$ with cyclohexane in a manner comparable to the technical system SL55 and Lanol99. As in the previous experiments, a polymer content of $\epsilon = 0.05$ was used. $C_{10}G_2$ is a quite efficient surfactant with $\tilde{\gamma} \approx 0.08$, hence no major shift of the X-point was achieved. In the base system the phase behaviour at $\alpha = 0.5$ is dominated by huge lamellar regions, nearly completely suppressing the bicontinuous microemulsion. The $L_{\alpha,2\Phi}$ phase extends almost to the X-point, leaving only a small **1** phase region for sample preparation between $\tilde{\gamma} \approx 0.08$ and $\gamma = 0.095$. At $\gamma = 0.10$, the **1** phase bicontinuous microemulsion is nearly completely suppressed by the rising $L_{\alpha,2\Phi}$. This lamellar phase is covering almost the whole region up to γ values of $\gamma = 0.20$, where another lamellar phase, $L_{\alpha,1\Phi}$ is formed. Only close to the phase boundaries to the $\underline{2}$ and $\overline{2}$ phases, small **1** phase regions are present.

A comparable behaviour is found in the case of F38, the dominant region is the $L_{\alpha,2\Phi}$ two phase region, in contrast to the pure system the $L_{\alpha,1\Phi}$ appears already at $\gamma = 0.15$.

Taking a look at the highly efficient polymers of **S3**, an important change in the phase behaviour is observed. In the systems containing F68, F88 or F108 the efficiency boosting leads to a X-point of $\tilde{\gamma}_{polymer} \approx 0.065 \pm 0.005$ with respect to the precision of the quite rough determination of the phase diagrams. Moreover, we found that these polymers are able to suppress the formation of the lamellar phases. In contrast to the pure system, the efficiency boosted systems show a bicontinuous single phase region up to $\gamma = 0.125$ in case of F68 or at least $\gamma = 0.10$ for F88 and F108. A comparable effect is described in the literature upon the use of amphiphilic diblock copolymers of the A-B type[6, 7]. Again, the expansion of the lamellar phases correlates with the polymer size. At $\gamma = 0.15$ the $\Delta\delta$ range of the $L_{\alpha,2\Phi}$ for F108 is increased compared to the one of F88 and F68. This finding is similar to the one for the technical system described in chapter 5.

*Series **2** and other*

For series **S2** the efficient polymers of the experiments performed with the technical grade surfactant were added to the pure $C_{10}G_2$ system. The phase diagrams of P104, P105 and F108 containing systems are shown in figure 6.4. The polymer P104 has only a slight effect on the phase boundaries, visible in an expansion of the $L_{\alpha,1\Phi}$ down to $\gamma = 0.15$. The X-point is found at $\tilde{\gamma}_{P104} \approx 0.090$, $\tilde{\delta}_{P104} \approx 0.104$. An increase of the PEO-content to 50 wt% reduces the lamellar phases without any significant effect on the X-point position ($\tilde{\gamma}_{P105} \approx 0.085$, $\tilde{\delta}_{P105} \approx 0.104$). In the system containing

P105, at $\gamma = 0.10$ no lamellar phases occur.

Also the addition of the smaller polymer P65 from **S1** suppresses the formation of the extend lamellar phases. The performance is better than in the case of the larger polymers of **S2**, without a significant influence on $\tilde{\gamma}$ ($\tilde{\gamma}_{P65} \approx 0.082$) and only a small increase of the co-surfactant content $\tilde{\delta}_{P65} \approx 0.102$. As an intermediate sized polymer between P65 and P105, P85 with an average molar mass of approximately 4600 g/mol was also applied to the pure $C_{10}G_2$ system (see figure 6.4, center). Here, no such efficient suppression of the L_α phases as in the case of P65 was observed.

Table 6.2: Position of the X-points in the system water / cyclohexane / $C_{10}G_2$(Pluronic) / 1-pentanol and the calculated efficiency boost factors f_B.

polymer name	M (g·mol^{-1})	ω(PEO) wt.%	$\tilde{\gamma}$	$\tilde{\delta}$	f_B
pure	-	-	0.080	0.095	-
P65	3400	50	0.082	0.102	0.51
P85	4600	50	0.078	0.085	1.51
P104	5900	40	0.090	0.104	-1.22
P105	6500	50	0.085	0.104	-0.18
F38	4700	80	0.085	0.093	-0.18
F68	8400	80	0.065	0.105	5.62
F88	11400	80	0.063	0.103	6.40
F108	14600	80	0.061	0.102	7.23

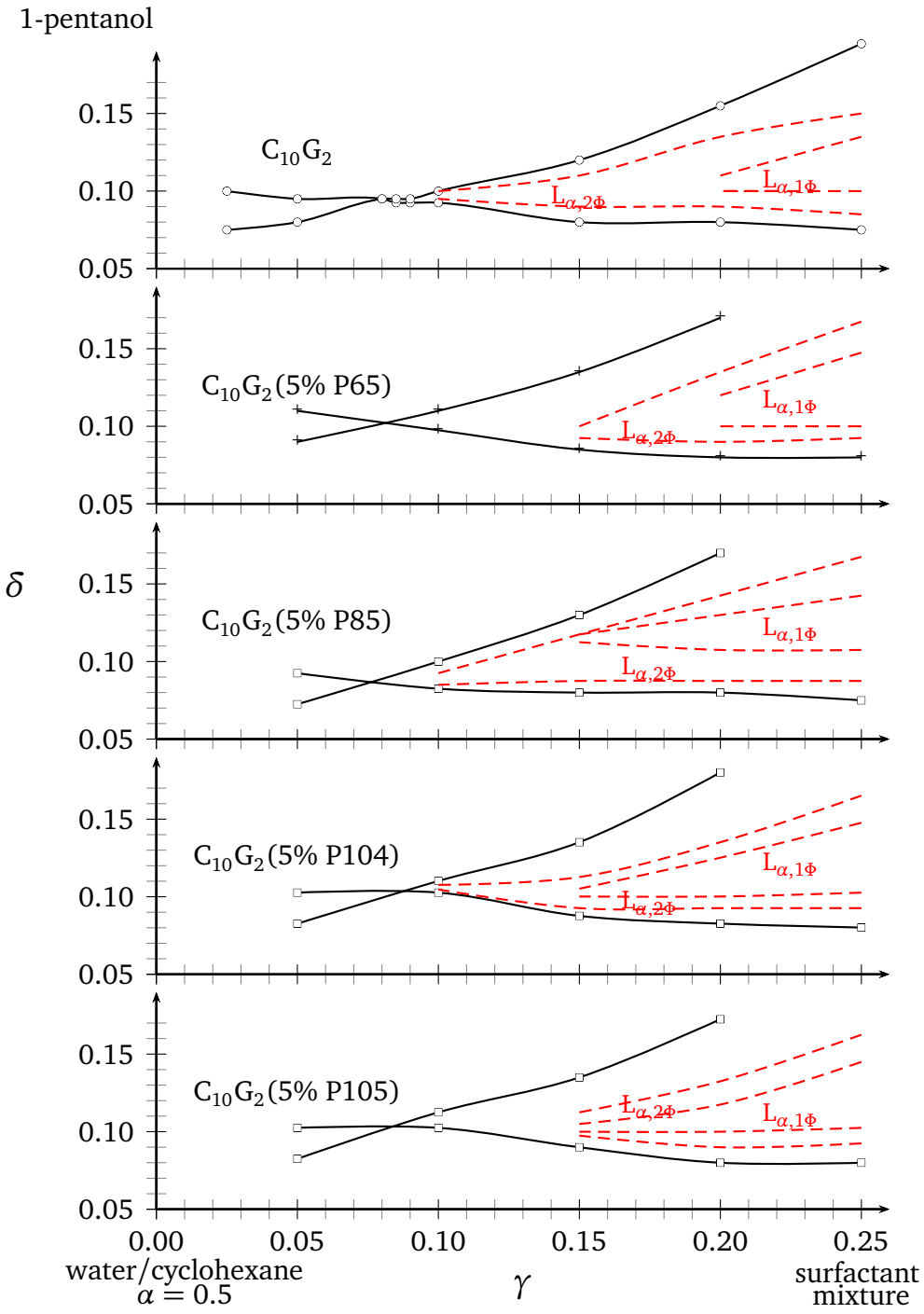

*Figure 6.4: Cut through the phase prism in the system water/cyclohexane/ $C_{10}G_2$/n-pentanol with the more efficient Pluronics of series **S1, S2** and P85. The pure system is shown on the top panel. Again the major effect of the Pluronic addition is the supression of the lamellar phase. This is similar compared to series **3**.*

6.2 Influence on the micro structure

SANS experiments were carried out at the Orphée reactor of the Laboratoire Léon Brillouin (Saclay, France) using the PAXY machine. The experiments were performed at three sample-to-detector distances of 1.255 m, 3.055 m and 6.801 m and at a neutron wavelength of 6 Å with a relative line width of $\Delta\lambda/\lambda = 0.1$. The data were collected with a BF_3 filled XY multidetector of 15500 cells of $5 \times 5\,mm^2$ and a overall size of $64 \times 64\,cm^2$. By replacing the water phase with D_2O the samples were prepared in bulk contrast. Figure 6.5 shows a series of different SANS patterns. The broad structure factor typical for bicontinuous microemulsion is observed in all samples. Solid lines are fits using the TS model performed with Origin using an implemented Levenberg-Marquardt algorithm. The treatment of the raw data such as bad pixel and beamstop masking, desmearing and background substraction was done with the software offered by the LLB [1].

6.2.1 Variation of the polymer content I - X-point

For the variations of the polymer content again F68 was applied, as it has been proven to be the most effective polymer in the previous experiments. The first set of samples of the system D_2O / cyclohexane / $C_{10}G_2$ / 1-pentanol was prepared close to the X-point of the investigated systems. The sample composition and the results of the TS analysis are given in table 6.3. As shown in figure 6.5, the typical broad signal of bicontinuous microemulsions is observed for all samples.

Table 6.3: Sample composition and results of the TS-analysis in the system water / cyclohexane / $C_{10}G_2$(F68) / n-pentanol with increasing polymer content. The bending elastic constant κ_{SANS} is discussed in section 6.2.4.

Polymer name	ϵ	γ	δ	ξ [nm]	d [nm]	κ_{SANS} k_BT
pure	0.0	0.095	0.098	14.25 ± 1.36	35.30 ± 1,39	0.34 ± 0.04
F68	1.0	0.082	0.094	16.05 ± 0.99	42.15 ± 1.13	0.32 ± 0.02
F68	2.5	0.078	0.093	16.29 ± 0.89	44.8 ± 1.07	0.31 ± 0.02
F68	5.0	0.074	0.093	16.37 ± 0.74	47.18 ± 0.92	0.30 ± 0.01
F68	10.0	0.070	0.093	16.43 ± 0.62	53.3 ± 0.79	0.26 ± 0.01

Increasing the F68 content shifts the $\tilde{\gamma}$ values of the systems to lower γ. All samples were prepared

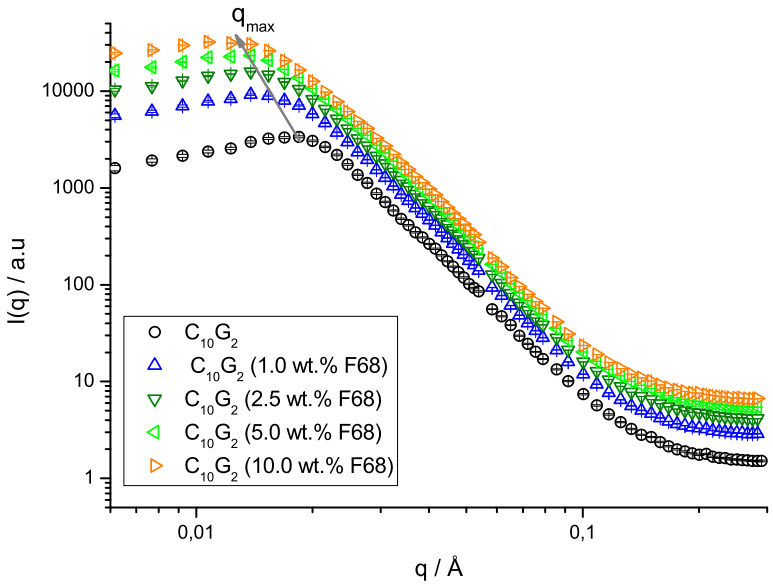

Figure 6.5: SANS pattern of the system D_2O / C_6H_{12} / $C_{10}G_2$ (F68) / 1-pentanol with increasing F68 content. All samples were prepared close to the X-point of the respective microemulsion. Due to the reduction of $\tilde{\gamma}$ the structure sizes grow and q_{max} shifts to lower q-values. The scattering patterns containing polymer are shifted to higher intensities with respect to each other for clarity.

at $\tilde{\gamma} + 0.01$, therefore the amount of surfactant available to form the interfacial layer is reduced with rising ϵ. This reduction leads to a swelling of the domain sizes in the structures resulting in a reduction of q_{max} which is observed in the scattering pattern. Figure 6.6 shows the results of the TS-analysis. Here d and ξ are plotted versus the F68 content (Fig 6.6, *left*) and the overall amphiphile content γ (Fig. 6.6, *right*), respectively. While ξ rises from 14.25 nm to 16.05 nm by replacing 1 wt.% $C_{10}G_2$ by F68, further polymer addition has only a marginal effect. At maximal polymer content of 10 wt.%, a correlation length of $\xi_{10wt\%F68} = 16.43$ nm is reached. In case of the domain size d the effect is larger. Upon polymer addition d rises from $d_{pure} = 35.30$ nm to $d_{1wt.\%\ F68} = 42.15$ nm. As shown by the fit (red line in Fig. 6.6, *right*), the increase of the domain size follows an exponential behaviour.

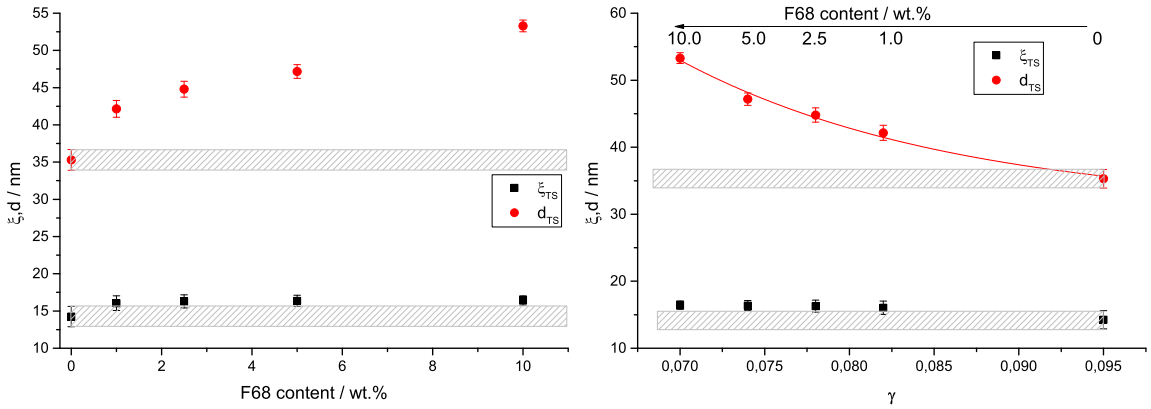

Figure 6.6: left: The obtained d (red circles) and ξ (black squares) values from the TS-analysis plotted versus the polymer content ϵ.

right: The d (red circles) and ξ (black squares) values plotted versus the amphiphile content γ. The gray boxes are a guide to the eye and embed the values of the base system within the errorbars. While the ξ values are only slightly increased, the domain size grows strongly with reduced γ correlating with the reduction of the amphiphilic film. The red line is a single exponential decay fit.

6.2.2 Variation of the polymer content II - Constant composition

At constant composition at $\alpha = 0.5$, $\gamma = 0.105$ and $\delta = 0.102$, five samples with an increasing F68-content were prepared to investigate the influence of the polymer on domain size and correlation length of the microemulsion. The resulting SANS pattern and the d and ξ values received by TS-analysis are shown in figure 6.7. In the surfactant amount the content of F68 was successively increased, starting from pure $C_{10}G_2$ with $\epsilon = 0.00$ up to the final value of $\epsilon = 0.11$. The samples containing 2.5 wt.% F68 show a significant variation in the results. Here, the cap was not sealed properly and cyclohexane evaporated during the experiment.

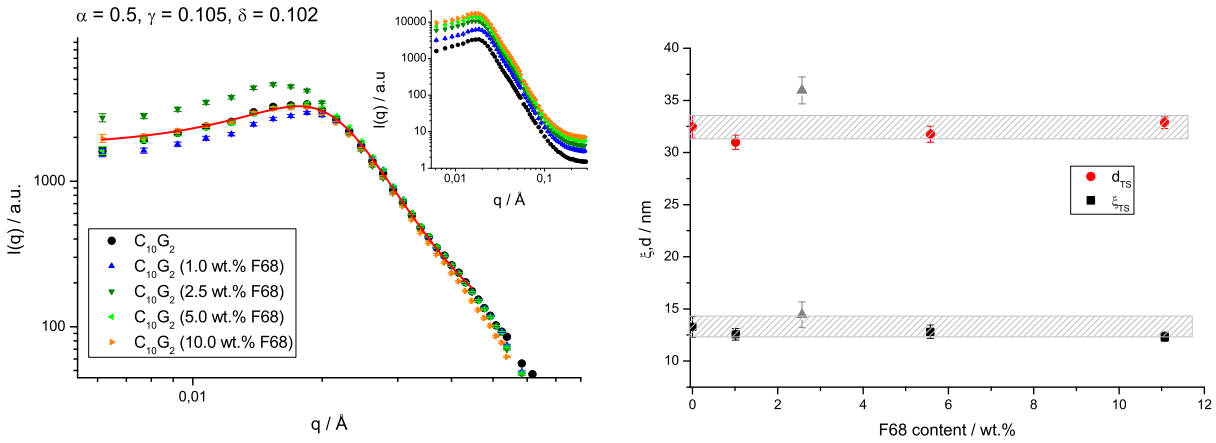

Figure 6.7: above: SANS pattern of the system D_2O / C_6H_{12} / $C_{10}G_2$ (F68) / 1-pentanol with increasing F68 content. All samples were prepared at $\alpha = 0.5$, $\gamma = 0.105$ and $\delta = 0.102$. The inset shows the complete q-range, here the curves are shifted in intensity. The red line is a fit with the TS-formula for the pure system. The sample with $\epsilon = 0.025$ showed phase separation during the experiment.
below: The obtained d (red circles) and ξ (black squares) values from the TS-fit plotted versus the F68 content. The gray boxes enclose the values for the base system within the errorbars.

As the sample was turbid after removal from the sample holder, phase separation occurred during the experiment and the results are excluded from further analysis. In all other samples, the good overlap of the resulting scattering pattern is observed (see Fig. 6.7, *left*). As seen before in the technical system, the addition of small amounts of polymer lead to a slight decrease in the domain size d. When the content of polymer rises, the domain size increases. For the correlation length the contrary effect is observed. Small amounts of polymer reduce the correlation length ξ, this effect is stronger when the amount of polymer is increased. But this influence is marginal in the studied

samples. Therefore, the change of the composition of the internal film had no significant influence on the structure size d or the correlation length ξ. The results of the TS-analysis of the scattering pattern shown in fig 6.7 are given in table 6.4.

Table 6.4: Sample composition and results of the TS-analysis in the system water / cyclohexane / $C_{10}G_2$(F68) / n-pentanol with increasing polymer content. All samples were composed at $\alpha = 0.5$, $\gamma = 0.105$ and $\delta = 0.102$.

Polymer name	ϵ	γ	δ	ξ [nm]	d [nm]	κ_{SANS} k_BT
pure	0.000	0.105	0.102	13.28 ± 1.00	32.45 ± 1.09	0.35 ± 0.03
F68	0.010	0.105	0.102	12.56 ± 0.55	30.99 ± 0.68	0.35 ± 0.02
F68	0.025	0.105	0.102	turbid after measurement		
F68	0.055	0.105	0.102	12.82 ± 0.64	31.76 ± 0.77	0.34 ± 0.04
F68	0.110	0.105	0.102	12.34 ± 0.44	32.68 ± 0.65	0.32 ± 0.01

6.2.3 Series 3, Variation of the polymer size

As shown in figure 6.8, a comparable result is observed upon addition of polymers of similar PEO-content and increasing polymer size. The influence of the different polymers of series **S3** was investigated by replacing 5 wt% of the pure surfactant by the **S3** polymers in the system D_2O / cyclohexane / $C_{10}G_2$ / 1-pentanol at $\alpha = 0.5$, $\gamma = 0.105$ and $\delta = 0.102$. Here again only small variations of the

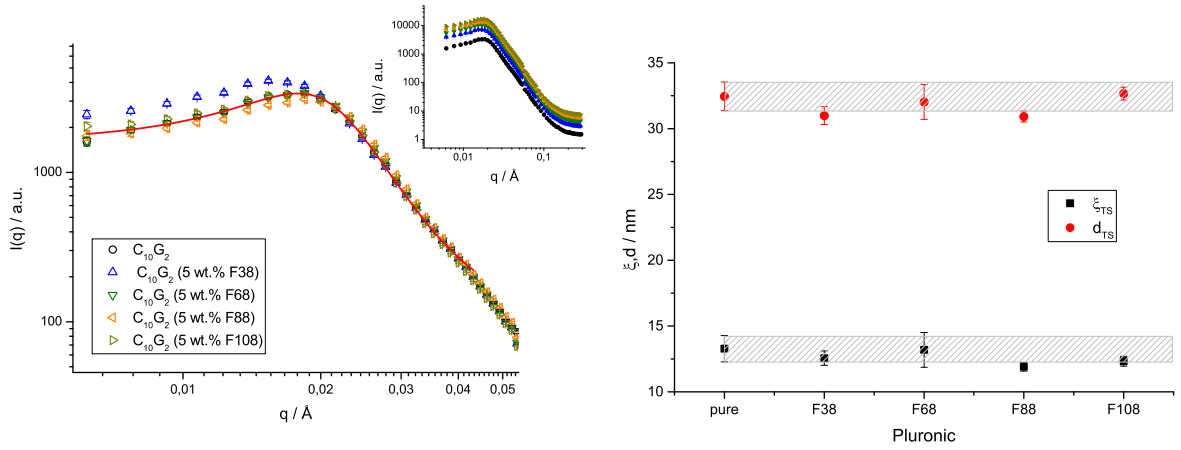

*Figure 6.8: SANS pattern of the **S3** variation of the system D_2O / C_6H_{12} / $C_{10}G_2$ (S3) / 1-pentanol at $\alpha = 0.50$, $\gamma = 0.105$ and $\delta = 0.10$. Shown is the q-region of q_{max}. In the inset the SANS patterns of the whole measured q-range are shown (data sets are shifted with respect to each other to increase the readability of the figure). Results of the TS analysis: d (red circles) and ξ (black squares) values plotted versus the applied Pluronic name. The gray boxes indicate the values of the pure $C_{10}G_2$ system. Within the experimental error no change of ξ and d is observable upon polymer addition.*

structure sizes are observed. In the technical system water / L 99 / SL 55 / 1-pentanol the addition of the polymers of series **S3** led to an increase of d accompanied by a decrease of ξ. Here, only a slight reduction of ξ is observed upon polymer addition. But the $C_{10}G_2$ containing samples are composed at $\gamma = 0.105$ with a domain size d in the range of 30 to 35 nm and a correlation length ξ of 13 to 15 nm. Compared to the Simulsol SL55 based system with $d \approx 17-20$ nm and $\xi \approx 5-7$ nm at $\gamma = 0.25$, there is less internal film in the $C_{10}G_2$ system. Therefore, the structure sizes in the microemulsion are larger than in the technical system. This leads to the conclusion that the polymer size has no strong influence on the structure sizes.

The samples prepared close to the X-point of the systems $\gamma = \tilde{\gamma} + 0.01$ show a comparable behaviour in case of the F38-samples. The effective Pluronics F68, F88 and F108 shift the X-point to $\tilde{\gamma} \approx 0.065$,

the samples were therefore prepared at $\gamma = 0.075$ for F88 and F108 and at $\gamma = 0.074$ for F68. Here, an increase of the size of the internal structures is observed, resulting in a shift of q_{max} to lower q-values as shown in figure 6.9. Analysis of the scattered intensity with the TS formula reveals to a comparable increase of d and ξ for all of the three Pluronics.

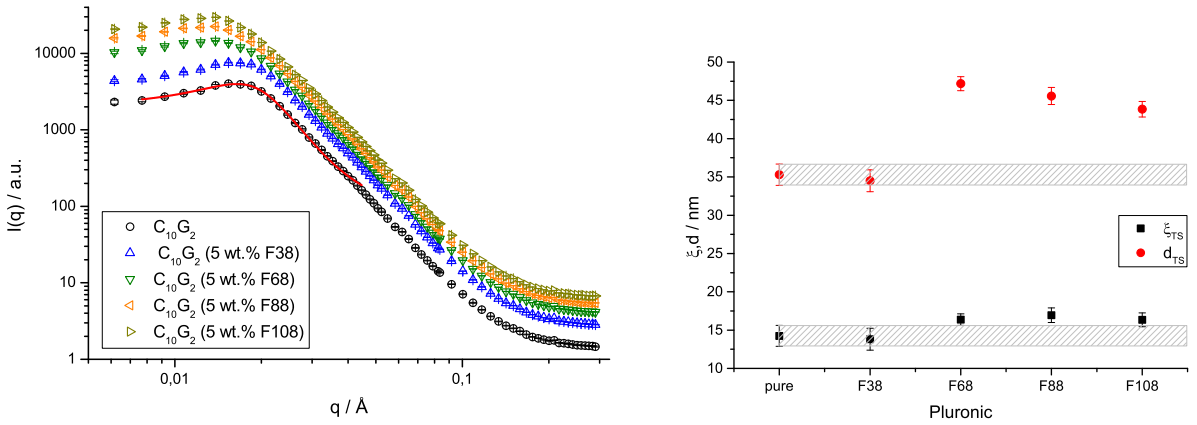

*Figure 6.9: left: SANS pattern of the **S3** variation of the $C_{10}G_2$ system at $\gamma = \tilde{\gamma} + 0.01$. The samples containing polymers are shifted in intensity with respect to each other in the sake of clarity of the presentation. For the pure system without Pluronics a fit with the TS-formula to the data is exemplarily shown as red line.*

right: Results of the TS analysis: d (red circles) and ξ (black squares) values plotted versus the applied Pluronic name. The gray boxes indicate the values of the pure $C_{10}G_2$ system. In case of the most efficient polymers, d and ξ are increased, compared to the microemulsion without polymer and the F38 containing system.

Table 6.5: Sample composition and results of the TS-analysis in the system D_2O / cyclohexane / $C_{10}G_2$(Pluronic) / n-pentanol. κ_{SANS} is the renormalized bending elastic constant according to equation (6.1) .

Polymer name	ϵ	γ	δ	ξ [nm]	d [nm]	κ_{SANS} k_BT
pure	0.00	0.105	0.102	13.28 ± 1.00	32.45 ± 1.09	0.35 ± 0.03
F38	0.05	0.105	0.102	12.56 ± 0.55	30.99 ± 0.68	0.33 ± 0.03
F68	0.05	0.105	0.102	13.19 ± 1.32	32.03 ± 1.23	0.34 ± 0.04
F88	0.05	0.105	0.102	11.91 ± 0.33	30.92 ± 0.42	0.33 ± 0.01
F108	0.05	0.105	0.102	12.33 ± 0.37	32.66 ± 0.48	0.32 ± 0.01
pure	0.00	0.095	0.098	14.25 ± 1.36	35.30 ± 1,39	0.34 ± 0.04
F38	0.05	0.095	0.086	13.82 ± 1.43	34.50 ± 1.44	0.34 ± 0.04
F68	0.05	0.074	0.093	16.37 ± 0.74	47.18 ± 0.92	0.30 ± 0.01
F88	0.05	0.075	0.089	16.95 ± 0.96	45.57 ± 1.12	0.32 ± 0.02
F108	0.05	0.075	0.084	16.35 ± 0.91	43.85 ± 1.02	0.32 ± 0.02

6.2.4 Bending elastic constant

From the results of the TS analysis (see equation (3.30)), the renormalized bending elastic constant κ_{SANS} can be obtained according to [8, 11, 17]

$$\frac{\kappa_{SANS}}{k_B T} = \frac{10\sqrt{3}\pi}{64}\frac{\xi_{TS}}{d_{TS}} \tag{6.1}$$

With respect to the experimental errors, the resulting κ_{SANS} values in the system D_2O / cyclohexane / $C_{10}G_2$(Pluronic) / n-pentanol have to be regarded carefully.

κ_{SANS} is in the range of $0.26\,k_BT < \kappa_{SANS} < 0.35\,k_BT$, and listed in the tables 6.3, 6.4 and 6.5. Comparable ranges of κ_{SANS} are known for the system D_2O / cyclohexane / C_9G_2 / n-pentanol ($\kappa_{SANS} = 0.25\,k_BT$ to $0.29\,k_BT$) [15] or the microemulsion systems based on the technical grade sugar surfactants listed in table 5.3. Here, values of κ_{SANS} are reported between $0.26\,k_BT$ to $0.28\,k_BT$) for water / RME / $C_{12/14}G_{1.3}$ / n-pentanol and $0.52\,k_BT$ to $0.57\,k_BT$) for D_2O / cyclohexane / $C_{8/10}G_{1.3}$ / n-pentanol.

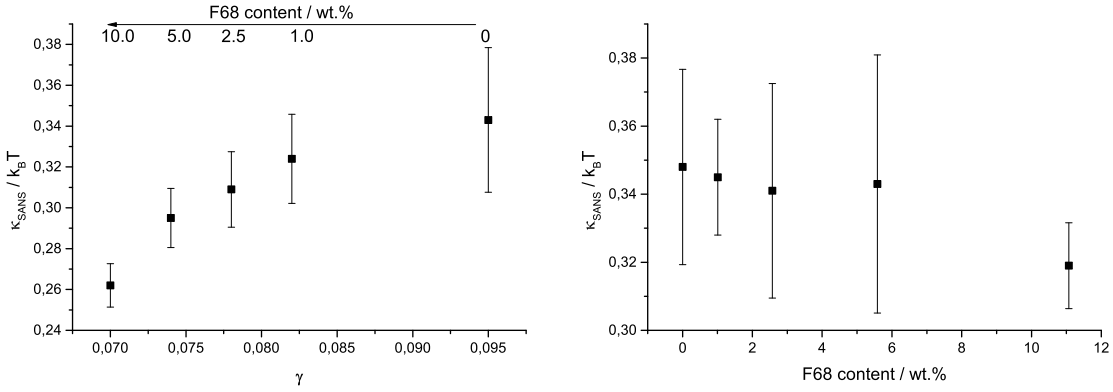

Figure 6.10: Left: Calculated renormalized κ_{SANS}/k_BT plotted versus the γ value of the measured sample close to the X-point. Right: Calculated κ_{SANS}/k_BT values plotted versus the F68 content at samples composed at $\alpha = 0.5$, $\gamma = 0.105$ and $\delta = 0.102$.

As shown in figure 6.10, κ_{SANS} is reduced upon increase of the F68 content in the samples measured at $\gamma = \tilde{\gamma} + 0.01$. The reduction of the overall amphiphile concentration in the system close to the X-point leads to an increase of the volume of the water and oil phases and therefore a higher flexibility of the film. On the right side of figure 6.10, κ/k_BT was calculated for five samples of identical composition at $\alpha = 0.5$, $\gamma = 0.105$ and $\delta = 0.102$. Here, a decrease of κ_{SANS} can be observed with increasing polymer content ϵ. This finding is comparable to the behaviour of homopolymers in C_iE_j

microemulsion systems, as reported by BYELOV *et al.* [3]. The same group reported a change in the renormalized bending rigidity κ_R of $\Delta\kappa_R \approx 0.11\,k_BT$ (κ_R in the range of $\kappa_R \approx 0.35$ to $0.47\,k_BT$) upon polymer addition [2]. But these homopolymers are known to reduce the surfactant efficiency, while the efficiency boosting diblock polymers increase the bending rigidity [3].

In the case of the Pluronic polymers one finds that, at constant sample composition, the spanned range of κ_{SANS} has a width of $\Delta\kappa_{SANS} \approx 0.03 k_BT$. The influence of the polymer content is smaller than the change of γ. With the large polymer molecules embedded in the internal film, the undulations of the film are reduced.

Applying Pluronic polymers seems to disturb the surfactant layer, reducing the bending elastic constant and creating a somewhat smoother surfactant layer. A possible interpretation of these findings may be the inception of the polymers in the surfactant layer. This reduces the stiffness of the internal film due to the long chains of the polymers, resulting in a higher flexibility and therefore a reduction of κ.

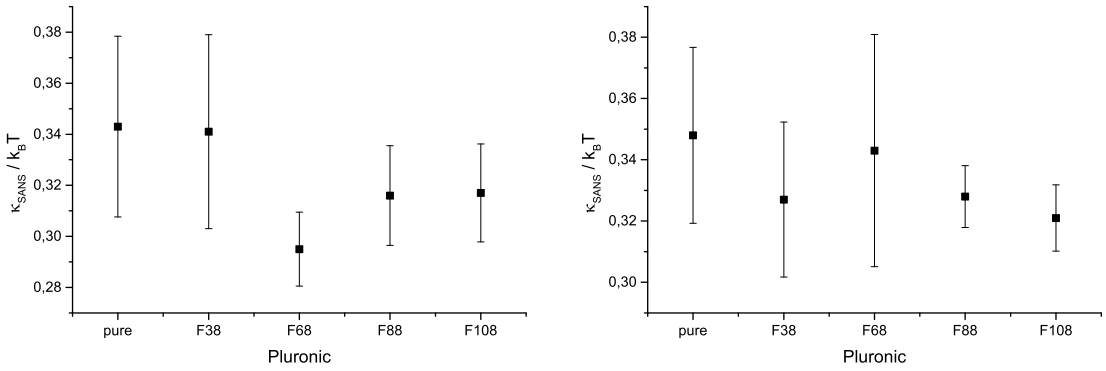

*Figure 6.11: Calculated renormalized κ_{SANS}/k_BT values plotted versus the **S3** Pluronic polymers. left: Samples prepared close to the X-point at $\delta = \tilde{\delta}$ and $\gamma = \tilde{\gamma} + 0.01$. right: Samples prepared at $\alpha = 0.50$, $\gamma = 0.105$ and $\delta = 0.10$.*

The samples containing series **S3** polymers close to the respective X-points of the systems, shown on the left side of figure 6.11, lead to a reduction of κ_{SANS}/k_BT for F68 ($\gamma = 0.074$), F88 and F108 (both $\gamma = 0.075$). The right side shows a set of samples with identical composition at $\alpha = 0.50$, $\gamma = 0.105$ and $\delta = 0.102$. All Pluronic polymers reduce the bending rigidity slightly compared to the pure system. This effect increases with increasing polymer size and can be correlated to stronger fluctuations at constant surface areas, resulting in a lowered mobility of the membrane[2, 3].

6.3 Influence on the membrane dynamics

6.3.1 Microemulsion dynamics measured by PCS

The normalized intensity time autocorrelation functions $g^2(q,\tau)$ were measured at 293 K for the five microemulsion samples which were also used for NSE experiments, subsequently. As shown in figure 6.12, the mean relaxation rate Γ resulting from a CONTIN analysis of the intensity correlation function is plotted versus the squared scattering angle q^2. The linear relationship indicates purely Fickian diffusion as the dominant collective dynamics of the bicontinuous samples. The increase of the polymer concentration reduces the motion of the microemulsion system. As the samples were composed close to the X-point of the microemulsion system, this result is a consequence of the rising structure sizes by reduction of the $\tilde{\gamma}$ values which is visualized in figure 6.13. The relaxation rate distributions resulting from the CONTIN analysis and the sample compositions are summed up in table 6.6.

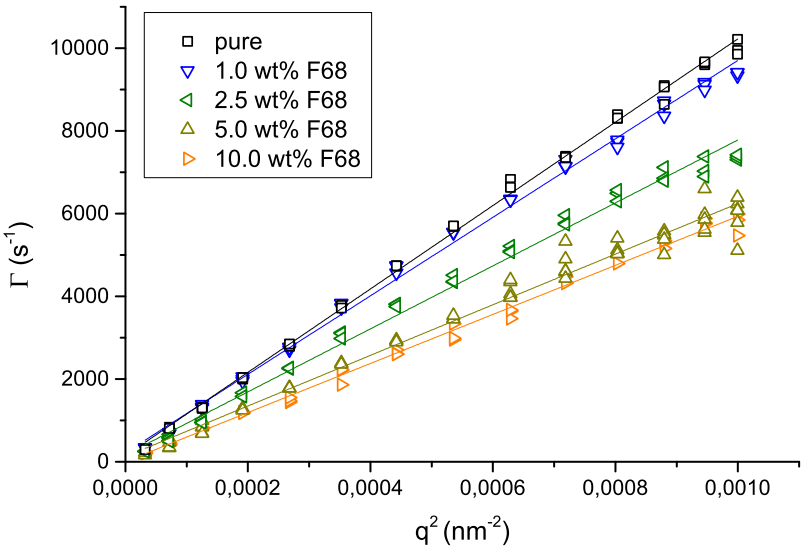

Figure 6.12: Results of the CONTIN analysis of the PCS experiments in the system D_2O / C_6D_{12} / $C_{10}G_2$ (F68) / 1-pentanol at 293 K as a plot of Γ versus q^2. Solid lines are linear fits to the data. The linear relationship indicates purely Fickian diffusion as the dominant collective dynamics of the bicontinuous samples.

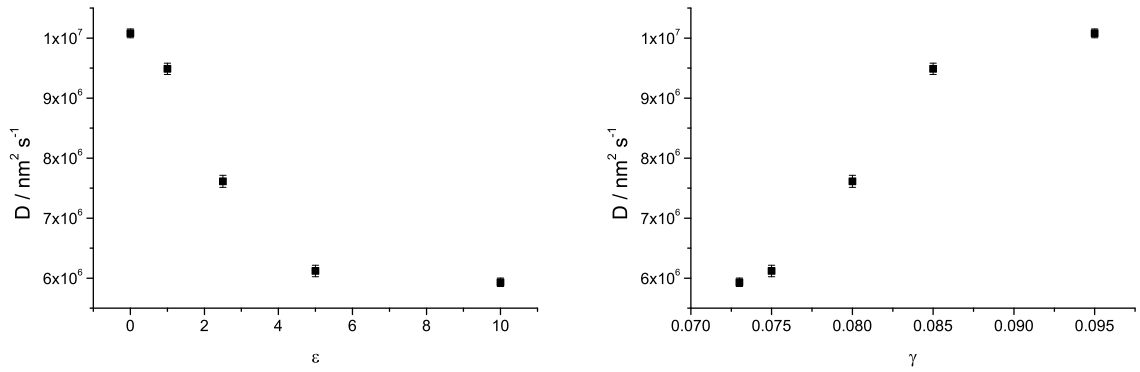

Figure 6.13: Left: Obtained diffusion coefficients D calculated from $\Gamma(q^2)$ linear regressions in figure 6.12 plotted versus the polymer content ϵ. Right: D versus the overall amphiphile content γ of the respective sample. The error bars are in the range of the size of the symbols.

Table 6.6: Results of the CONTIN-analysis of the PCS-data measured at 293 K in the system water / C_6D_{12} / $C_{10}G_2$(F68) / n-pentanol. The F68 content was increased from 0 wt% in the pure system up to 10 wt%. All samples were composed close to the resulting X-point in the respective system.

	α	γ	δ	ϵ	D $\left[\frac{nm^2}{s}\right]$	ΔD
pure	0.500	0.095	0.090	0.000	$1.01 \cdot 10^{-7}$	$7.37 \cdot 10^{-10}$
1.0 wt% F68	0.500	0.082	0.085	0.010	$9.49 \cdot 10^{-8}$	$9.26 \cdot 10^{-10}$
2.5 wt% F68	0.500	0.080	0.084	0.025	$7.61 \cdot 10^{-8}$	$1.01 \cdot 10^{-9}$
5.0 wt% F68	0.500	0.075	0.080	0.050	$6.12 \cdot 10^{-8}$	$9.58 \cdot 10^{-10}$
10.0 wt% F68	0.500	0.073	0.085	0.100	$5.93 \cdot 10^{-8}$	$6.93 \cdot 10^{-10}$

6.3.2 Microemulsion dynamics by NSE

Neutron spin echo spectroscopy has already been used in previous works to detect the thermally excited fluctuations of the interfacial surfactant film in a bicontinuous microemulsion. [21, 14, 10]. The Zilman-Granek description of a fluctuating flat membrane has proven to be a good model for the analysis of the intermediate scattering functions. It can also be used in the present case, since on the length scale resolved by NSE, the film in the bicontinuous microemulsion can be described as an ensemble of randomly oriented but locally flat membrane plaquettes [25]. Hence, using this approach, one can compute the bending rigidity κ_{NSE}. In the approximation by Zilman and Granek [25, 24], the intermediate scattering function can be described by a stretched exponential function

$$\frac{S(q,\tau)}{S(q,0)} = \exp(-(\Gamma_{ZG}\tau)^{\beta}). \tag{6.2}$$

with the stretching exponent β predicted to be $\beta = 2/3$. The relaxation rate Γ_{ZG} is related to κ_{NSE} by:

$$\Gamma_{ZG} = 0.025\gamma_{ZG}\left(\frac{\kappa_{NSE}}{k_BT}\right)^{0.5}\frac{k_BT}{\mu}q^3. \tag{6.3}$$

Hence, the relaxation rate is expected to show a linear q^3 dependence, which is also observed in Zimm polymer dynamics. Here, μ is the viscosity of the solvent that surrounds the surfactant membrane. The pre-factor γ_{ZG} depends on κ and can be calculated according to equation 6.4 [13]:

$$\gamma_{ZG} = 1 - 3(\frac{k_BT}{4\pi\kappa})\ln(q\xi_{TS}). \tag{6.4}$$

For values of the bending rigidity $\kappa >> k_BT$, $\gamma_{ZG} \approx 1$ can be used. Due to the lack of reliable ξ_{TS} values, this estimation is used in the following.

With respect to the contribution of the hydrodynamic motion, as received from DLS measurements, the decay of the normalized intermediate scattering function can be described by

$$\frac{S(q,\tau)}{S(q,0)} = \exp(-(\Gamma_{Diff}\tau)\left(A + (1-A)\exp(-(\Gamma_U\tau)^{\beta}\right). \tag{6.5}$$

where Γ_{Diff} is the relaxation rate of the collective hydrodynamic modes based on the diffusion coefficient received from DLS measurements according to the dispersion relation $\Gamma_{Diff} = Dq^2$ [21]. A series of NSE measurements were performed with bicontinuous samples close to the X-point with an increasing F68-content. The samples were measured at 293 K in the range of $q = 0.02\,\text{Å}^{-1}$ to $q = 0.17\,\text{Å}^{-1}$, using neutron wavelengths of $\lambda = 10\,\text{Å}$ and $\lambda = 16\,\text{Å}$. The pure sample was less stable at 293 K, therefore is was measured at 299 K. Examples of the obtained data are shown in figure 6.14.

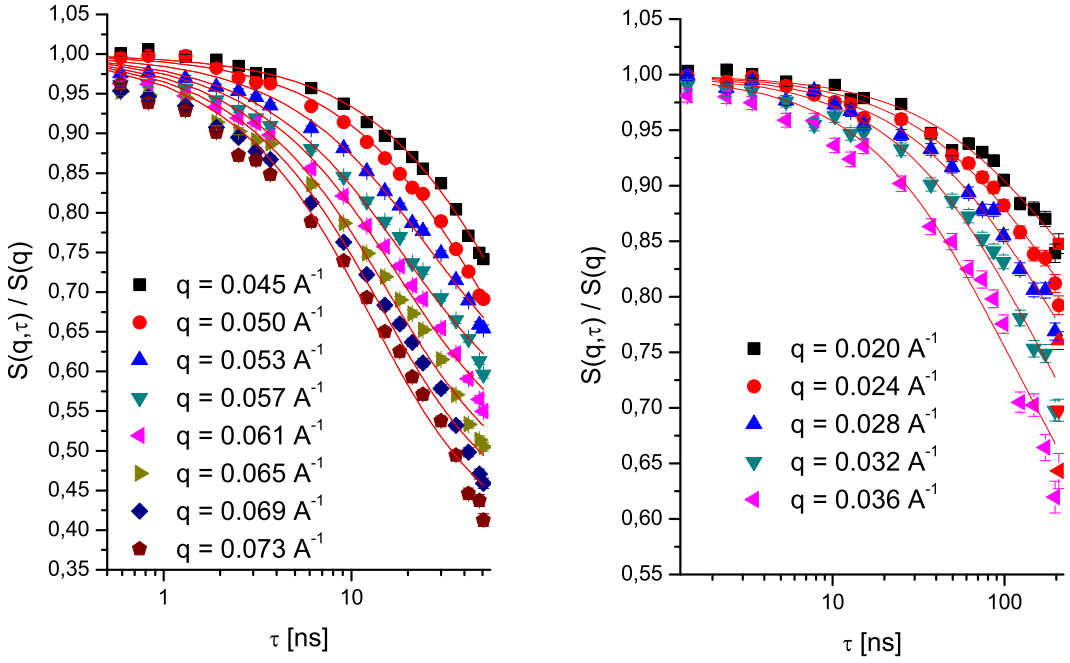

Figure 6.14: Examples of the normalised intermediate scattering function $S(q,\tau)/S(q,0)$ from the NSE measurements. The solid lines are fitting curves to eq. (6.5).

The lines are fits according to the model described in equation (6.5) using the Γ_{Diff} obtained from DLS measurements and $\beta = 2/3$. The influence of the performed background correction with D_2O only lead to an overcorrection of S(q). As the polarization of cyclohexane-d12 is three times higher than the one of water-d2, this has a higher influence at low q-values. As a result, the calculated Γ_U values for $\lambda = 10\,\text{Å}$ were shifted to higher values compared to the ones measured at $\lambda = 16\,\text{Å}$. As only the slope is relevant for further analysis, the y-offset was corrected by baseline-subtraction. The resulting undulation relaxation rates Γ_U plotted versus q^3 are shown in figure 6.15. In good accordance with the theoretical approach described in eq. (6.3), the linear q^3-dependence of Γ_U is observed for all microemulsion samples.

The bending elasticity constant κ_{NSE} was calculated according to equation 6.3. Here, the effective viscosity μ was simply used as the arithmetic middle of the dynamic viscosity of D_2O and cyclohexane-d12 and $\gamma_{ZG} \approx 1$. Therefore the effect of the polymers added to the samples on the overall sample viscosity is not taken into account.

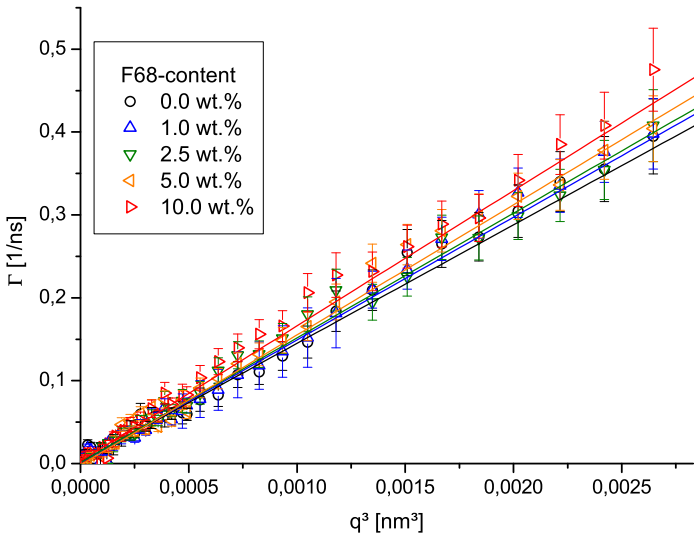

Figure 6.15: Plot of the relaxation rates Γ_U versus q^3. Γ_U of the undulation motion results from fits according to equation (6.5) *for the five different microemulsion samples. The lines are linear fits with slope C summed up in table 6.7.*

In table 6.7, the values of κ calculated from the slope of the linear fit of Γ_U versus q^3 are summarized. All samples are composed close to the X-point in the respective systems. Hence, the composition of the samples changes in γ and due to the shift in the phase diagrams in δ.

Interestingly, the values calculated using the simplification $\gamma_{ZG} \approx 1$ are comparable to those calculated from the SANS measurements presented in section 6.2.4. From the SANS measurements κ_{SANS} values in the range of $0.26\,k_BT < \kappa_{SANS} < 0.35\,k_BT$ were found. For the film contrast samples κ_{NSE}, where only the undulations of the membrane is taken into account, the values were in the range of $0.21\,k_BT < \kappa_{NSE} < 0.30\,k_BT$. In both samples the bending elasticity constants κ are significantly reduced at low γ values. As it is known from the addition of homopolymers and amphiphilic polymers to C_iE_j based microemulsion systems, the influence of the surfactant content γ and the resulting structure size on κ is larger than the effect of the polymers [14]. The reduction of the bending elasticity constant indicates an increase in the undulation of the amphiphilic membrane. Holderer *et al.* [9] reported a comparable behaviour for homopolymers (polyethyleneoxide (PEO) and polyethylenepropylene (PEP)) in a microemulsion system based on D_2O, d-decane and the surfactant $C_{10}E_4$. They observed a decrease of κ_{NSE} in the range of $\approx 0.3\,k_BT < \kappa_{NSE} < 1.0\,k_BT$

Table 6.7: Slope C of the linear fit of the plot Γ_U versus q^3 and the calculated values of κ_{NSE} in units of k_BT from the analysis with equation (6.5).

Sample composition				C	κ_{NSE}
α	γ	δ	ϵ	$[A^3/ns]$	$[k_B\ T]$
0.500	0.095	0.090	0.000	143.0 ± 3.9	0.303 ± 0.018
0.500	0.082	0.085	0.010	148.1 ± 3.9	0.296 ± 0.016
0.500	0.080	0.084	0.025	150.4 ± 3.5	0.287 ± 0.015
0.500	0.075	0.080	0.050	157.1 ± 3.5	0.266 ± 0.013
0.500	0.073	0.085	0.100	163.2 ± 3.8	0.208 ± 0.012

with increasing homopolymer concentration and increasing homopolymer size.

For the calculation of κ_{NSE} several simplifications were used. The influence of the polymers on the effective solvent viscosity close to the amphiphilic film was neglected and, due to the lack of reliable SANS data, $\gamma_{ZG} = 1$ was used for the calculation of κ_{NSE}, which is only valid for $\kappa >> k_BT$ [14]. Usually the bicontinuous phase imply low membrane rigidity, and in literature typically values of κ_{NSE} in the range of $\kappa_{NSE} \approx 1k_BT$ are found [14, 9, 21]. The resulting κ_{NSE} values from the rough estimation made here are significantly lower than the ones usually reported in literature. But nevertheless, they are in good agreement with the renormalized κ_{SANS} values (as shown in figure 6.17), obtained from the SANS measurements performed in the bulk contrast samples and found for comparable microemulsion systems based on sugar surfactants [19].

As the bending elasticity constant can be interpreted as the work required for the deformation of the surfactant membrane compared to the spontaneous curvature of the film [22], the combined polymer sugar surfactant microemulsion system investigated here shows strong fluctuations at constant surface area.

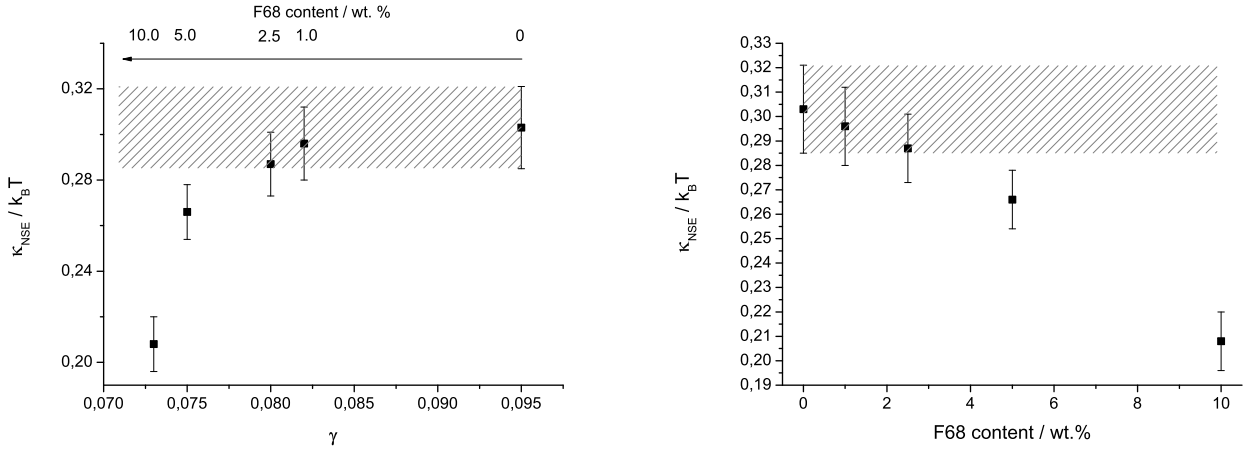

Figure 6.16: Bending elastic constant κ_{NSE} in units of k_BT as a function of γ (left) and the F68 - content (right). Data from table 6.7. The shaded area represents the polymer free system with respect to the error bars.

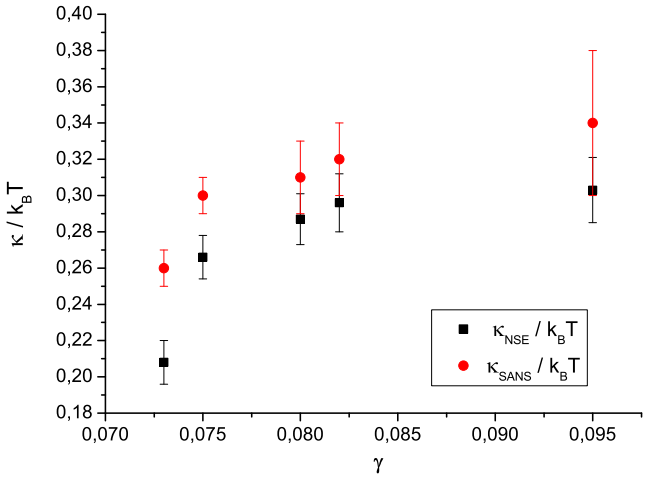

Figure 6.17: Bending elastic constant κ_{NSE} and the renormalized bending elastic constant κ_{SANS} in units of k_BT as a function of γ. κ_{SANS} calculated from the SANS experiments of the bulk contrast samples in section 6.2.4.

6.4 Conclusion

The phase diagram of the system water / cyclohexane / $C_{10}G_2$ / 1-pentanol is dominated by extended lamellar regions in the "fish"-tail. As the surfactant itself is already quite efficient, the observed efficiency boosting effects of the applied Pluronic polymers are smaller compared to the technical system based on SL55. But nevertheless the correlation between structure and size of the polymer used in the microemulsion system is identical. The large Pluronics with a high PEO content, namely F68, F88 and F108 again show the highest efficiency boost factors f_B. Again, the best results were achieved with Pluronic F68, which drives the X-point to $\tilde{\gamma} = 0.065$, corresponding to a $f_B = 5.6$ by simultaneous reduction of the lamellar region. In case of the microemulsion system with the extended lamellar structures this effect is of interest as it offers a larger bicontinuous region in the phase diagram. Upon addition of the small polymers the suppression of the formation of lamellar structures has been observed.

With small angle scattering experiments the influence of the different Pluronic polymers was investigated. At a constant composition the polymers have no longer a significant influence on domain size d and correlation length ξ. As the samples were composed at low γ values and therefore larger structure sizes, the molecular size of the polymers themselves seems to have no influence on the length scales of the internal structure.

Upon polymer addition the stabilization of microemulsion structures with lower surfactant content is achieved. Therefore, the interfacial surfactant film is formed by less molecules, consequently larger structure sizes are available. With the pure microemulsion system $d_{max} = 35nm$ at $\tilde{\gamma}$, by replacing 10% surfactant with polymer, structure sizes of $d_{max} \approx 53nm$ are available. The renormalized bending rigidity κ_{SANS} estimated by SANS is comparable to the results of sugar surfactant based microemulsion systems found in the literature. The bending elastic constants κ_{NSE} of the film contrast samples, obtained from the combination of dynamic light scattering measurements with neutron spin echo experiments, are in good agreement with the κ_{SANS} values. With diffusion coefficients in the range of $D = 5.93 \times 10^{-8} cm^2 s^{-1}$ to $D = 1.01 \times 10^{-7} cm^2 s^{-1}$ for the collective motions, the calculated κ_{NSE} values are in the range of $0.21\, k_B T < \kappa_{NSE} < 0.30\, k_B T$. This finding can be interpreted as a result of the polymers being a part of the amphiphilic film and therefore reducing the overall mobility of the membrane by introducing strong fluctuations at the surface.

6.5 References

[1] A. Brulet et al. “Improvement of data treatment in small-angle neutron scattering”. In: *Journal of Applied Crystallography* 40.1 (2007), pp. 165–177. DOI: 10.1107/S0021889806051442.

[2] D. Byelov et al. “Microemulsion Efficiency Boosting and the Complementary Effect. 1. Structural Properties”. In: *Langmuir* 20 (2004), pp. 10433–10443.

[3] D. Byelov et al. “SANS studies of polymer efficiency boosting in microemulsions - diblock copolymers versus homopolymers.” In: *Physica B,* 350 (2004), pp. 931–933.

[4] F. Caboi and M. Monduzzi. “Didodecyldimethylammonium Bromide Vesicles and Lamellar Liquid Crystals. A Multinuclear NMR and Optical Microscopy Study”. In: *Langmuir* 12.15 (1996), pp. 3548–3556.

[5] B.E. Conway. *Ionic Hydration in Chemistry and Biophysics*. Ed. by B.E. Conway. Elsevier, Amsterdam, 1981.

[6] C. Frank et al. “Coexisting lamellar phases in water-oil-surfactant systems induced by the addition of an amphiphilic block copolymer”. In: *Journal of Colloid and Interface Science* 312.1 (2007), pp. 76–86.

[7] C. Frank et al. “Influence of Amphiphilic Block Copolymers on Lyotropic Liquid Crystals in Water-Oil-Surfactant Systems”. In: *Langmuir* 21.20 (2005), pp. 9058–9067.

[8] G. Gompper and D. M. Kroll. “Membranes with Fluctuating Topology: Monte Carlo Simulations”. In: *Phys. Rev. Lett.* 81 (11 1998), pp. 2284–2287.

[9] O. Holderer et al. “Dynamic properties of microemulsions modified with homopolymers and diblock copolymers: The determination of the bending moduli and renormalization effects.” In: *J. Chem. Phys.* 122 (2005), p. 094908.

[10] O. Holderer et al. “Hydrodynamic effects in bicontinuous microemulsions measured by inelastic neutron scattering”. In: *European Physical Journal E* 22 (2007), pp. 157–161.

[11] O. Holderer et al. “Soft fluctuating surfactant membranes in supercritical CO2-microemulsions”. In: *Phys. Chem. Chem. Phys.* 13 (8 2011), pp. 3022–3025.

[12] B. Jakobs. *Amphiphile Blockcopolymere als ’Efficiency Booster’ für Tenside: Entdeckung und Aufklärung des Effektes*. Cuvillier Verlag Goettingen, 2001.

[13] M. Klostermann et al. “Structure and dynamics of balanced supercritical CO_2-microemulsions”. In: *Soft matter* 8 (2012), pp. 797–807.

[14] M. Mihailescu et al. “Dynamics of bicontinuous microemulsion phases with and without amphiphilic block-copolymers”. In: *Journal of Chemical Physics* 115 (2001), pp. 9563–9577.

[15] R. Neubauer. “Diffusion of proteins inside crowded structures generated using microemulsions”. Phd Thesis. Universität Bayreuth, 2013.

[16] R.M. Pashley et al. “Attractive forces between uncharged hydrophobic surfaces: direct measurements in aqueous solution”. In: *Science* 13 (1985), pp. 1088–1089.

[17] P. Pieruschka, S.A. Safran, and S.T. Marcelja. “Comment on Fluctuating interfaces in microemulsion and sponge phases”. In: *Phys. Rev. E.* 52 (1995), pp. 1245–1247.

[18] C. Schulreich. “Mikroemulsionen auf Basis von Zuckertensiden: Struktureigenschaftsbeziehungen, Stabilität und Enzymkinetik”. Phd Thesis. Universität Bielefeld, 2015.

[19] C. Schulreich et al. “Bicontinuous microemulsions with extremely high temperature stability based on skin friendly oil and sugar surfactant”. In: *Colloids and Surfaces A: Physicochemical and Engineering Aspects* 418 (2013), pp. 39–46.

[20] C Stubenrauch et al. “A new approach to lamellar phases (Lα) in water – non-ionic surfactant systems”. In: *Liq. Cryst.* 1 (2004), p. 39.

[21] S. Wellert et al. “Temperature dependence of the surfactant film bending elasticity in a bicontinuous sugar surfactant based microemulsion: a quasielastic scattering study”. In: *Physical Chemistry Chemical Physics* 13.8 (2011), pp. 3092–3099.

[22] S. Wellert et al. “The DFPase from loligo vulgaris in sugar surfactant based bicontinuous microemulsions: Structure, dynamics and enzyme activity”. In: *European Biophys. J.* 40 (2011), pp. 761–774.

[23] C. Whiddon and O. Soederman. “Unusually Large Deuterium Isotope Effects in the Phase Diagram of a Mixed Alkylglucoside Surfactant Water System”. In: *Langmuir* 17.6 (2001), pp. 1803–1806.

[24] A. G. Zilman and R. Granek. “Membrane dynamics and structure factor”. In: *Chemical Physics* 284.1-2 (2002), pp. 195–204.

[25] A. G. Zilman and R. Granek. “Undulations and Dynamic Structure Factor of Membranes”. In: *Phys. Rev. Lett.* 77 (23 Dec. 1996), pp. 4788–4791.

Chapter 7

Skin Decontamination

There are mainly two ways chemical warfare agents (CWA) are incorporated: Via the respiratory system and via the skin [17, 27]. With approximately 2 m^2 of surface area and a mass of 11 kg, human skin is the largest organ.[3] It is a complex, three layered system consisting of epidermis, dermis and subcutaneous fat, as shown in figure 7.1 [1]. The epidermis serves as the first barrier of the body against exogenous material, including chemicals or microbes, as it consists of several alternating hydrophilic and lipophilic layers with a low water content [3]. Unfortunately this barrier is easily penetrated by the lipophilic CWAs within a short time window [18].

For that reason, an immediate and extensive decontamination of the involved skin is essential. An overview of decontamination methods actually in use is given in the textbook by RICHARDT [18].

The chemical hydrolysis of CWAs can be performed by simple soap solutions. The limiting factor is the low reaction rate of the hydrolysis, but the availability of this simple decontaminant led to an intense use during world war I in combination with bleach (calcium hypochlorite) [12].

In many surveys the efficiency of decontaminants composed of 'house hold' chemical is proven [12, 13, 20]. The prime reason for the efficiency of a decontamination medium is the physical removal of the threat from the involved surface which avoids further assimilation of the warfare agent. However, the low diffusion rate and the poor water solubility of the CWA still are a major challenge [13, 20] .

Microemulsions, such as the microemulsion system with biodiesel as oil phase recently published by WELLERT and co-workers, are able to decontaminate CWAs [28, 10, 9]. In this juncture the oil domain of the microemulsion system operates as a solvent for the lipophilic CWA. Decontamination takes place at the amphiphilic interface, the active species are usually water soluble and therefore

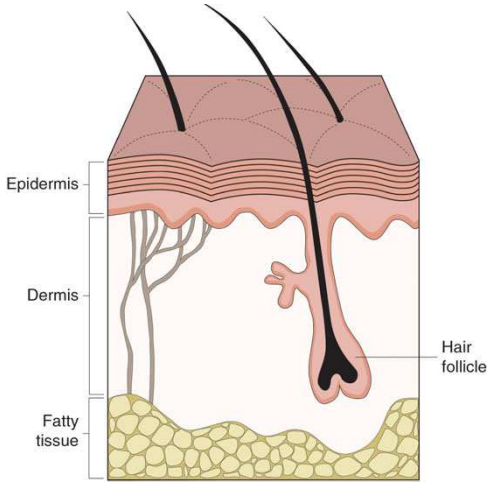

Figure 7.1: Human skin consists of three main parts: the hypodermis (fatty subcutaneous tissue), the dermis (collagenous tissue from which fibroblasts can be isolated) and the epidermis (stratifying epithelial tissue consisting mainly of keratinocytes and also other cell types including melanocytes). Human hair is a complex mini-organ of which keratinocytes in the outer root sheath are differentiating inward to produce the keratin of the growing hair. These cells can be isolated for culture by plucking or dissecting the hair. Pictures and description from Aasen, T. and Belmonte, J.C.I: Isolation and cultivation of human keratinocytes from skin or plucked hair for the generation of induced pluripotent stem cells, Nature Protocols 2010, 5, 371–382. Copyright Nature publishing group. Reproduced with permission.

dissolved in the water domain. The way the decontamination is performed is of secondary importance. Generally alkaline hydrolysis, oxidation or enzymatic depletion are used in the deactivation step. The promising method in this case is the enzymatic decontamination performed with diisopropyl fluorophosphatase (DFPase), as only small amounts of enzyme in the microemulsion system are necessary to reduce a large amount of CWA effectively [18, 19, 4].

In the present thesis, the systems developed by our group are used as a starting point for further investigations. In this context a special focus is given to the cyclohexane model system and the biodiesel system published by WELLERT *et al.* which serve as base systems [28].

Variation of single components were performed to increase the skin compatibility, trying to create a model system able to serve as potential skin decontaminant. In the following chapter the results of the respective investigations are shown.

7.1 System variation I: Non-polar phase

The hydrophobic phase of the microemulsion has to fulfil several requirements for application in skin decontaminants. First of all the chemical and physical needs: Not only solubility of the CWA and the ability to remove CWAs from different surfaces are requested, the used oil should also show a long term stability without ageing effect influencing its properties. Additionally the oil must be non toxic and non irritating to the skin. Preferable is an approval as pharmaceutical component to ease the fast availability of the final product. An overview of the requirements of an ideal decontaminant are given in section 2.3.

Cyclohexane is categorized as flammable, harmful and irritating to skin, therefore it can only serve as oil component in the model systems (see chapter).

First improvement was the skin friendly system developed by HELLWEG ET AL. using the emollient isononyl-isononate (Lanol 99, Seppic, Paris, Frankreich) as oil phase [11]. This system was improved by addition of Pluronics (see chapter 5).

Unfortunately the extraction performance of this microemulsion system did not reach the expected requirements [14]. Therefore the development of new microemulsion systems with skin friendly oil phases was necessary.

The next step was the introduction of ethyl laurate and ethyl caprate based systems, where we tried to improve the extraction properties of the oil phase. The most promising system is the fatty acid methyl ester (FAME) system, where rapeseed methyl ester (RME) was used.

7.1.1 Ethyl laurate and ethyl caprate

To increase the extraction ability of the Lanol 99 based microemulsion to the level of the biodiesel system, alternative oil phases for environmentally friendly skin decontamination are needed. Ethyl laurate and ethyl caprate are both produced on an industrial scale and are ethyl esters of the carboxylic acids lauric acid (dodecanoic acid) and decanoic acid. Both are used either in food processing or cosmetics industry as fragrance or aroma [21]. Therefore, we expect the resulting microemulsion system to satisfy the regulatory requirements with regard to safety aspects.

The decanoic ester ethyl caprate has a lower viscosity compared to ethyl laurate. Hence, we expect a higher diffusion rate into the surfaces and a better extraction performance.

Table 7.1: Physical data of the two oil phases ethyl laurate and ethyl caprate.

Properties	Unit	Ethyl caprate	Ethyl laurate
Chemical formula		$CH_3(CH_2)_8COOC_2H_5$	$CH_3(CH_2)_{10}COOC_2H_5$
Molar mass	g/mol	200,32	228,37
Density (20°C)	g/cm^3	0,86	0,86
Solubility (20°C)	g/L	0.016	insoluble
Flash point	°C	104	113
Viscosity (298.15 K)	mPa·s	2.10	3.02

Phase behaviour

For both of the new oil phases the phase diagrams with the two surfactants Glucopon 220 and Simulsol SL55 were recorded at a constant $\alpha = 0.5$, using n-pentanol as co-surfactant. The resulting cuts are shown in Figure 7.2 for ethyl caprate and in Figure 7.3 for ethyl laurate, respectively. In both cases the influence of the surfactant alkyl chain length can be seen. Upon usage of the larger surfactant Simulsol SL55 (average alkyl chain length is increased by an ethyl unit compared to Glucopon G220), less co-surfactant is necessary to reach the one phase body.

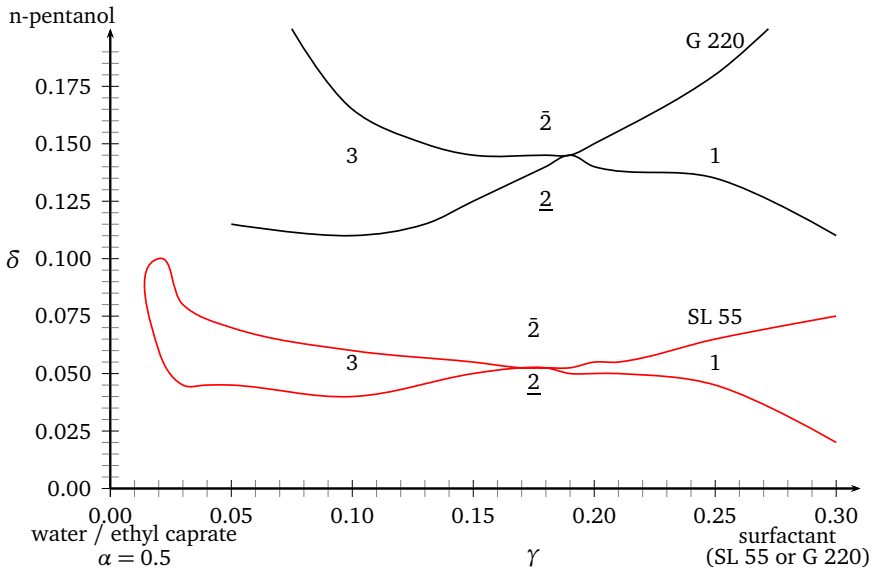

Figure 7.2: Phase diagrams of the system water / ethyl caprate / Glucopon 220 / n-pentanol (black) and water / ethyl caprate / Simulsol SL55 / n-pentanol (red). In both cases $\alpha = 0.5$.

In the case of ethylcaprate the amount of surfactant needed to solubilize the oil and water ($\tilde{\gamma}$) is comparable for both technical surfactants. For the system water-ethyl caprate-Glucopon G220-pentanol the X-point is at $\tilde{\gamma}_{G220} = 0.19$, for the larger surfactant SL 55 at $\tilde{\gamma}_{SL55} = 0.177$ (water-ethyl caprate-SL55-pentanol). In contrast, the alcohol content is reduced by almost $\frac{2}{3}$ from $\tilde{\delta}_{G220} = 0.145$ to $\tilde{\delta}_{SL55} = 0.055$.

A quite similar behaviour is observed when ethyl laurate is applied. Taking the structural and physical resemblance of the two carboxylic esters into account, this is not surprising. Here, we also observe a clear reduction of the co-surfactant needed to form a bicontinuous microemulsion structure when SL55 is used instead of G220. The X-points in the ethyl laurate systems are located at $\tilde{\gamma}_{G220} = 0.19$, $\tilde{\delta}_{G220} = 0.135$ for water-ethyl laurate-Glucopon G220-pentanol and at $\tilde{\gamma}_{SL55} = 0.20$, $\tilde{\delta}_{SL55} = 0.0575$ in the case of water-ethyl laurate-SL55-pentanol.

The slightly higher hydrophobic character of ethyl laurate leads to the shift of the one phase region to higher surfactant and co-surfactant contents.

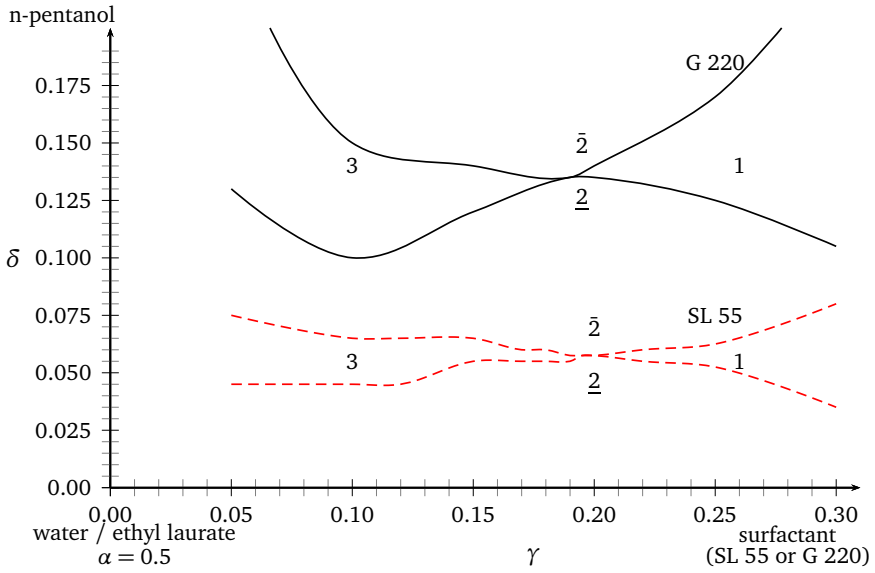

Figure 7.3: Phase diagrams of the system water / ethyl laurate / Glucopon 220 / n-pentanol (black) and water / ethyl laurate / Simulsol SL55 / n-pentanol (red) at $\alpha = 0.5$.

α-Variation, Water / ethyl caprate / SL55 / n-pentanol

For the decontamination purpose $\alpha = 0.5$ may not be the ideal oil to water ratio. Therefore, a set of phase diagrams at different oil-to-water proportions was recorded to localize the phase boundaries of the bicontinuous microemulsion phase **1**. This was exemplary performed with ethyl caprate, which is expected to have a higher diffusion rate and therefore a stronger removal capacity for CWA due to the faster interpenetration of the surfaces. Simulsol SL55 was chosen as surfactant based on the higher solubilisation capacity and the lower demand of co-surfactant. Hence, the system water / ethyl laurate / SL55 / n-pentanol is expected to be more relevant for application.

Figure 7.4 shows the experimentally obtained X-points of this system for varying α values between $\alpha = 0.1$ and 0.9 in steps of 0.1, the position of the X-points is summarized in the table on the right side of the graph.

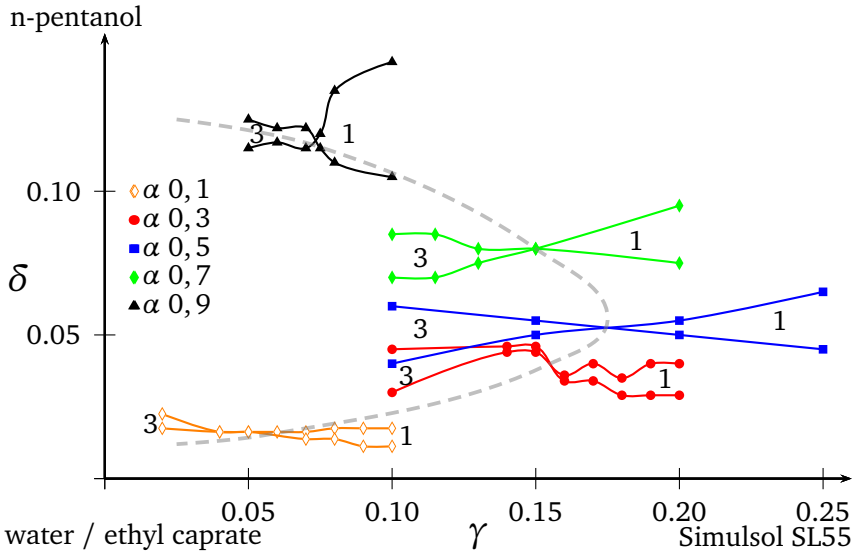

α	$\tilde{\gamma}$	$\tilde{\delta}$
0.1	0.055	0.015
0.3	0.155	0.040
0.5	0.175	0.055
0.7	0.150	0.080
0.9	0.073	0.116

Figure 7.4: Phase diagrams of the system water / ethyl caprate / Simulsol SL55 / pentanol. α is increased from $\alpha = 0.1$ to $\alpha = 0.9$ in steps of 0.2. The shift of the position of the X-points can be described by a parabola (dashed line). The position of the X-points at different α values is given in the table.

Depending on their composition, the position of the X-points in the $\delta(\gamma)$ plot can be described by a parabola. This distribution has been firstly described by SOTTMANN and STREY for C_iE_j surfactant systems [24].

Remarkable is the fact, that even upon employing technical sugar surfactant mixtures, the systems

show a comparable systematic behaviour of the X-points in dependency of α similar to the pure model systems investigated by SOTTMANN and STREY [24]. There is, of course, a deformation of the fish-shape. This is typical for technical surfactants, but the major shift of the X-point shows a similar change compared to the systems with pure surfactants.

At a low oil content less surfactant and co-surfactant are needed to solubilize the oil. Increasing the amount of oil to $\alpha = 0.5$ leads to a growth of the interfacial layer needed to formulate an one phase microemulsion. More surfactant has to be added to the system before the one phase region rises. When the oil to water ratio ascends, the size of the amphiphilic film is reduced, the X-point is shifting to lower $\tilde{\gamma}$ values. In contrast the demand of co-surfactant still rises. While the water solubility of n-pentanol is negligible, it is soluble in the oil phase, increasing the hydrophilic properties of the oil phase. As the amount of alcohol dissolved in the oil phase is not available at the amphiphilic film, additional alcohol has to be provided.

Efficiency boosting

Water / ethyl caprate / Simulsol SL55 / n-pentanol

For the system based on ethyl caprate only a single phase diagram was taken. As described in the experimental part, the recording of the phase diagram is a very time consuming method and the behaviour of ethyl caprate and ethyl laurate is quite similar. The shift in the system water / ethyl caprate / Simulsol SL55 / n-pentanol presented in figure 7.5 was achieved by replacement of 9 % surfactant by Pluronic F68. This results in a shift of the X-point from $\tilde{\gamma} = 0.175$ in the pure system to auf $\tilde{\gamma}_{F68} = 0.105$ in the polymer containing system, correlating with a boost factor of $f_B = 14.3$. The polymer slightly broadens the **1** phase region (fish tail), but the position of the X-point and the phase boundaries shift to higher co-surfactant amounts.

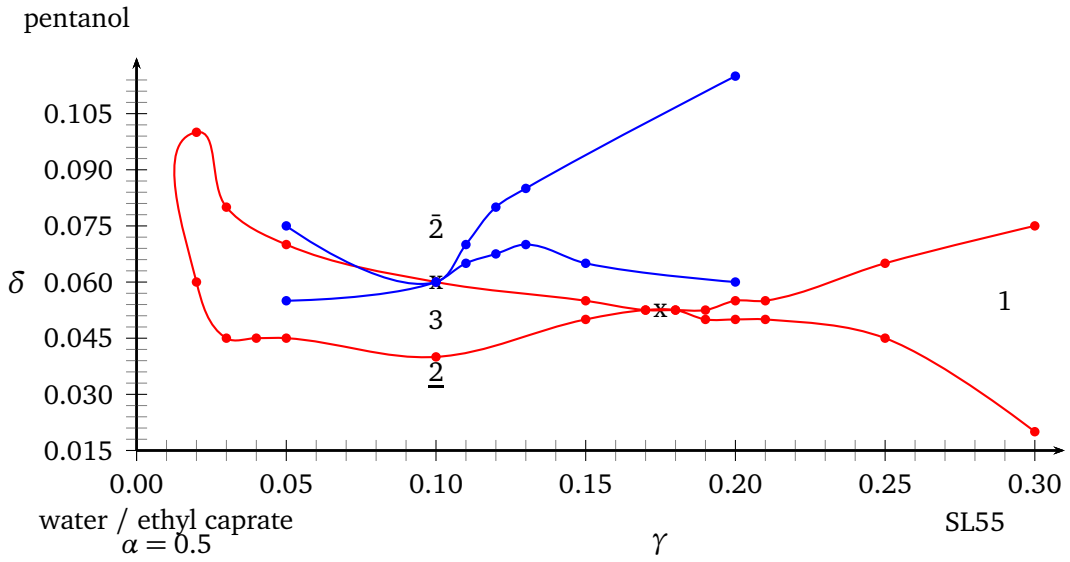

Figure 7.5: Phase diagram of the system water / ethyl caprate / Simulsol SL55 / n-pentanol (red) and water / ethyl caprate / Simulsol SL55 - 9% F68 / n-pentanol (blue).

Water / ethyl laurate / Simulsol SL55 / n-pentanol

For the skin friendly microemulsion systems with ethyl laurate serving as oil component the influence of polymers on the phase behaviour was investigated. We focussed on the pluronic polymer F68, as it showed the largest influence in the preliminary experiments.

Figure 7.6 shows the resulting phase diagrams of the system water / ethyl laurate / Simulsol SL55 /

n-pentanol at $\alpha = 0.5$ with a stepwise increased F68 content in the total amphiphile. The resulting phase diagrams offered a spreading of the **1** phase region close to the X-point. Here, the spreading of the bicontinuous region upon addition of 5 wt.% F68 is clear to see at higher γ values.

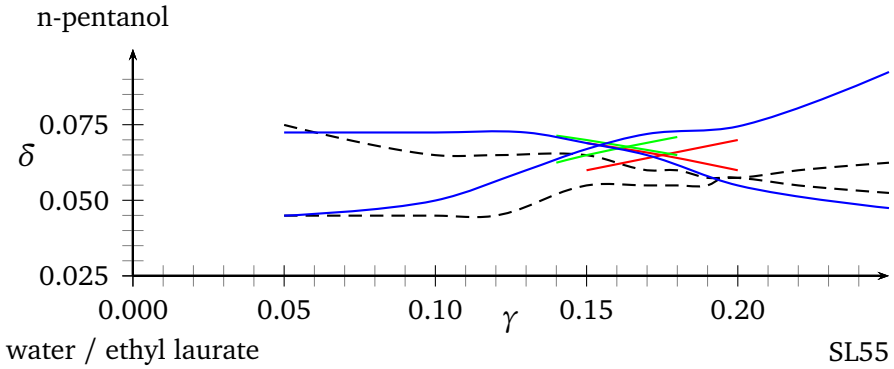

Figure 7.6: Shift of the phase diagram in the system water / ethyl laurate / Simulsol SL55 / n-pentanol at $\alpha = 0.5$ with increasing F68 content. The pure system is drawn in black (dashed lines), the shift was achieved by replacement of SL55 with F68 starting from 1 wt.% (red) to 2.5 wt.% (green) and 5 wt.% (blue). For reasons of clarity only the region close to the X-point are shown in case of the efficiency boosted systems with 1% and 2.5 % F68.

The resulting efficiency boost factors f_B in relation to the F68 content are summarized in table 7.2.

Table 7.2: Characteristics and resulting efficiency boost factor f_B in relation to the F68 content in the system water / ethyl laurate / Simulsol SL55 / n-pentanol at $\alpha = 0.5$.

	ϵ	$\tilde{\gamma_0}$	$\tilde{\gamma}$	f_B
1.0 wt.% Pluronic F68	0.010	0.2	0.175	12.1
2.5 wt.% Pluronic F68	0.025	0.2	0.163	9.5
5.0 wt.% Pluronic F68	0.050	0.2	0.153	7.1

As seen before in the Lanol 99 based system (see 5), the effect decreases with higher F68 amounts. Due to the lower amount of surfactant needed to form the bicontinuous microemulsion phase in the pure ethyl laurate system, the effect of the efficiency boosting is reduced in comparison to the Lanol 99 based system.

Microstructure

The following results of the small angle X-ray scattering were measured with the ID01 beamline at the European Synchrotron Radiation Facility (ESRF, Grenoble, France).
First, the influence of 5 wt.% F68 ($\tau = 0.05$) on the structure of the bicontinuous microemulsion is compared to the system water / ethyl laurate / Simulsol SL55 / n-pentanol. Starting with the polymer free sample composed at $\alpha = 0.5$, $\gamma = 0.22$ and $\delta = 0.06$, a second sample with Pluronic F68 with $\tau = 0.05$ and identical α, γ and δ values was composed.
The results of the fit according to TEUBNER and STREY to the scattering intensities of the two samples, shown in figure 7.7, are given in table 7.3.

Table 7.3: Sample composition and resulting domain sizes d and correlation lengths ξ from the TS-fit to the scattering intensity in the system water / ethyl laurate / Simulsol SL55 / n-pentanol.

	α	γ	δ	ξ (nm)	d (nm)
SL55	0.50	0.22	0.06	4.5	12.9
SL55 (5% F68)	0.50	0.22	0.06	4.6	13.1

In the second series the influence of the polymer content on the structure sizes of the microemulsion was investigated. Due to the boosting of the surfactant efficiency by adding F68, the **1** phase region shifts to lower γ values. Therefore, the bicontinuous phase is reached with surfactant amounts lower than the ones needed in the pure microemulsion. The change in the internal structure sizes upon the addition of the polymer is investigated by the SAXS experiments. As shown in figure 7.6 a higher co-surfactant content is necessary to reach the **1** phase region when Pluronic polymers are applied. To keep the co-surfactant content δ constant, the samples were composed at co-surfactant contents below $\tilde{\delta}$ and higher γ values. The overall surfactant contents of the samples were chosen to ensure a stable microemulsion phase at $\delta = 0.06$ for the samples with increasing F68 content from 0% to 1 %, 2.5 % and 5 %. The exact sample composition and the results of the TS-fit are given in table 7.4.
The resulting scattering intensities of the SAXS experiments are shown in figure 7.8.
The calculated domain sizes d and correlation lengths ξ resulting from the parameters of the TS-fits are summarized in table 7.4 and visualized in 7.9 as function of the amphiphile content γ. With increasing surfactant content the internal surface grows, this finding correlates with the decrease of

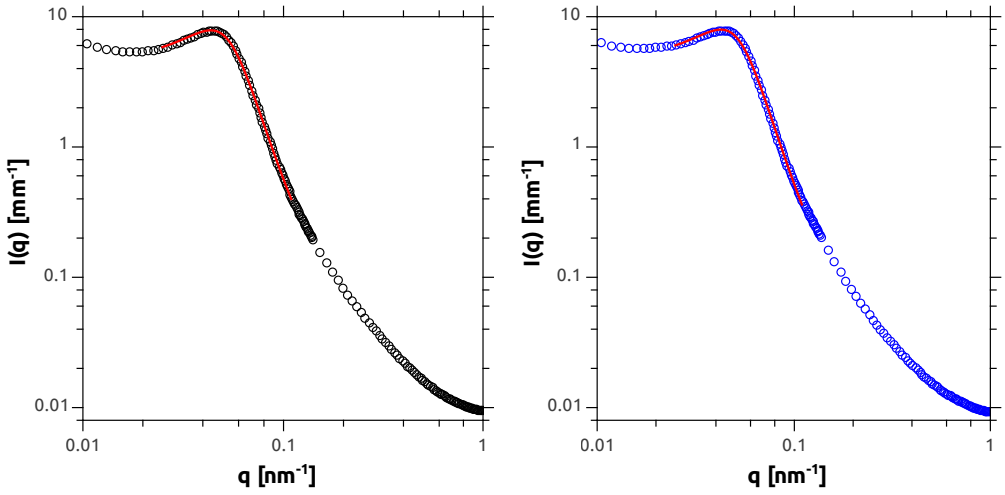

Figure 7.7: Scattering intensities of the SAXS experiments. Samples of the system water / ethyl laurate / Simulsol SL55 / n-pentanol composed at $\alpha = 0.5$, $\gamma = 0.22$ and $\delta = 0.06$. The pure SL55 is shown in black, the sample with F68 ($\tau = 0.05$) in blue. The red lines are fits according to TS.

the domain sizes d and the correlation length ξ in the microemulsion systems.

Related to the results of the system with Lanol 99 as oil phase, the ethyl laurate containing system shows a linear relation between the structure sizes and the surfactant content. Here, the influence of the polymer addition is only marginal. Upon variation of the F68 content added to the microemulsion system the changes in the internal structures were in the range of the experimental error. The efficiency boosting of the surfactant by addition of polymer can be seen as an useful tool to reach bicontinuous phases with low surfactant contents. The second effect is the stabilisation of the microemulsion **1** phase region at a constant surfactant content, observed as a growth of the bicontinuous region upon polymer addition in the phase diagrams.

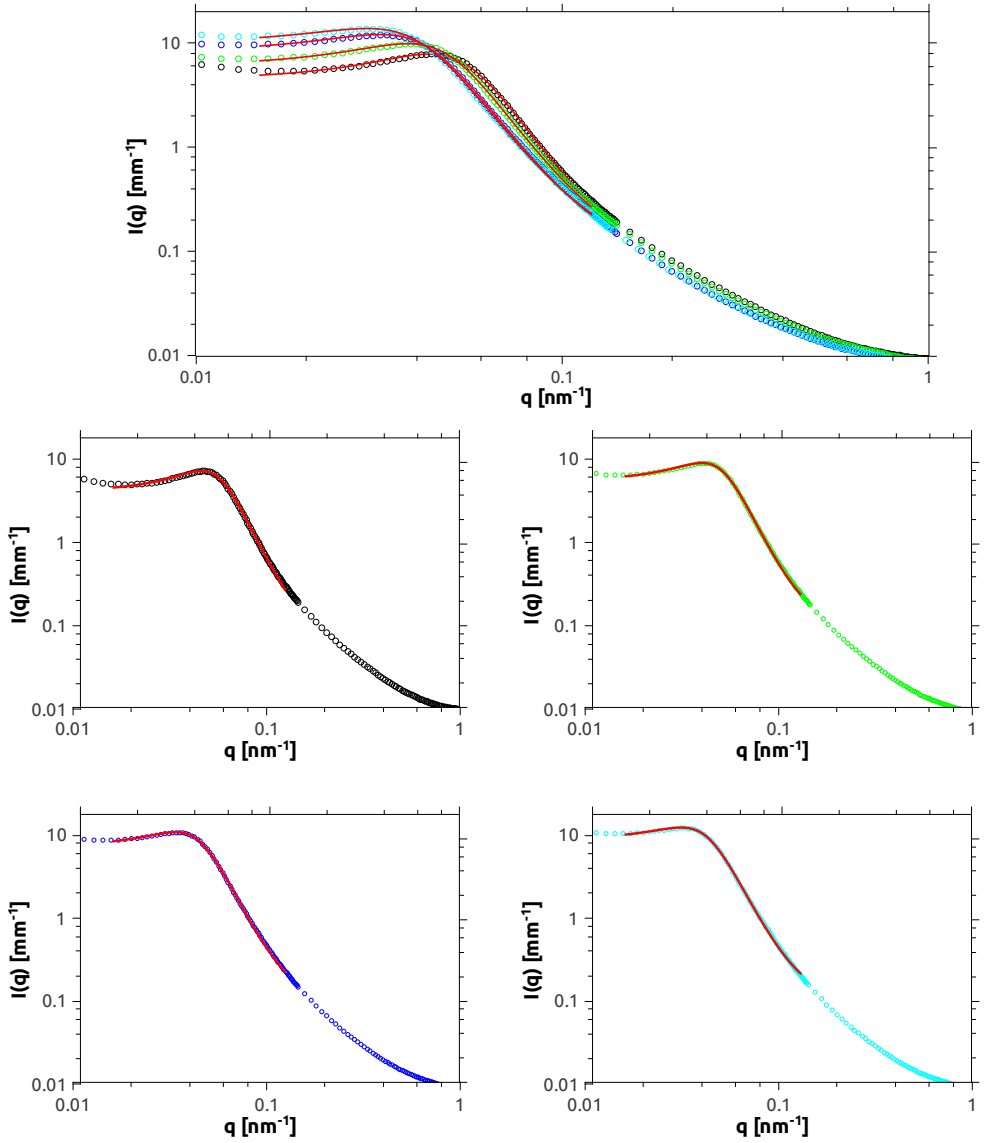

Figure 7.8: Scattering intensities of the samples composed in the bicontinuous region of the system water / ethyl laurate / Simulsol SL55 / n-pentanol at constant $\alpha = 0.5$ and $\delta = 0.06$. Top: Overview of the resulting scattering intensities. γ was reduced starting from the pure system at $\gamma = 0.22$ (black) to $\gamma = 0.20$ in the system with 1 % F68 (green), $\gamma = 0.185$ with 2.5 % F68 (blue) down to the 5 % F68 containing sample at $\gamma = 0.17$ (cyan). Bottom: Single scattering intensities, the red lines are fits according to the Teubner Strey theory.

Table 7.4: Sample compositions and resulting structure sizes from the SAXS experiments analysed with the TS-fit in the bicontinuous phase of the water / ethyl laurate / Simulsol SL55 / n-pentanol system.

label	α	γ	δ	τ	ξ (nm)	d (nm)
22-06-00	0.50	0.22	0.06	0.00	4.5	12.9
20-06-01	0.50	0.20	0.06	0.01	4.8	14.6
185-06-025	0.50	0.185	0.06	0.025	5.1	16.8
17-06-05	0.50	0.17	0.06	0.05	5.2	17.9

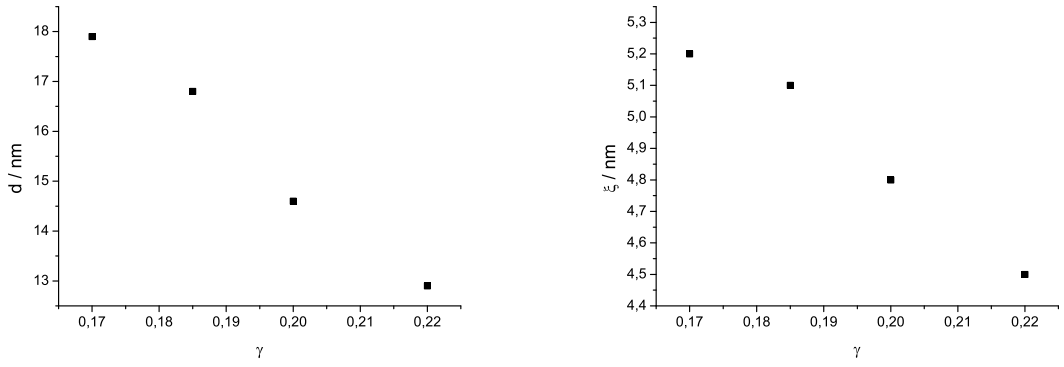

Figure 7.9: Plot of the domain size d (left side) and the correlation length ξ (right side) as a function of the surfactant content γ in the system water / ethyl laurate / Simulsol SL55 / n-pentanol. The F68 content declines with rising γ starting from 5 % F68 ($\gamma = 0.17$) to 2.5 % F68 ($\gamma = 0.185$) and 1 % F68 ($\gamma = 0.20$). The sample at $\gamma = 0.22$ is the pure system without polymer. The samples were, where possible, composed at $\delta = 0.06$ and $\gamma = \tilde{\gamma} + \approx 0.02$, in the case of the sample containing 1 wt.% F68 at $\gamma = \tilde{\gamma} + 0.025$.

Microemulsion dynamics by PCS

The motion of the oil and water domains is a collective breathing mode of the microemulsion. As the bicontinuous region of the different microemulsions show no overlap in the region of interest, the composition of samples with identical α, γ and δ in the **1** phase region is not possible. So all samples were composed close to the X-point, as it is the crucial point in all of the phase diagrams. The diffusion coefficient D is lowered with an increase of the surfactant content. On the other hand an increase of co-surfactant δ leads to higher values of D. So only samples composed quite close to the X-point allow an interpretation of the influence of the oil component on the collective diffusion of the sample. All samples were composed with n-pentanol as co-surfactant. The results of the Contin analysis of the PCS measurements are given in table 7.5.[1]

Table 7.5: Composition and dynamic behaviour of the water / oil / Simulsol SL55 / n-pentanol microemulsion samples. As oil components Lanol 99, ethyl caprate and ethyl laurate were used. In the case of ethyl caprate a sample with Glucopon 220 as surfactant was measured.

Oil / surfactant	α	γ	δ	$D_{eff}[m^2/s]$
Lanol 99/SL 55	0.5	0.28	0.09	8.00 ($\pm$0.21) $\cdot 10^{-12}$
Ethyl laurate/SL 55	0.5	0.22	0.06	8.87 ($\pm$0.08) $\cdot 10^{-12}$
Ethyl caprate/SL 55	0.5	0.22	0.0525	9.68 ($\pm$0.05) $\cdot 10^{-12}$
Ethyl caprate/Glucopon 220	0.5	0.22	0.145	1.16 ($\pm$0.02) $\cdot 10^{-11}$

The collective diffusion coefficient increases from Lanol 99 over ethyl caprate to ethyl laurate. This effect can be related to the decrease in molecular weight and viscosity of the oil component, which decreases from approximately 5.8 mPa·s for Lanol 99 over 3.02 mPa·s (ethyl laurate) to 2.10 for ethyl caprate. The change of the surfactant from SL 55 to Glucopon 220 leads to a high amount of co-surfactant needed to form the bicontinuous phase, as shown in the phase diagrams (figure 7.2). This leads to a higher diffusion coefficient.

[1] Unpublished results, in cooperation with Ralf Stehle

7.1.2 Rapeseed methyl ester

Due to the high availability of the oil phase the biodiesel based microemulsion system developed by HELLWEG *et al.* [28] is an interesting decontamination system. It reaches the requirements of the NATO standard for decontamination and has been characterized in detail [11]. Biodiesel is usually a technical mixture of different fatty acid methyl esters with several additives to improve its properties as fuel. The composition changes due to the varying needs in dependence of the seasons. These seasonal changes in the composition had an influence on the phase behaviour, especially the additives added to reduce the gelation temperature in winter caused problems. Therefore a model system with constant properties was developed with an available, low cost technical oil phase.
The major part of biodiesel is rapeseed methyl ester, a mixture of methyl esters of different fatty acids in the range of C16 to C22. The RME used as a replacement is sold as Synative ES ME TI 05 by Cognis GmbH (BASF Personal Care and Nutrition GmbH, Germany). It has a carbon chain length distribution mainly between C_{14} and C_{18}, with a content of 82 % C_{18}. The main advantage is the possibility to use the resulting microemulsion system for skin decontamination, as the used RME is not harmful.
In table 7.6 the properties of the RME are compared to the requirements of biodiesel as given by EN 14214 [7].

Table 7.6: Comparision of the RME properties with the requirements of EN 14214.

		Biodiesel threshold		Synative ES ME TI 05
	Unit	lower limit	upper limit	Batch CE10260010
Density (15°C)	kg/m^3	860	900	874 (20°C)
Water content	mg/kg	-	500	200
Viscosity (40°C)	mm^3 / s	3,5	5,0	4,1
Acid value	mg KOH/g	-	0,5	0,04
Iodine number	-	-	120	91,3
Linolic acid methyl ester	%	-	12	1,6

Phase diagram of the system water / RME / Simulsol SL55 / n-pentanol

As we expected, the phase behaviour of the system water / RME / Simulsol SL55 / n-pentanol at $\alpha = 0.5$ is nearly identical to the one of the biodiesel based system. As shown in figure 7.10, the **1** phase region starts at high surfactant contents γ. The X-point is located at $\tilde{\gamma} = 0.24$ and $\tilde{\delta} = 0.065$.

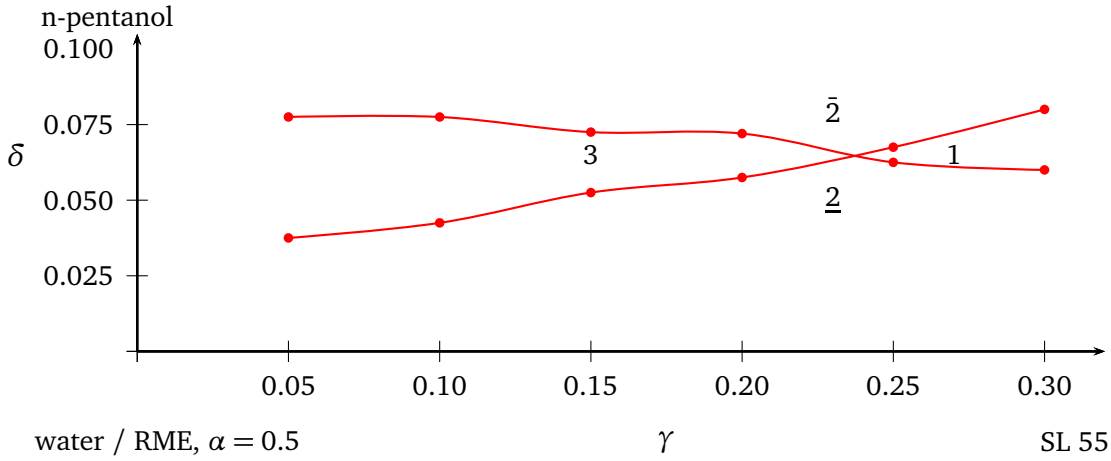

Figure 7.10: Phase diagram (Kahlweit-„fish“) of the system water / RME / Simulsol SL55 / n-pentanol at $\alpha = 0.5$. The X-point is located at $\tilde{\gamma} = 0.24$ and $\tilde{\delta} = 0.065$.

Thus this reference system is slightly more efficient than the biodiesel system, where the bicontinuous system is found at a X-point with $\tilde{\gamma} = 0.26$ and $\tilde{\delta} = 0.07$ [28].

α-variation

As described before, the balanced oil to water ratio of $\alpha = 0.5$ is not necessarily the best for decontamination purposes. Therefore, an α variation was performed for the system water / RME / Simulsol SL55 / n-pentanol. The resulting phase diagrams are shown in figure 7.11.

At low oil content and low surfactant concentrations one observes that the formation of lamellar structures is favoured. At $\alpha = 0.1$ a dominant L_α phase occurs. The very small **3** phase body is followed by a tail, where the bicontinuous phase region behind the X-point is almost completely suppressed by the formation of lamellar structures. At a surfactant content of about $\gamma = 0.23$ the first **1** phase regions occur, which remain stable over an extended δ-range at $\gamma \geq 0.25$.

This observation was made in the mixtures with very low oil content. In more balanced mixtures with an oil content of $\alpha = 0.3$ a clear, stable **1** phase region is observed behind the X-point. Upon

further changes of the oil to water ratio bicontinuous microemulsions without the appearance of lamellar phases are formed up to $\alpha = 0.7$. Again the positions of the X-points show the parabolic trend within the variation of α.

The related $\tilde{\gamma}$ and $\tilde{\delta}$ values of the x-points are summarized in table 7.7.

Table 7.7: Position of the X-points in relation to the α value in the system water / RME / Simulsol SL55 / n-pentanol.

α	$\tilde{\gamma}$	$\tilde{\delta}$
0.1	0.145	0.025
0.3	0.215	0.04
0.5	0.24	0.065
0.7	0.20	0.085

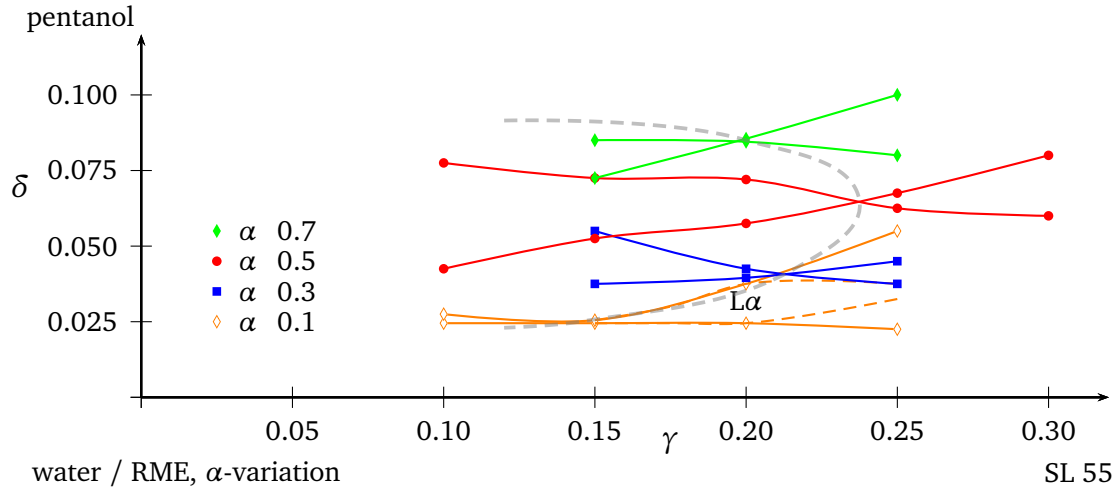

Figure 7.11: Phase diagrams close to the X-point in the system water / RME / Simulsol SL55 / n-pentanol at different values of α in the range of α = 0.1 to α = 0.7. The position of the X-point follows a parabola shape, indicated by the dashed line.

Efficiency boosting

Also for the system water / RME / Simulsol SL55 / n-pentanol a phase diagram with 5% F68 was recorded. Again the polymer induces an enlarged bicontinuous phase and a shift of the x-point from $\tilde{\gamma}_{pure} = 0.24$ to approximately $\tilde{\gamma}_{5\%F68} = 0.17$. In contrast to the systems with a pure oil phase, such as Lanol 99 or ethyl laurate and caprate no significant increase of the amount of co-surfactant is observed when the technical RME is used as an oil phase. The amount of pentanol needed to form the bicontinuous phase is with $\tilde{\delta}_{5\%F68} = 0.060$ slightly reduced compared to the pure system ($\tilde{\delta}_{pure} = 0.065$).

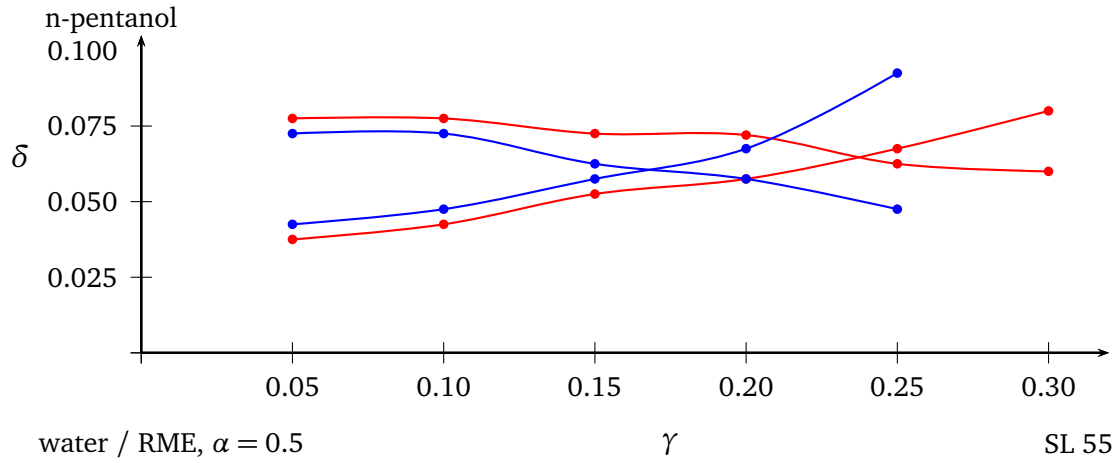

Figure 7.12: Phase diagram (Kahlweit-„fish“) of the system water / RME / Simulsol SL55 / n-pentanol (red) and water / RME / Simulsol SL55 (5% F68) / n-pentanol (blue) at $\alpha = 0.5$.

7.2 System variation II: Co-surfactant

In all systems presented until now, n-pentanol was used as co-surfactant. For model systems, n-pentanol is an excellent choice, as it is a medium sized alcohol showing negligible water solubility. In all systems investigated n-pentanol was able to tune the curvature of the internal surfactant film within adequate co-surfactant contents. Moreover, it can be purchased perdeuterated and contrast variation SANS experiments can be performed.

But all of these advantages are useless in terms of skin decontamination, as the toxicity of n-pentanol is increased compared to the short chain alcohols. Therefore, application in skin friendly microemulsions designed for human decontamination is not favourable. 1,2-octane-diol has been reported by KAHLWEIT *et al.* to be an appropriate non-toxic replacement for n-pentanol [16]. Unfortunately, 1,2-octane-diol is a solid, resulting in an intense rise of the amount of work for recording phase diagrams. Therefore liquid alcohols are preferred due to easy handling.

The requirements for the new co-surfactants are a pharmaceutical certificate on the one hand and the ability to tune the phase behaviour of APG-based microemulsions on the other hand. As a plus, the one phase region should appear at low alcohol concentrations.

With benzyl alcohol and eugenol, we found two alcohols meeting our requirements. Both of them have been used as anaesthetics, therefore medical or pharmaceutical certification exists for dermal use. Skin CWA such as Mustard are able to penetrate skin within minutes, the resorption of the CWA and the following period of several hours are reported to be free from symptoms [27], so the analgesic effect is not required. Taking into account that the alcohols are used in high concentrations when applied as local anaesthetic even the high demand of co-surfactant for microemulsion formation should not exceed harmful limits.

Both alcohols are aromatic alcohols, the structure is depicted in Figure 7.13. Benzyl alcohol or phenylmethanol can be found in essential oils, such as jasmine or ylang-ylang oil [6]. It is suitable as disinfectant or preservative agent, amongst others it is added as preservative to intravenous medication solutions. In addition, it is a food additive (E1519) for flavour production. In 2009 a 5% solution of benzyl alcohol was approved for dermal application as a treatment to head lice infection suitable for children from an age of 6 months [8]. Hence, we expect benzyl alcohol containing microemulsions to be applicable for dermal use.

The second alcohol, eugenol is a phenylpropene (2-methoxy-4-(2-propenyl)-phenol) is known to

be a potential antimicrobial substance and is with a content of 70 - 90 % the main constituent of natural clove oil[5, 15]. In combination with zinc oxide, eugenol is used as a dental cement (zinc oxide eugenol) or as an anaesthetic. A diluted eugenol solution containing up to 5% eugenol are used against inflammation in the oropharynx [5, 15, 2]. Therefore the dermal application of microemulsions containing higher amounts of eugenol for decontamination purposes is acceptable.

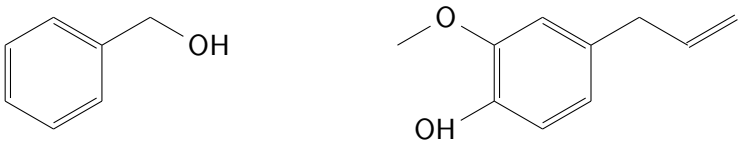

Benzyl alcohol Eugenol

Figure 7.13: Chemical structure of the two co-surfactants benzyl alcohol and eugenol used in the skin friendly microemulsion compositions.

7.2.1 Phase behaviour

The use of of benzyl alcohol and eugenol as co-surfactants in microemulsion formulation was tested in well known systems.

The phase behaviour of the system water / Lanol 99 / Simulsol SL55 / alcohol was studied with the aim to locate the bicontinuous microemulsion region. As shown in the figures 7.14 and 7.15, both alcohols are effective co-surfactants for the formulation of skin friendly microemulsions. Figure 7.14 shows a section through the phase tetrahedron at $\alpha = 0.5$ in the system water / Lanol 99 / Simulsol SL55 / benzyl alcohol. The fish shape of this cut through the phase tetrahedron of the microemulsion system is distorted at low γ values. Here, the three phase body reaches δ values up to $\delta = 0.20$. This is a typical finding, as the alcohol is able to act as co-surfactant and as a co-oil (see additives to microemulsions, section 3.3). As a co-oil, parts of the added alcohol dissolve in the oil phase, increasing the hydrophilic properties of this phase. Hence, the benzyl alcohol dissolved in the oil phase leads to a loss of co-surfactant at the amphiphilic interface. To compensate this loss a higher amount of alcohol is needed to form a balanced interfacial film and therefore, the shape of the fish is distorted at low γ values [25, 26]. The System is a bit less effective compared to the pentanol system, the position of the X-point is shifted from $\tilde{\gamma}_{pentanol} = 0.23$ to $\tilde{\gamma}_{benzylalcohol} = 0.265$,

the fraction of alcohol is increased from $\tilde{\delta}_{pentanol} = 0.085$ to $\tilde{\delta}_{benzylalcohol} = 0.13$.

For the eugenol system at $\alpha = 0.5$ shown in Figure 7.15, this effect is not observed at $\gamma = 0.05$. Lower surfactant concentrations were not investigated as they are not part of the field of interest. Here, again the classical fish shape of the phase boundaries appears, the system is the most efficient of the three investigated systems, the major disadvantage is the high co-surfactant fraction. The X-point is located at $\tilde{\gamma}_{eugenol} = 0.175$ and $\tilde{\delta}_{eugenol} = 0.16$.

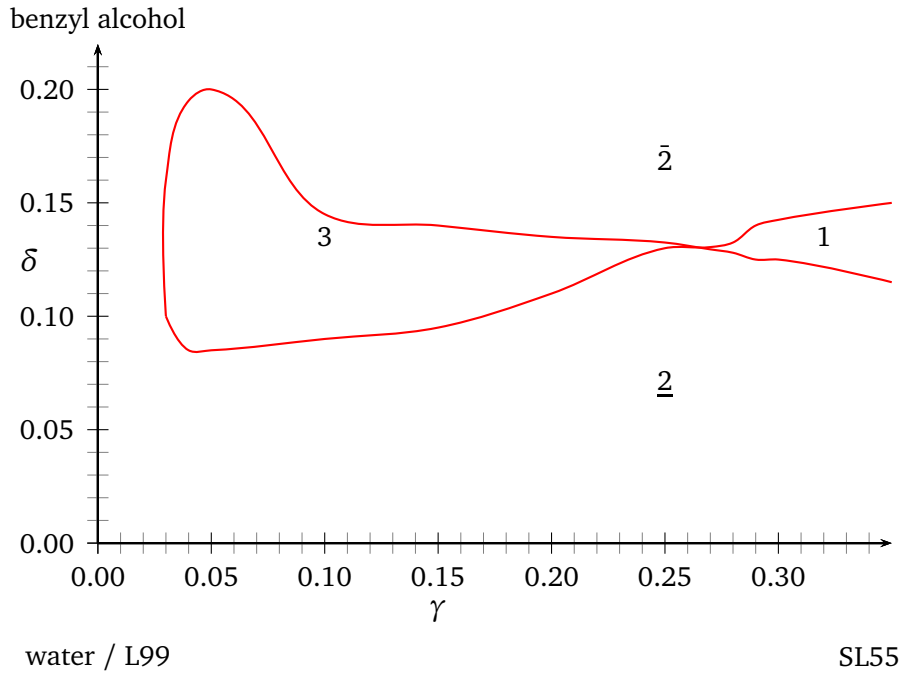

Figure 7.14: Phase diagram of the system water / Lanol 99 / Simulsol SL55 / benzyl alcohol at $\alpha = 0.5$. The X-point is located at $\tilde{\gamma} = 0.265$ and $\tilde{\delta} = 0.13$.

The results are visualized in Figure 7.16, where the fish tail regions of the recorded phase diagrams at $\alpha = 0.5$ are compared with the pentanol base system. The shift of the X-points and the whole single phase region (**1**) to higher $\tilde{\delta}$ values is clearly shown. As mentioned before, eugenol as co-surfactant reduces , benzyl alcohol increases the surfactant fraction. Pentanol, the smallest alcohol is the most effective alcohol to tune the curvature of the internal surfactant film. The co-surfactant content upon utilisation of eugenol is increased compared to benzyl alcohol and nearly twice the amount compared to pentanol is needed.

In Table 7.8 the composition of the microemulsions at the X-point are summed up. Additional

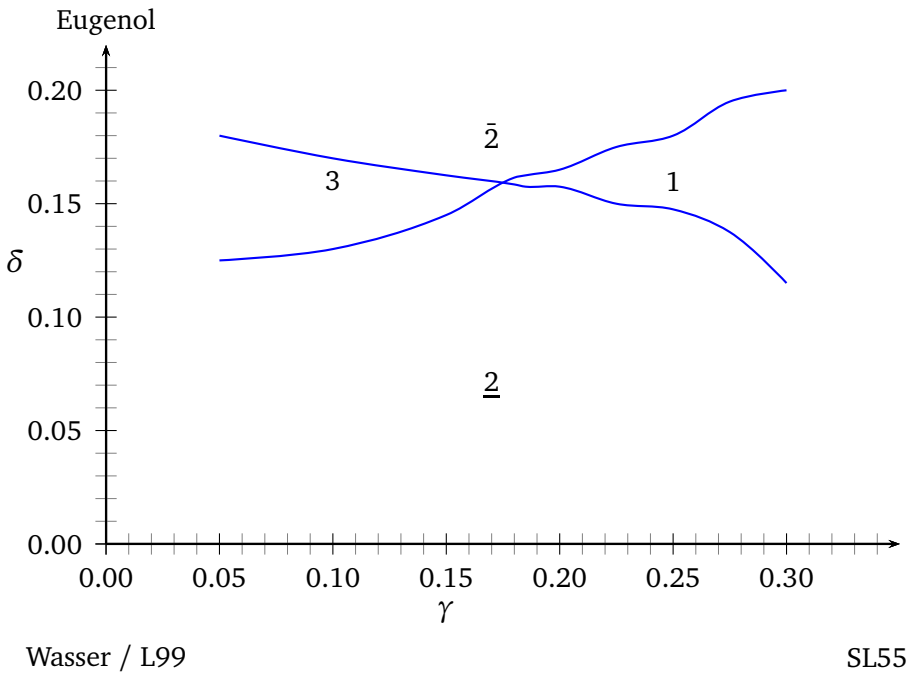

Figure 7.15: Phase diagram of the system water / Lanol 99 / Simulsol SL55 / eugenol at $\alpha = 0.5$. The X-point is located at $\tilde{\gamma} = 0.175$ and $\tilde{\delta} = 0.16$.

information is given about the molar mass of the single alcohols. Using these data, the molality b of the alcohols in the microemulsion can be calculated. The molality b is obtained according to equation 7.1, as volume of the solvent the sum of the volume of oil and water were used.

$$b = \frac{n_{alcohol}}{m_{solvent}} = \frac{n_{alcohol}}{m_{water} + m_{oil}} \tag{7.1}$$

Comparing the molality b of the different alcohols shows that the increase of the co-surfactant amount of eugenol correlates with the higher molecular weight. Benzyl alcohol has a lowered efficiency as co-surfactant, possible reasons may be the increased water solubility compared to pentanol (benzyl alcohol: 39 g/L ; pentanol: 28 g/L) and a resulting decrease of available alcohol molecules in the amphiphilic film.

Table 7.8: Position of the X-point in the system water / Lanol99 / SL55 / co-surfactant depending on the used co-surfactant. Additionally the values of the molar mass and the calculated molality b at the X-point are given.

alcohol	α	$\tilde{\gamma}$	δ	molar mass M g/mol	molality b mmol/g
Pentanol	0.5	0.23	0.085	88.15	0.964
Benzyl alcohol	0.5	0.265	0.13	108.14	1.202
Eugenol	0.5	0.175	0.16	164.20	0.976

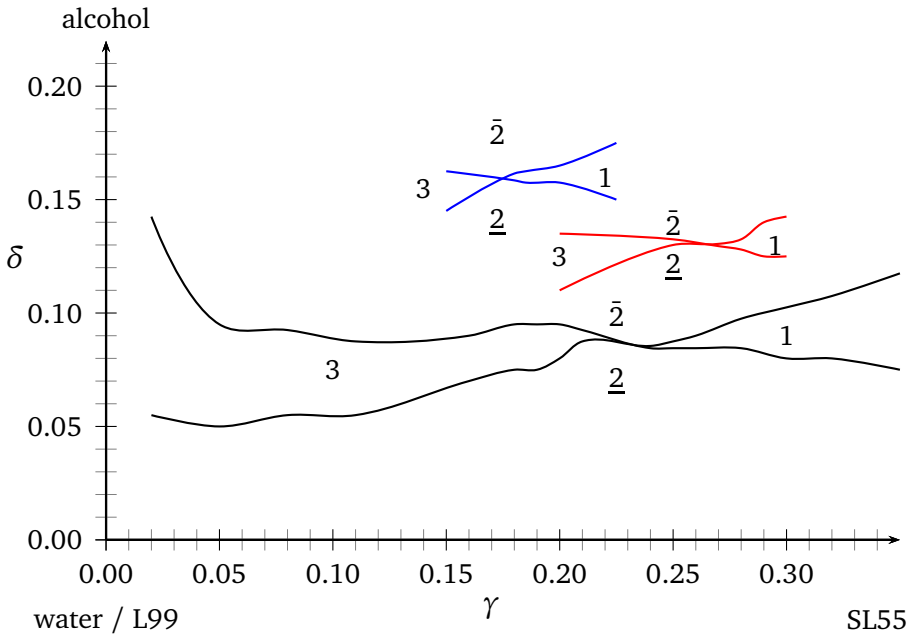

Figure 7.16: Phase diagram of the system water / Lanol 99 / Simulsol SL55 / co-surfactant at $\alpha = 0.5$ with different co-surfactants. For clarity reasons only the area around the X-point of the systems containing Eugenol (blue) and benzyl alcohol (red), for comparison the base system water-SL55-Lanol99-pentanol (black) is shown.

7.2.2 SANS-measurements, system water / Lanol 99 / SL55 / benzyl alkohol

Extensive SANS studies of the system water / Lanol 99 / SL55 / benzyl alkohol, using the PAXY instrument at the LLB (Saclay, France), were performed in cooperation with CHRISTOPH SCHULREICH. The results were published in the *Journal of Colloid and Interface Science* [23]. We were able to show that this microemulsion system shows an extremely low temperature dependence in the range of 261 K to 343 K. Detailed information of this results will be part of the thesis of CHRISTOPH SCHULREICH and are therefore not included in this work [22].

Here, just the first experiments investigating the bicontinuous microemulsion phase in this system by SANS experiments at the FRM II (Garching, Munich) are shown to compare them with the pentanol system.

The systems are optically homogeneous, information about the internal nano structure is gained utilising different scattering methods. For scattering contrast reasons the water phase was replaced by D_2O, the samples were prepared as 'bulk contrast' samples.

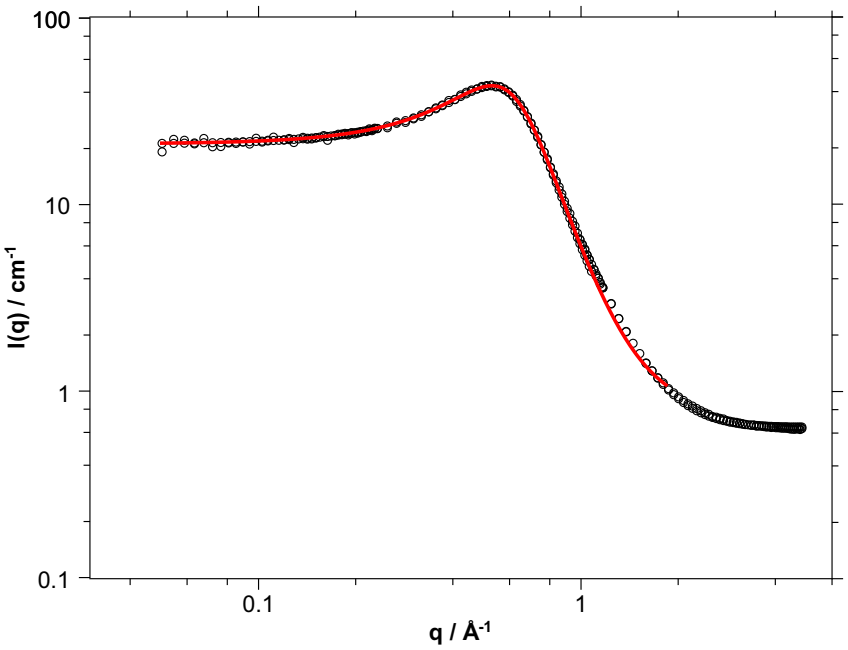

Figure 7.17: SANS data of the system D_2O / Lanol 99 / SL 55 / benzyl alcohol at $\alpha = 0.5$, $\gamma = 0.35$ and $\delta = 0.115$. The red lines are fits according to the Teubner-Strey approximation.

In Figure 7.17 the resulting scattering curve is shown.

The results of the data analysis are summarised in table 7.9 and compared with the results of a SANS experiment performed by HELLWEG *et al.* on a sample at $\gamma = 0.34$ and $\delta = 0.0825$ of the base system D_2O / Lanol 99 / SL55 / n-pentanol at the Laboratoire Léon Brillouin (LLB, Saclay, France) (Data taken from reference [11]).

Table 7.9: Sample composition and results of the TS analysis of the SANS experiments in the system D_2O / Lanol 99 / SL55 / benzyl alcohol. For comparison the results for the system D_2O / Lanol 99 / SL55 / n-pentanol are given (original data see reference [11].

	α	γ	δ	T / °C	ξ/nm	d/nm	κ/k_BT
Benzyl alcohol	0.5	0.35	11.5	20.0	4.3	10.9	0.395
Pentanol	0.5	0.34	0.0825	21.7	4.7	9.7	0.416

The comparison of the correlation length and the domain size obtained from Teubner-Strey analysis shows that in both systems a bicontinuous microemulsion phase exists. The domain size d is the quasi periodical distance of the water and oil domains, the correlation length ξ describes the dispersion of d in the bicontinuous structure. In the benzyl alcohol system, the d is slightly larger, while the correlation length ξ is reduced. This may indicate an increase of the volume of the water phase as a result of the higher solubility of the benzyl alcohol compared to pentanol.

7.3 System water / ethyl ester / SL55 / benzyl alcohol

On the roadmap to a new microemulsion system suitable for skin decontamination, the ethyl esters introduced in section 7.1.1 were combined with benzyl alcohol. The new systems contain only components that already are used in pharmaceutical application or in cosmetics. When the extraction abilities reach the demands of the NATO standard for decontamination media, a use of this new skin friendly system will be possible.

The resulting phase diagrams at $\alpha = 0.5$ are shown in Figure 7.19 for ethyl caprate and figure 7.18 for ethyl laurate respectively. Both systems show a low surfactant efficiency, the bicontinuous region starts with both oils at $\tilde{\gamma} = 0.23$. The three phase body (**3**) and the one phase region (**1**) are rather small between $\gamma = 0.15$ and $\gamma = 0.23$, which impedes the correct determination of the X-point.

Compared with the Lanol 99 containing system, the alcohol demand is significantly lowered. The X-point is reached upon addition of 6.0 wt% in case of the ethyl caprate ($\tilde{\delta}_{EC} = 0.06$), elongating

the oil alkyl chain by an ethyl unit leads to a slightly higher alcohol content of 6.5 wt% for ethyl laurate ($\tilde{\delta}_{EL} = 0.065$).

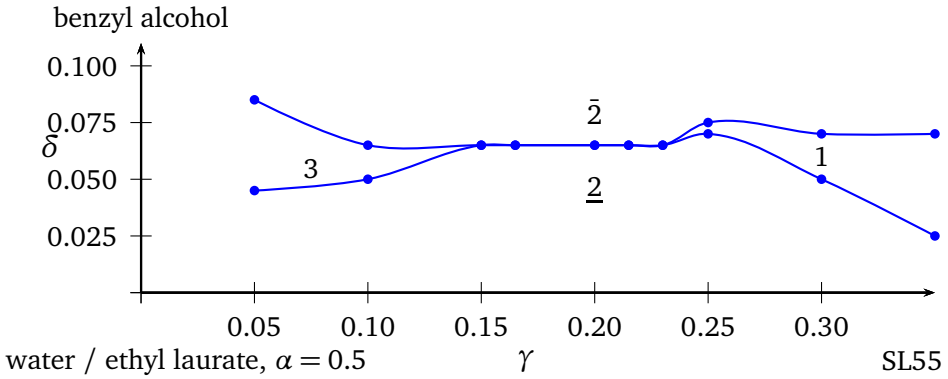

Figure 7.18: Phase diagram of the system water / ethyl laurate / SL55 / benzyl alcohol at $\alpha = 0.5$.

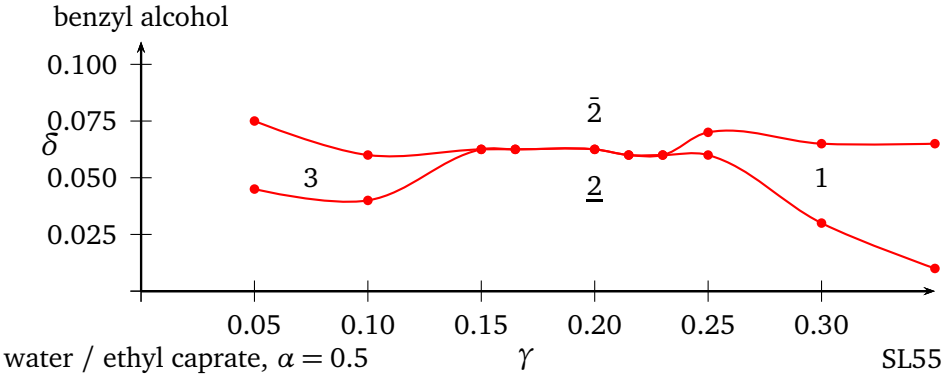

Figure 7.19: Phase diagram of the system water / ethyl caprate / SL55 / benzyl alcohol at $\alpha = 0.5$.

In both systems the formation of a bicontinuous microemulsion phase was achieved, the necessary amount of alcohol is in a range comparable to the concentrations used in pharmaceutical applications. Therefore, this system is highly recommended for skin decontamination purposes.

7.4 Conclusion

Microemulsions are a promising media for decontamination purposes. But the systems existing up to date are based on chemicals not suitable for the decontamination of the human skin. Therefore, the cyclohexane or diesel fuel in the technical systems was modified. As possible replacements ethyl esters and rapeseed methyl ester were successfully tested. All systems offered a suitable bicontinuos microemulsion phase at acceptable co-surfactant contents. For systems based on water / ethyl caprate / Simulsol SL55 / n-pentanol and water / RME / Simulsol SL55 / n-pentanol an α variation was performed. As comparable results to the well-known behaviour of the C_iE_j surfactant based systems were observed, by variation of the oil to water ratio the extraction abilities of the microemulsion system can be tuned. The influence of the Pluronic polymers is comparable to the observations made in the system based on water / Lanol 99 / SL 55 / n-pentanol. Upon addition of F68 the efficiency of the sugar surfactant Simulsol SL55 was increased. This finding allows the formation of long time stable microemulsions, using a surfactant / polymer mixture instead of the pure surfactant as amphiphilic film. Additionally, a significant reduction of the amount of surfactant needed to form a bicontinuos microemulsion phase is achieved. With the replacement of n-pentanol by benzyl alcohol or eugenol, which are both used in pharmaceutical applications, microemulsion systems suitable for skin decontamination were developed. The new alcohol components allow formulations with anaesthetic effects on the skin, containing only components which are already used in pharmaceutical applications or cosmetics.

Therefore, the transfer from purely technical usage to in-field use for the decontamination of human skin is possible. Keeping the requirements of an ideal decontamination system in mind, which were summarized in table 2.2, the properties of the new systems are matched to that requirements. This comparison, shown in table 7.10, shows that the new microemulsion systems fulfil many of the requirements of an ideal decontamination medium and outperform the macroemulsion systems used nowadays.

Table 7.10: Comparison of the requirements of an ideal skin decontamination medium (see 2.2) with the properties of new developed microemulsion systems. ✓ (fulfilled), o (partly fulfilled), - (not fulfilled)

Aspect	Ideal decontamination media	Our systems
Safety	non irritating and non allergic	o containing only components used in cosmetics/drugs.
	non hazardous	✓ formulations possible.
	environmentally compatible	✓ components are natural extracts or renewables.
	non corrosive	o no increase to common in use macroemulsions expected.
Usability	easy to employ	✓ liquids with high surface activity.
	quick to hand	✓ premixed stable systems possible.
	single and mass use devices available	✓ easy scale up due to thermodynamic stability.
Stability	Temperature range from -40 °C to +50 °C	Stability between -12 °C and +45 °C proven[23].
	long storage life	✓ some samples stable for several years now.
	no separation effects	✓ thermodynamically stable.
Economy	low costs	- but surfactant saving possible.
	available in large amounts	✓ all components available in industrial scales.
	easy to scale-up	✓ liter scale used for decontamination tests at WIS Munster.
	constant quality	✓ formation of systems with technical grade chemicals possible.
Efficiency	quick and complete decontamination	o (depending on active agent)
	no formation of toxic products	o (depending on active agent)
	no increase of percutaneous uptake	no data available, but not induced for the components used.

7.5 References

[1] T. Aasen and J.C.I Belmonte. “Isolation and cultivation of human keratinocytes from skin or plucked hair for the generation of induced pluripotent stem cells”. In: *Nature Protocols* 5 (2010), pp. 371–382.

[2] W. Ax et al. *Lehrbuch der pharmazeutischen Biologie*. Springer Berlin Heidelberg, 1996.

[3] K. Bauer, K.-H. Froemming, and C. Fuehrer. *Lehrbuch der Pharmazeutischen Technologie*. Wissenschaftliche Verlagsgesellschaft mbH Stuttgart, 2006.

[4] M.-M. Blum et al. “Binding of a Designed Substrate Analogue to Diisopropyl Fluorophosphatase: Implications for the Phosphotriesterase Mechanism”. In: *Journal of the American Chemical Society* 128.39 (2006), pp. 12750–12757.

[5] F. von Bruchhausen, S. Ebel, and E. Hackenthal. *Hagers Handbuch der Pharmazeutischen Praxis: Stoffe A-K*. Bd. 1. Springer, 1999.

[6] S (ed.) Budavari. *The Merck Index: An Encyclopedia of Chemicals, Drugs, and Biologicals*. Merck, 1989.

[7] *DIN EN 14214:2012-11, Fluessige Mineraloelerzeugnisse - Fettsaeure-Methylester (FAME) zur Verwendung in Dieselmotoren und als Heizoel - Anforderungen und Pruefverfahren*.

[8] *FDA Label for ULESFIA*. Food and Drug Administration.

[9] F. Gonzaga et al. “New microemulsions for oxidative decontamination of mustard gas analogues and polymer-thickened half-mustard”. In: *New J. Chem.* 25 (2001), pp. 151–155.

[10] T. Hellweg. “Microemulsions: A Versatile Carrier for Decontamination Agents”. In: *Decontamination of Warfare Agents*. Ed. by A. Richardt and M.-M. Bum. Wiley-VCH, Weinheim, 2008.

[11] T. Hellweg, R. Stehle, and C. Schulreich. *Herstellung von Struktur-Wirkungsbeziehungen für Mikroemulsionen zur Dekontamination*. 2009.

[12] C.J. Hilmas, J.K. Smart, and B.A. Hill. “Medical Aspects of Chemical and Biological Warfare - Textbook of Military Medicine”. In: ed. by R. Zajtchuk and R.F. Bellamy. Office of The Surgeon General Department of the Army, United States of America, 2008. Chap. 2. History of Chemical Warfare, p. 9.

[13] C. van Hooidonk et al. “CW Agents and the Skin: Penetration and Decontamination.” In: *Proceedings of the International Symposium on Protection against Chemical Warfare Agents. Umea, Sweden: National Defence Research Institute*. 1983, pp. 153–160.

[14] *Internal communication, no published results.*

[15] B.K. Jadhav et al. “Formulation and evaluation of mucoadhesive tablets containing eugenol for the treatment of periodontal diseases”. In: *Drug Dev Ind Pharm.* 30.2 (2004), pp. 195–203.

[16] M. Kahlweit, G. Busse, and B. Faulhaber. “Preparing Nontoxic Microemulsions”. In: *Langmuir* 13 (1995), pp. 5249–5251.

[17] H. Marquardt and S.G. Schaefer. *Lehrbuch der Toxikologie*. Ed. by H. Marquardt and S.G. Schaefer. BI-Wissenschafts-Verlag, 1994.

[18] A. Richardt and M.M. Blum. *Decontamination of Chemical Warfare Agents*. Wiley VCH, 2008.

[19] A. Richardt, M.M. Blum, and S. Mitchell. “Was wissen Calamari über Sarin? Enzymatische Dekontamination von Nervenkampfstoffen.” In: *Chemie in unserer Zeit* 40.4 (2006), pp. 252–259.

[20] H. Salem, A.L. Ternay, and J.K Stuart. “Chemical Warfare Agents - Chemistry, Pharmacology, Toxicology and Therapeutics”. In: ed. by J.A. Roman, B.J. Lukey, and H. Salem. CRC Press, 2008. Chap. Brief History and use of Chemical Warfare Agents in Warfare and Terrorism.

[21] W. Schroeder, J. Teschner, and A. Wanninger, eds. *Taschenbuch der Chemie*. Verlag Harri Deutsch, 2005.

[22] C. Schulreich. “Mikroemulsionen auf Basis von Zuckertensiden: Struktureigenschaftsbeziehungen, Stabilität und Enzymkinetik”. Phd Thesis. Universität Bielefeld, 2015.

[23] C. Schulreich et al. “Bicontinuous microemulsions with extremely high temperature stability based on skin friendly oil and sugar surfactant”. In: *Colloids and Surfaces A: Physicochemical and Engineering Aspects* 418 (2013), pp. 39–46.

[24] T. Sottmann and R. Strey. “Shape Similarities of Ultra-Low Interfacial Tension Curves in Ternary Microemulsion Systems of the Water-Alkane-CiEj Type”. In: *Berichte der Bunsengesellschaft für physikalische Chemie* 100.3 (1996), pp. 237–241.

[25] C. Stubenrauch, B. Paeplow, and G. H. Findenegg. “Microemulsions Supported by Octyl Monoglucoside and Geraniol. 1. The Role of the Alcohol in the Interfacial Layer”. In: *Langmuir* 13.14 (1997), pp. 3652–3658.

[26] C. Stubenrauch et al. “Phase behavior of the quaternary system water - decane - decyl monoglucoside - decanol”. In: *Tenside Surfactants Deterg.* 33 (1996), p. 237.

[27] H.-W. Vohr. *Toxikologie Band 2: Toxikologie der Stoffe*. Ed. by H.-W. Vohr. Vol. 2. Wiley VCH Verlag GmbH & Co KGaA, 2010.

[28] S. Wellert et al. “Structure of biodiesel based bicontinuous microemulsions for environmentally compatible decontamination: A small angle neutron scattering and freeze fracture electron microscopy study”. In: *J.Colloid Interf.Sci.* 325.1 (2008), pp. 250–258.

Chapter 8

Summary and future perspectives

Bicontinuous microemulsion phases are promising decontamination media, as they provide a water and an oil phase, separated by an enormous amphiphilic film. While the oil phase serves as solvent for the toxic agent, the water phase is the carrier for the active decontamination agent, such as DFPase. But the high demand of sugar surfactants is a limiting factor for the industrial use of the microemulsion systems.

Since the discovery of the efficiency boosting effect, the interaction of polymers with surfactant films was widely investigated. Usually amphiphilic polymers of the A-B type, synthesized in laboratory size batches were used. This thesis is connecting the efficiency boosting effect with technical grade A-B-A polymers (Pluronic, BASF), available in industrial scale. These polymers are commercially available in a variety of different sizes and block length compositions. Some of them are able to increase the efficiency of the surfactant strongly. In all investigated systems the observed trends between polymer structure or size and effect on the sugar surfactant were similar.

8.1 Lanol system

Based on the well known system water / Lanol 99 / Simulsol SL55 / n-pentanol the influence of the Pluronic polymers on the phase behaviour of the microemulsion system was systematically studied. The strength of the influence on the surfactant efficiency is closely connected to the polymer size and composition. Pluronic polymers with a low PEO content decrease the efficiency of the surfactant, and therefore lead to a shift of the X-point to higher values of γ. With the change in the polymer composition to higher PEO contents, an increase of the surfactant efficiency was observed. The

resulting $\tilde{\gamma}$ values are reduced, the best effects were reached with the Series **S3** of polymers of a PEO-content of 80 wt.%. In all cases the amount of co-surfactant needed to form a bicontinuous structure was found at higher $\tilde{\delta}$ values compared to the pure system.

In contrast to the classical efficiency boosting effect with A-B type amphiphilic polymers, a saturation effect was observed. The sugar surfactant efficiency is increased up to a concentration of 10 wt.% polymer in the amphiphile. Further increase of the surfactant amount replaced by polymer, lead to a break of the microemulsion structure. In the samples containing 15 wt.% Pluronic no bicontinuous phase was observed throughout the investigated region. Therefore a standard polymer concentration of 5 wt.% was applied throughout this work.

However, this effect was also connected to the polymer size. An increase of the overall polymer size usually leads to a higher surfactant efficiency, even though less polymer molecules are available in the internal membrane. As the large polymers tend to form extended lamellar phases, the best results were obtained with the Pluronic F68. Depending on the polymer type and the concentration, the surfactant amount needed to form a stable bicontinuous microemulsion phase was reduced by $\approx$ 10 to 40 %. This impressive effect and the resulting cost savings come together with an observed increased stability. Although the samples were composed close to the X-point, the microemulsion phases containing Pluronic polymers showed an increased long time stability. In some cases the samples are stable for more than 4 years.

Furthermore, the influence of the polymers on the microstructure was investigated by SAXS experiments. Here, the smaller polymers of Series **S2**, which show small effects on the surfactant efficiency, lead to a slight reduction in the domain size d while the correlation length ξ is slightly increased. In contrast to that, the polymer series **S3** increases d compared to the pure system, by a reduction of ξ. The real advantage of the polymer addition is the increase of the structure size available. In a microemulsion system the available internal structure size is limited by the position of the X-point. By simply adding a small amount of polymer, this size can be increased by 14 % from 17.7 nm to 20.2 nm at a constant γ value.

The PCS experiments showed that the motion of the amphiphilic membrane is reduced upon polymer addition. This is interpreted as a result of the integration of the large polymers into the membranes. The reduction of the diffusion coefficient D is connected to the mass of the polymer.

The results related to the classical efficiency boosting effect as described by JAKOBS *et al.*, are an

important improvement of technical grade sugar surfactant microemulsion systems.

8.2 $C_{10}G_2$ system

To avoid the influence of impurities of the technical grade systems and to allow contrast variation by deuteration the model system based on the pure sugar surfactant n-decyl-β-D-maltoside ($C_{10}G_2$) was investigated. In case of the system water / cyclohexane / $C_{10}G_2$ / 1-pentanol extended lamellar phases are observed. Here, the addition of Pluronic polymers leads to similar changes of the phase behaviour. An additional advantage is the suppression of the formation of lamellar phases, offering large bicontinuous regions at low γ values. As the system is quite effective with $\tilde{\gamma} = 0.080$, the boost factors were rather small. With F108 a $f_B = 7.23$ was reached, corresponding to a $\tilde{\gamma} = 0.061$.
The pure system offers maximum structure sizes in the range of $\xi = 14.25$ nm and d = 35.30 nm close to the X-point. Upon polymer addition no significant changes were observed at constant sample compositions, as shown by SANS experiments. However, the addition of polymers enables stable bicontinuous structures with $\xi = 16.43$ nm and d = 53.30 nm, that corresponds to an increase of the correlation length ξ of 15 %. In case of the domain size an increase of 50 % was achieved by replacing 10% surfactant with F68 polymer.
The internal motion of the amphiphilic film was investigated by PCS and NSE experiments. In all cases the resulting bending rigidity κ_{PCS} and the bending rigidity κ_{NSE} are slightly reduced upon polymer addition. This correlates to our interpretation of the polymer being a part of the amphiphilic film and therefore reduce the overall mobility of the membrane.

8.3 Skin decontamination

As the current systems are not suitable for the decontamination of the human skin due to the alcohol component or the oil phase used, an improvement of the existing systems is necessary. The extraction ability of the Lanol 99 based system was below the expectations, therefore the oil phase was modified.
As the new microemulsion systems using ethyl laurate, ethyl caprate or RME as oil phases, and benzyl alcohol or eugenol as co-surfactants, these systems are no longer hazardous mixtures according to the Globally Harmonized System of Classification and Labelling of Chemicals (UN-GHS). All components were chosen carefully, with priority on substances that already have pharmaceuti-

cal permission or are used as food additives. Again, the addition of Pluronic polymers lead to an increase of the surfactant efficiency.

All newly developed systems showed the desired bicontinuous microemulsion phases. Furthermore, we expect the system based on the fatty acid methyl ester to show extraction results comparable to the biodiesel system developped by WELLERT *et al.*. After the identification of the best suited oil phase for the decontamination process, which is done in extraction experiments by the Wehrwissenschaftliches Institut für Schutztechnologien – ABC-Schutz (WIS), further refinements of the systems can be envisaged. With the possibility to tune the structure sizes of the microemulsion domains by simply adding Pluronic polymers, the mobility of the DFPase in the system can easily be increased.

Comparing the properties with the requirements of an ideal skin decontamination medium (see table 2.2 in section 2.3), we expect the newly developed systems to be versatile carriers for decontamination. Safety aspects require a non irritating, non allergic and non hazardous decontamination system, which is environmentally safe and non corrosive. The sugar surfactant based microemulsions are non hazardous mixtures according to the Regulation (EC) No 1272/2008. Even though the used alcohols are known to be potentially allergen, we were able to formulate systems using concentrations below the level of other pharmaceutical products. Here, a combination of different co-surfactants is a future task for further improvement.

As an aqueous mixture, the microemulsion systems are potentially corrosive, but as the systems are composed at pH values in the range of pH = 7 - 8, corrosion should be negligible. The usage of compounds derived from natural raw material leads to a high environmental compatibility of the microemulsion system, they are weakly hazardous to water and both, surfactant and oil phase, are biodegradable. Furthermore, even the microemulsion samples composed close to the phase boundaries showed a good long term stability up to 4 years. Therefore, we suggest the usage of premixed solutions, which are easy to deploy and show no separation effect, as microemulsions are thermodynamically stable systems. In addition, the efficiency boosting concept with technical grade Pluronic polymers and the resulting saving of sugar surfactant can be transferred completely to the skin friendly microemulsion systems.

Depending on the used co-surfactant, the temperature stability is given in the range from -10 °C to +45 °C. The samples we cooled below the freezing point remained bicontinuous after thawing, therefore even storage as frozen samples is possible. Especially for the enzymatic decontamination this is interesting, as the stability of the enzyme DFPase depends on the storage temperature.

Here, the combination of a freshly produced or premixed decontamination system stored at room temperature with an enzyme containing stock solution is possible with our microemulsion systems. The efficiency of the decontamination media depends on two factors. First the CWA has to be extracted from the surface. Here, microemulsions show excellent wetting abilities, as they offer low surface tensions and are, due to the oil phase, suitable solvents for the lipophilic CWA. The second step, the destruction of the CWA depends on the used active agent. Here, the enzymatic decontamination is favoured in combination with sugar surfactants, as these surfactants are known to preserve the tertiary structure of enzymes. In addition, the mobility of the enzyme in the microemulsion can be increased by tuning the internal structure sizes by simply adding Pluronic polymers.
Regarding the advantages of the skin friendly microemulsion systems, we are convinced that these systems have great potential as decontamination media for both, equipment and human decontamination. This work shows that the technical systems designed for the field use can be transferred to skin friendly systems without a loss of the properties and the advantages of microemulsion based decontamination systems.

Appendix

List of Figures

List of Tables

List of Publications

1. S. Hoehn, C. Schulreich, and T. Hellweg, ”Efficiency Boosting in Technical Grade Sugar Surfactant Based Microemulsions Using Pluronics.”, *Tensides Surf. Det.*, 51 (2014) 1, 32-39.

2. C. Schulreich, C. Angermann, S. Hoehn, R. Neubauer, S. Seibt, R. Stehle, A. Lapp, A. Richardt, A. Diekmann, and T. Hellweg, “Bicontinuous microemulsions with extremely high temperature stability based on skin friendly oil and sugar surfactant.” *Colloids and Surfaces A: Physicochemical and Engineering Aspects*, 418 (2013), 39-46.

3. R. Neubauer, S. Hoehn, C. Schulreich, and T. Hellweg, “Protein diffusion in a bicontinuous microemulsion. Inducing sub-diffusion by tuning the water domain size.”, *in preparation*

4. R. Neubauer, S. Hoehn, C. Schulreich, S. Seibt, and T. Hellweg, ‘Protein diffusion in a system crowded with monodisperse spheres”, *in preparation*

Abbreviations

APG	Alcylpolyglycoside (Surfactants)
BCP	Block Copolymer
CMC	Critical Micelle Concentration
CMT	Critical Micelle Temperature
C_iE_j	Alkyl Polyglycolether (Surfactants)
C_nG_m	Alcylpolyglucoside; n = number C-Atoms, m = polymerization degree
$C_{10}G_2$	n-decyl-β-D-maltoside
CWA	Chemical Warfare Agent
CWC	Chemical Weapons Convention
DFPase	Diisopropyl Fluorophosphatase
DLS	Dynamic Light Scattering
FAME	Fatty Acid Methyl Ester
FFEM	Freeze-Fracture Electron Microscopy
G220	Glucopon 220
ICF	Intensity Correlation Function
NMR	Nuclear Magnetic Resonance Spectroscopy
NSE	Neutron Spin Echo Spectroscopy
OPCW	Organisation of the Prohibition of Chemical Weapons
PCS	Photon Correlation Spectroscopy
PEO	Poly(ethylene oxide)
PEP	Poly(ethylene propylene)
PIT	Phase Inversion Temperature
PPO	Poly(propylene oxide)
SAS	Small Angle Scattering
SANS	Small Angle Neutron Scattering
SAXS	Small Angle X-Ray Scattering
SL55	Simulsol SL 55
SLS	Static Light Scattering
TS	Teubner - Strey (equation)

Danksagung

An dieser Stelle sei all jenen gedankt, die mich in der (langen) Zeit der Promotion unterstützt haben.
Besonderer Dank gilt meinem Doktorvater Prof. Dr. Thomas Hellweg, der mir nicht nur ein spannendes Forschungsthema überlassen hat, sondern durch sein Vertrauen und den Freiraum zur Gestaltung viele spannende Projekte ermöglicht hat.
Auch Prof. Dr. Stefan Förster möchte ich für die freundliche Aufnahme in seinen Arbeitskreis danken, wodurch die praktischen Arbeiten in Bayreuth vollendet werden konnten.
Meinen Freunden und Kollegen in Bayreuth und Bielefeld danke ich für das hervorragende Arbeitsklima. Eure Ratschläge, die diversen Liter gemeinsamer Kaffee inklusive fachlicher und nichtfachlicher Diskussionen waren klasse.
Der Dank für spannende Messzeiten gilt den Messteams und Local Contacts: A. Lapp (LLB), P. Falus (ILL), sowie P. Boeseke, M. Sztucki, T. Narayanan und J. Gummel (ESRF). Die Forschungsaufenthalte am ESRF, ILL (beide Grenoble) und am LLB (Saclay) werden für mich immer ein "highlight" meiner Forschung bleiben.
Der mechanischen Werkstatt und F. Fischer gilt mein Dank für die tatkräftige Unterstützung und Praxiswissen, wenn die Röntgengeneratoren mich zur Verzweiflung gebracht haben. Stellvertretend für die guten Seelen im Hintergrund möchte ich K.H. Lauterbach, E. Düngfelder und S. Gericke meinen Dank für allen Themen im Unialltag außerhalb der Forschung aussprechen.
Meinen Lektoren (allen voran Ralph und Martin) gebührt die Ehre aus meinen Texten ein lesbares Werk gemacht zu haben.
Meiner Familie und meinen Freunden sei für die moralische (Kaffee! Schokolade!) Hilfe und tatkräftige (Kinderbetreuung!) Unterstützung herzlich gedankt. Ohne Euch würde ich heute noch schreiben.

Von ganzen Herzen möchte ich mich bei Lisa bedanken.
Und bei Andreas, Georg, Martin und Ulrich

- für Eure Geduld und die Zeit an den Wochenenden,
die eigentlich Euch gehört hätte.

Erklärung zur Dissertation

Hiermit erkläre ich, dass ich diese Arbeit selbständig verfasst und keine anderen als die von mir angegebenen Quellen und Hilfsmittel benutzt habe.

Ferner habe ich nicht versucht, anderweitig mit oder ohne Erfolg eine Dissertation einzureichen oder mich der Doktorprüfung zu unterziehen.

Altenplos, 12. Dezember 2015

Sebastian G. A. Höhn